PISCES

A Morphodynamic Coastal Area Model
First Annual Report

T J Chesher
H M Wallace
I C Meadowcroft
H N Southgate

Report SR 337
April 1993

HR Wallingford

Registered Office: **HR Wallingford Ltd.** Howbery Park, Wallingford, Oxfordshire, OX10 8BA, UK
Telephone: 0491 835381 International + 44 491 835381 Telex: 848552 HRSWAL G.
Facsimile: 0491 832233 International + 44 491 832233 Registered in England No. 2562099.
HR Wallingford Ltd is a wholly owned subsidiary of HR Wallingford Group Ltd.

Contract

This report describes work funded by the Ministry of Agriculture, Fisheries and Food under Contract Number CSA 2090, for which the nominated officer was Mr B D Richardson and the HR Wallingford (HR) nominated officer was Dr W R White. Allied work funded by the Commission of the European Communities Directorate General for Science, Research and Development under Contract Number MAST 0035-C is reported here as well. The HR job number was USS 11. This report is published on behalf of the Ministry of Agriculture, Fisheries and Food, but any opinions expressed in this report are not necessarily those of the funding Ministry. The work was carried out by T J Chesher, I C Meadowcroft and Dr H M Wallace and the project was managed by Dr H N Southgate.

Prepared by T J Chesher (name) Project Engineer (Job title)

Approved by H N Southgate Project Manager

Date 5 May 1993

Summary

PISCES

A Morphodynamic Coastal Area Model
First Annual Report

T J Chesher
H M Wallace
I C Meadowcroft
H N Southgate

Report SR 337
April 1993

This report describes work carried out during year one of a three year research study funded by MAFF, to develop an integrated morphodynamic coastal area numerical model. The model is designed primarily to investigate the response of a particular coastal system to short term events (up to a spring-neap cycle) by simulating the relevant hydrodynamics, sediment transport and resulting sea bed level changes.

In this first year the main emphasis has been on integrating existing wave, tidal current and sediment transport models, together with a new morphodynamic model, into one overall model.

Testing has been carried out on a number of idealised test cases, with increasing complexity, and results to date indicate that where the natural behaviour of the particular test case is understood, the model reproduces the main features accurately. Where the natural behaviour is not documented, due to lack of data, or because the test case has been schematised it is shown that the model behaves in a realistic manner. Further development and application of the model will help provide a better understanding of complex coastal morphological systems.

This report is unrestricted and contains the outcome of original research. It is intended primarily for numerical modellers in civil engineering hydraulics. For further information regarding this study please contact Dr H N Southgate in the Marine Sediments Group.

List of symbols

A	coefficient in sand transport formula
B	wave stirring coefficient in sand transport formula
C	seabed celerity
C_D	drag coefficient
C_x	seabed celerity in x direction
C_y	seabed celerity in y direction
c_0	seabed celerity along a streamline
c_1	seabed celerity normal to a streamline
D_{50}	median grain diameter
D_*	non-dimensional grain diameter
d	water depth
g	gravitational acceleration
h	seabed level relative to model datum
hu	seabed level on model u-face relative to model datum
hv	seabed level on model v-face relative to model datum
n	exponent in sand transport formula
p	bed porosity
Q	fluid flux
q_b	bedload sediment flux
q_s	suspended load sediment flux
q_t	total load sediment flux
q_{t+}	wave-enhanced total load sediment flux
q_{t+g}	wave-enhanced total load sediment flux with slope effect
q_x	sediment flux in x direction
q_y	sediment flux in y direction
r	deposition rate
s	streamwise coordinate
U	streamwise velocity
U_{cr}	threshold speed for sediment motion
u	current velocity in x direction
v	current velocity in y direction
z	free surface elevation relative to model datum
α	angle of spreading of point source relative to streamline
β	bed slope coefficient in sand transport formula
ΔT_m	morphodynamic timestep
ν	kinematic viscosity of water
ρ	water density
ρ_s	sediment density
σ	sediment specific density
τ_{bx}	bed shear stress in x direction
τ_{by}	bed shear stress in y direction
τ_{wx}	wave breaking stress in x direction
τ_{wy}	wave breaking stress in y direction

Contents

Contents continued

Figures

Contents *continued*

Contents *continued*

1 Introduction

This report describes the development of a fully interactive numerical model of the distribution of waves and currents, the resulting sediment transport, and the response of the coastline and coastal bathymetry, in complex coastal areas. The model is based on existing models at HR Wallingford (HR) for waves and currents separately, complemented by our recent advances in the understanding of sediment transport in such conditions. The model will be capable of tackling the response of a complex coastal area both to engineering works and to natural changes such as rising sea level.

The model development work was commissioned by the Ministry of Agriculture, Fisheries and Food to cover a period of three years starting in January 1992. The studies of the test cases of river outflow and semicircular bay were funded by the Commission of the European Communities Directorate General for Science, Research and Development as part of the G6M Coastal Morphodynamics research programme.

This report covers the initial development of the model undertaken during the first year. The report is structured as follows. In Chapter 2 the background to the development of the coastal area model is discussed. Chapter 3 contains the formulation of the model including the theory behind each individual module and describes any amendments or enhancements. In Chapter 4 the model is applied to a number of test cases and the performance of each aspect of the model is discussed. Finally, in Chapter 5 a number of areas for future development of the model are presented.

2 Background

It was recognised some years ago that many of the coastal problems on which HR has been asked to advise concerning the movement of sediment would be best undertaken with a numerical model capable of simulating the many interacting physical processes involved in areas with complex topography. Such a model must simulate: the wave distribution at each tidal level; the tidal, wind-induced, and wave-induced currents; the various interactions between the waves and the currents; the wave-enhanced sediment transport; and the morphodynamic response of the sea-bed. At the time it was felt that there were too many unknown factors to be able to tackle such a comprehensive model straight away. As a first step, attention was focused on the development of a one-dimensional coastal profile model which could be applied to straight or mildly curved coasts. Many of the modelling problems could be solved on this simpler, Nearshore Profile Model (now called COSMOS, see Southgate 1989, Southgate and Nairn, 1993, Nairn and Southgate 1993), and the model is also of considerable practical value in its own right.

However there are many coastal areas which are not amenable to COSMOS because their topography is too complex: such areas include irregular coastlines, river mouths, harbours, headlands and bays, and offshore sandbanks. Here the area must be modelled fully two-dimensionally.

Having gained experience with COSMOS, and through research into the physical processes a better understanding of the problems involved has been achieved. The development of a full coastal area model would greatly strengthen the ability to predict possible deleterious effects of proposed engineering works, as well as giving an indication of the capacity of the coastal zone to protect itself against rising sea level and increasing wave climate. Furthermore, HR is involved in the EC-funded MAST Coastal Morphodynamics collaborative research programme, which will enable the pursuit of research avenues complementary to the development of the coastal area model, as well as giving access to the experience of researchers from many of the leading European hydraulics institutes who have been striving to develop similar models.

The aim of this particular study is to develop an integrated, fully interactive coastal morphodynamic model for use primarily to investigate the response to short-term (usually storm) events. It is also envisaged that the model will be developed further to study long-term morphological processes. On the spatial scale, the model is intended for regions of coastline from tens of metres to tens of kilometres. Initial plans for the development of the model, including the basis for each module and their integration, were described in an interim report (Southgate, 1991).

3 Formulation of the integrated model, PISCES

The coastal area model is based on existing flow, wave and sediment transport models at HR which have been extensively applied to a variety of coastal applications. Each of these models has been under continual development over a number of years to incorporate the latest theories, the most appropriate parameter settings based on up-to-date data, and the most efficient numerical methods. By these means the existing models provide a sound basis for the development of an integrated coastal area model.

The main tasks for this first stage of the study comprise the development of a morphological update module, linking and interfacing routines between the modules, and a framework for the overall model to handle the data input and output and timestepping information. The new model is given the name PISCES.

3.1 Overall model framework

The framework for PISCES has been developed on the architecture of the HR TIDEWAY modelling suite, an integrated package designed for tidal current modelling and tidal process modelling (e.g. sand, heat, and pollutant transport). By this means the setting up of model geometries, the derivation of the required boundary conditions, output of the model results and subsequent post-processing can utilise existing, well-established routines, with the minimum of effort. A flow diagram describing the main model structure and links between the modules is presented in Figure 1. This design also means that each module can be run as a stand-alone sub-model; for example, a wave propagation analysis for a specified model area can be carried out without the need to consider the other aspects of the morphodynamic modelling system.

The wave module was developed separately from the TIDEWAY format and therefore an interface was required to link automatically the current and wave modules. The sediment transport module, and morphodynamic update module

were both developed on the TIDEWAY format. The overall package is 2D in plan, based on regular gridded geometry, and for each module the numerical solution is obtained by finite difference methods.

Output from the model is in the form of data files referring to each particular element of the model, comprising wave, current, and sediment transport fields, and updated bathymetry. The morphodynamic timestepping information is also stored as a means of assessing the development in time of the seabed bathymetry.

Presentation of model results was greatly facilitated by developing PISCES on the TIDEWAY framework. A range of post-processing programmes are available to view model output, including contour and vector plots, time-series at specific locations and cross-sectional histograms. Colour animations have also been developed and this medium provides a means of displaying results in an attractive presentational manner, as well as being useful at the development stage in providing a clear indication of the sequence of morphodynamic changes.

3.2 Wave transformation module

The wave module determines the transformation of surface waves incorporating the combined effects of refraction and diffraction, and dissipation by bottom friction and breaking. Random wave spectra, current refraction effects, and wind growth can be included at later stages. Further details of this model are given in Southgate and Goldberg (1989) and a summary of the basic processes is presented in Appendix 1.

The wave module is based on steady-state conditions, and the normal mode of operation is to run for a specific stage of the tide at a particular plane water level. This module was amended for PISCES by inclusion of the water elevation field from the current module. This factor becomes important in shallow coastal areas where wave setup and tidal pressure setup become significant, and the water surface is no longer level. This amendment to the module results in a more accurate representation of the wave-induced current-driving forces.

3.3 Interface between the wave module and the current module

Because the wave module was developed according to a separate grid configuration to that employed in the remainder of PISCES, an interface to dynamically link the two was required. This system has the advantage that the wave and current/sand transport modules can work on grids of different sizes, and alignments. An added advantage is that it is not always the case that high definition of the current field is required at the same places as the wave field. This is a much more efficient and flexible means of developing the integrated model than by reconfiguring and revalidating either the existing current or wave module.

3.4 Current module

The current module is based on the depth-integrated TIDEFLOW-2D package from the HR TIDEWAY suite. The module is formulated on the well-established depth-averaged shallow water equations defining the conservation of mass and momentum of water. Details of the basic flow modelling package including the effects of waves are given in Appendix 2. Development of the current module was based on a previous study where current-driving wave forces had been included (HR Wallingford, 1991). In this study the model had been developed on HR's AMT DAP (Distributed Array Processor), using an explicit finite difference method, and it seemed prudent to take advantage of these advances for the development of PISCES.

3.4.1 Adjustment to the boundary values for wave effects

In previous studies (see for example HR Wallingford, 1991) adjustment of the boundary values to account for the effects of waves was not considered, resulting in spurious flow patterns that in some cases could affect the solution well into the model area. For PISCES it was necessary to determine methods to reduce or eliminate the errors associated with this deficiency. Two approaches were identified; the first solution involved a nested grid system, whereby the required model area forms part of a larger model. The combined waves+currents field is calculated over the larger model (which will contain the errors described above, though much further away), and the flows in the vicinity of the required sub-model are therefore more accurately determined.

The second approach involves an estimation of the wave-related fields at the boundaries, based on an assumption of longshore uniformity and negligible cross-shore current velocity. By definition, therefore, it is only strictly applicable to model boundaries in straight stretches of coastline (and bathymetry). Correction for the wave setup is outlined in Southgate, Goldberg and Cooper (1989), and for the more general case of wave setup and wave-driven longshore currents by Roelvink (1992). The details of this approach regarding the current module are summarised below.

Consider the equation for continuity of momentum for both components of the velocity field (ignoring viscous and Coriolis effects):

$$\frac{\partial u}{\partial t} + u\frac{\partial u}{\partial x} + v\frac{\partial u}{\partial y} = -g\frac{\partial z}{\partial x} - \frac{\tau_{bx}}{\rho d} + \frac{\tau_{wx}}{\rho d} \qquad (1)$$

$$\frac{\partial v}{\partial t} + u\frac{\partial v}{\partial x} + v\frac{\partial v}{\partial y} = -g\frac{\partial z}{\partial y} - \frac{\tau_{by}}{\rho d} + \frac{\tau_{wy}}{\rho d} \qquad (2)$$

where	u,v	are the velocity components in the x-,y- direction (m/s)
-	g	is the acceleration due to gravity (m/s^2)
-	z	is the free-surface elevation (m)
-	τ_{bx}, τ_{by}	are the bed shear stress components (N/m^2)
-	τ_{wx}, τ_{wy}	are the driving forces due to waves (N/m^2)
-	ρ	is the water density (kg/m^3)
-	d	is the water depth (m)

Consider an anti-clockwise coordinate system with x-axis normal to the coast. The assumption of steady flow, longshore uniformity and negligible cross-shore mean flow reduces (1) and (2) to:

$$0 = -g\frac{\partial z}{\partial x} + \frac{\tau_{wx}}{\rho d} \tag{3}$$

$$0 = -g\frac{\partial z}{\partial y} - \frac{\tau_{by}}{\rho d} + \frac{\tau_{wy}}{\rho d} \tag{4}$$

which can be solved to define the longshore wave driven current (according to the friction law relating the bed shear stress to the velocity), and the cross-shore mean water level setup z (by assuming zero setup offshore).

This method was implemented for the simulation of a river outflow into a coastal zone, described in Chapter 4.

3.5 Sediment transport module

Deterministic sediment transport numerical models usually fall into two main categories, distinguished by the degree of complexity involved in the calculation of the sediment flux. The first and simplest case is the potential transport model, whereby the sediment flux is directly related to the power of the flow. This relation can be expressed either by an empirically derived formula, such as that determined by van Rijn (1984), or by an energetics based approach as first described by Bagnold (1966).

The second and more elaborate transport model uses a more dynamic approach, and involves the solution of a continuity equation for the mass of sand in suspension. Examples of such models are described in Galappatti and Vreugdenhil (1985). The interaction between the sediment transport and the governing flow parameters is usually expressed in a similar manner to that described for the potential models, i.e. either empirically or by an energetics based argument, but include lag functions to allow for the reaction time of the sand. By this means hysteresis effects can be simulated (see for example Wild (1988)). Dynamic models have the compensating disadvantage in that they are usually more computationally expensive because firstly they involve more elaborate code, and secondly there is an inherent timestepping restraint imposed by the solution of the continuity equation.

Initial plans for PISCES (Southgate 1991) favoured the development of a potential sediment transport module, with the proviso that the HR SANDFLOW - 2D dynamic model (incorporating quasi 3D effects) could be incorporated at a later stage. This plan was adopted and two alternative potential sand transport routines were developed into the sand transport module; an energetics based routine after Bailard (1981) and Stive (1986), and an empirically based routine after van Rijn (1984) adapted for wave effects using the method of Grass (1981), as follows:

The van Rijn formula for currents only is:

$$q_b = 0.005\ Ud \left(\frac{U - U_{cr}}{[(\sigma-1)gD_{50}]^{0.5}} \right)^{2.4} \left(\frac{D_{50}}{d} \right)^{1.2} \quad (5)$$

$$q_s = 0.012\ UD_{50} \left(\frac{U - U_{cr}}{[(\sigma-1)gD_{50}]^{0.5}} \right)^{2.4} D_*^{-0.6} \quad (6)$$

where q_b, q_s are the bedload, suspended load sediment fluxes ($m^3/m/s$)
- D_{50} is the median grain diameter (m)
- σ is the sediment specific density = ρ_s/ρ
- ρ_s is the sediment density
- U_{cr} is the threshold speed (m/s)

$D_* = D_{50} \left[\frac{(\sigma-1)g}{\nu^2} \right]^{1/3}$ is a non-dimensional grain diameter (7)

- ν is the kinematic viscosity of water (m^2/s)
- U is the streamwise velocity (m/s)

These formulae for currents only are written in total load flux form as:

$$q_t = AU(U - U_{cr})^{n-1} \quad (8)$$

where A is constant for a particular grain size, but varies with water depth
- n is 3.4

By appealing to the method of Grass, the wave enhanced sediment transport formula, including a threshold velocity, is defined as suggested by Soulsby (private communication) by:

$$q_{t+} = AU[(U^2 + BW^2)^{0.5} - U_{cr}]^{n-1} \quad (9)$$

where $B = 0.08/C_D$
- W is the r.m.s. wave orbital velocity (m/s)
- C_D is the drag coefficient

Equation 9 is modified to include the effect of bed slope according to Struiksma and Crosato (1989) to give:

$$q_{t+g} = q_{t+} \left(1 - \beta \frac{\partial h}{\partial s} \right) \quad (10)$$

where s is the streamwise coordinate
- β is a constant of order 1
- h is the bed level relative to a fixed model datum (m)

For convenience and speed of operation the module was developed to work on the HR DAP parallel processor.

3.6 Morphodynamic update module

The change in bed level is determined according to the continuity equation:

$$(1-p)\frac{\partial h}{\partial t} - \frac{\partial q_x}{\partial x} - \frac{\partial q_y}{\partial y} = 0 \qquad (11)$$

where q_x is the sediment transport rate in the x-direction ($m^3/m/s$)
- q_y is the sediment transport rate in the y-direction ($m^3/m/s$)
- p is the porosity of the bed

Equation 11 states that the change in bed level in an elemental volume is related to the divergence of the sediment flux field. The staggered mesh in PISCES lends itself to a centred scheme whereby the elemental volume is the cell size, and q_x, q_y are the sediment fluxes through the east and south cell faces respectively (Figure 2). A space-centred solution to Equation 11 gives the change in bed level in the centre of the cell, and an interpolation routine is required to calculate the new bed levels at the cell sides, defined as hu for the east face and hv for the south face.

According to Equation 11 the deposition rate, r, is given by:

$$r = -\frac{1}{(1-p)}\left(\frac{\partial q_x}{\partial x} + \frac{\partial q_y}{\partial y}\right) \qquad (12)$$

In this module at each grid cell, r is calculated by:

$$r_{ij} = \frac{1}{(1-p)}\left[\frac{(q_x)_{i-1,j} - (q_x)_{ij}}{\Delta x} + \frac{(q_y)_{i,j} - (q_y)_{i,j-1}}{\Delta y}\right] \qquad (13)$$

Having defined the deposition rate, the bed deposits Δh_{ij} representing accretion or erosion in each model cell are calculated according to a variety of schemes described in section 3.6.2 below.

3.6.1 The morphodynamic timestep

Earlier tests with morphological models (see for example Chesher, 1992) identified the concept of a limiting morphodynamic timestep associated with the calculation of the bed level changes. This aspect of the bed update scheme is central to PISCES as it effectively defines the timestepping period of the main loop as described in Figure 1. The technique involves a calculation of the celerity of the bed over the entire model domain, and selection of the maximum morphological timestep consistent with a stable solution of the explicit formulation of the bed update equation.

Equation 11 is rewritten as:

$$\frac{\partial h}{\partial t} - C_x\frac{\partial h}{\partial x} - C_y\frac{\partial h}{\partial y} = 0 \qquad (14)$$

where

$$C_x = \frac{\frac{1}{(1-p)}\frac{\partial q_x}{\partial x}}{\frac{\partial h}{\partial x}} = \frac{1}{(1-p)}\frac{\partial q_x}{\partial h} \qquad (15)$$

$$C_y = \frac{\frac{1}{(1-p)}\frac{\partial q_y}{\partial y}}{\frac{\partial h}{\partial y}} = \frac{1}{(1-p)}\frac{\partial q_y}{\partial h} \qquad (16)$$

Equations 15 and 16 define the bed celerities in the x and y directions respectively.

If the sediment transport relation follows a simple power law, as in the empirically based option in PISCES, these celerities can be estimated accordingly,

$$q_t = A.U^n = A.\left(\frac{Q}{h}\right)^n \quad \Rightarrow \quad \frac{\partial q_t}{\partial h} = -\frac{nq_t}{h} \qquad (17)$$

where Q is the fluid flux along a streamline. A simple analysis indicates that an assumption behind this relationship is a rigid lid on the water surface. For most applications of PISCES the water level is not expected to be strongly affected by the bed level changes and therefore the assumption appears valid. Furthermore, initial tests have indicated that this criterion has proved accurate in determining the optimum morphodynamic timestep.

For an explicit solution to Equation 14 there is the familiar CFL stability criterion in two dimensions,

$$2(C_x^2 + C_y^2)\left(\frac{\Delta t}{\Delta x}\right)^2 \leq 1 \qquad (18)$$

(assuming $\Delta x = \Delta y$).
which yields the morphodynamic timestep ΔT_m,

$$\Delta T_m \leq \frac{\Delta x}{\sqrt{2\,(C_x^2 + C_y^2)}} \qquad (19)$$

3.6.2 Bed update schemes

(a) First order upstream scheme
An alternative upstream scheme was devised using the following methodology:

If $(q_x)_{i,j} > 0$, $\Delta hu_{i,j} = \Delta h_{i,j}$
- $(q_x)_{i,j} \leq 0$, $\Delta hu_{i,j} = \Delta h_{i+1,j}$

If $(q_y)_{i,j} < 0$, $\Delta hv_{i,j} = \Delta h_{i,j}$
- $(q_y)_{i,j} \geq 0$, $\Delta hv_{i,j} = \Delta h_{i,j-1}$

In terms of fluxes, this scheme on the u-face for positive flux gives:

If $(q_x)_{i,j} > 0$, $\Delta hu_{i,j} = -\Delta T_m . r_{ij}$

$$- \qquad = -\frac{\Delta T_m}{(1-p)}\left[\frac{(q_x)_{i-1,j} - (q_x)_{i,j}}{\Delta x} + \frac{(q_y)_{i,j} - (q_y)_{i,j+1}}{\Delta y}\right] \qquad (20)$$

and is equivalent to assigning the cell u-depth change to the upstream central depth change. A simple analysis of this scheme indicates that it is non-conservative for diverging or converging flow conditions where the fluxes

change direction, which makes it unreliable for all except known unidirectional flow cases. Furthermore it is only accurate to first order.

A stability analysis yields the requirement:

$$\Delta T_m \leq \frac{\Delta x}{\sqrt{2(C_x^2 + C_y^2)}} \tag{21}$$

(assuming $\Delta x = \Delta y$)

(b) First order centred scheme

In this case the bed deposit is simply the product of the deposition rate and the morphodynamic timestep, ΔT_m:

$$\Delta h_{i,j} = -\Delta T_m \, r_{ij} \tag{22}$$

Initial tests with this scheme using a simple model indicated it to be unconditionally unstable, although the interpolation scheme in PISCES may provide sufficient smoothing to stabilise the bed.

Physical smoothing in the form of the slope term in the sand transport relation may also be sufficient to maintain stability in some cases. However, due to its inherent lack of robustness this scheme was not adopted for any test cases, but the inclusion of second order terms yields the conditionally stable Lax Wendroff scheme described in the next section.

(c) Second order Lax Wendroff scheme

The centred difference scheme described above can be stabilised by inclusion of second order terms. Consider the Taylor Expansion of the bed deposits:

$$\Delta h_{i,j} = \Delta t \left(\frac{\partial h}{\partial t}\right)_{i,j} + \frac{\Delta t^2}{2} \frac{\partial}{\partial t}\left(\frac{\partial h}{\partial t}\right)_{i,j} + \cdots \tag{23}$$

Expanding the second term of the rhs and substituting with equations 11, 15 and 16:

$$\frac{\partial}{\partial t}\left(\frac{\partial h}{\partial t}\right) = \frac{\partial}{\partial t}\left(\frac{1}{(1-p)}\left(\frac{\partial q_x}{\partial x} + \frac{\partial q_y}{\partial y}\right)\right) = \frac{\partial}{\partial x}\left(\frac{1}{(1-p)}\frac{\partial q_x}{\partial t}\right) + \frac{\partial}{\partial y}\left(\frac{1}{(1-p)}\frac{\partial q_y}{\partial t}\right)$$

$$= \frac{\partial}{\partial x}\left(\frac{1}{(1-p)}\frac{\partial q_x}{\partial h}\cdot\frac{\partial h}{\partial t}\right) + \frac{\partial}{\partial y}\left(\frac{1}{(1-p)}\frac{\partial q_y}{\partial h}\cdot\frac{\partial h}{\partial t}\right)$$

$$= \frac{\partial}{\partial x}\left[C_x\left(\frac{1}{(1-p)}\left(\frac{\partial q_x}{\partial x} + \frac{\partial q_y}{\partial y}\right)\right)\right] + \frac{\partial}{\partial y}\left[C_y\left(\frac{1}{(1-p)}\left(\frac{\partial q_x}{\partial x} + \frac{\partial q_y}{\partial y}\right)\right)\right] \tag{24}$$

Yielding:

$$\Delta h_{i,j} = -\Delta T_m r_{i,j} - \frac{\Delta T_m^2}{2}\left[\frac{\{(C_x . r)_{i+1,j} - (C_x . r)_{i-1,j}\}}{2\Delta x} + \frac{\{(C_y . r)_{i,j+1} - (C_y . r)_{i,j-1}\}}{2\Delta y}\right] \tag{25}$$

A stability analysis yields the requirement:

$$\Delta T_m \leq \frac{\Delta x}{\sqrt{2(C_x^2 + C_y^2)}} \tag{26}$$

(assuming $\Delta x = \Delta y$)

(d) Alternative Lax Wendroff scheme

As an alternative to the Lax Wendroff scheme above, the following analysis was carried out:

Consider Equation 11 rewritten in the form:

$$\frac{\partial h}{\partial t} - C\left(\left|\frac{\partial h}{\partial x}\right| + \left|\frac{\partial h}{\partial y}\right|\right) = 0 \tag{27}$$

where

$$C = \frac{\frac{1}{(1-p)}\left(\frac{\partial q_x}{\partial x} + \frac{\partial q_y}{\partial y}\right)}{\left|\frac{\partial h}{\partial x}\right| + \left|\frac{\partial h}{\partial y}\right|} \tag{28}$$

From Taylor's expansion:

$$\Delta h_{i,j} = \Delta t.C_{i,j}\left[\left|\frac{\partial h}{\partial x}\right| + \left|\frac{\partial h}{\partial y}\right|\right]_{i,j} + \frac{\Delta t^2}{2}\frac{\partial}{\partial t}\left[C\left|\frac{\partial h}{\partial x}\right| + C\left|\frac{\partial h}{\partial y}\right|\right]_{i,j}$$

$$= \Delta t.C_{i,j}\left[\left|\frac{\partial h}{\partial x}\right| + \left|\frac{\partial h}{\partial y}\right|\right]_{i,j} + \frac{\Delta t^2}{2}\left[\frac{\partial C}{\partial t}\left(\left|\frac{\partial h}{\partial x}\right| + \left|\frac{\partial h}{\partial y}\right|\right) + C\frac{\partial}{\partial t}\left(\left|\frac{\partial h}{\partial x}\right| + \left|\frac{\partial h}{\partial y}\right|\right)\right]_{i,j}$$

$$\approx \Delta t.\left[\frac{1}{(1-p)}\left(\frac{\partial q_x}{\partial x} + \frac{\partial q_y}{\partial y}\right)\right]_{i,j} + \frac{\Delta t^2}{2}C_{i,j}\left[\pm\frac{\partial}{\partial x}\left(\frac{\partial h}{\partial t}\right) \pm \frac{\partial}{\partial y}\left(\frac{\partial h}{\partial t}\right)\right]_{i,j}$$

$$= -\Delta t.\ r_{i,j} + \frac{\Delta t^2}{2}C_{i,j}\left[\pm\frac{\partial}{\partial x}\left[\frac{1}{(1-p)}\left(\frac{\partial q_x}{\partial x} + \frac{\partial q_y}{\partial y}\right)\right] \pm \frac{\partial}{\partial y}\left[\frac{1}{(1-p)}\left(\frac{\partial q_x}{\partial x} + \frac{\partial q_y}{\partial y}\right)\right]\right]_{i,j}$$

$$\Rightarrow \Delta h_{i,j} \approx -\Delta t.r_{i,j} - \frac{\Delta t^2}{2}C_{i,j}\left[\pm\frac{\partial r}{\partial x} \pm \frac{\partial r}{\partial y}\right]_{i,j} \tag{29}$$

Yielding:

$$\Delta h_{i,j} \approx -\Delta T_m r_{i,j} - \frac{\Delta T_m^2}{2}C_{i,j}\left[\pm\frac{(r_{i+1,j} - r_{i-1,j})}{2\Delta x} \pm \frac{(r_{i,j+1} - r_{i,j-1})}{2\Delta y}\right] \tag{30}$$

The assumption behind this method is that:

$$\frac{\partial C}{\partial t}\left(\left|\frac{\partial h}{\partial x}\right| + \left|\frac{\partial h}{\partial y}\right|\right) \ll C\frac{\partial}{\partial t}\left(\left|\frac{\partial h}{\partial x}\right| + \left|\frac{\partial h}{\partial y}\right|\right) \tag{31}$$

The selection of the positive and negative options depends on the protocol:

$$\text{Select +ve if } \frac{\partial h}{\partial x} > 0, \text{ -ve if } \frac{\partial h}{\partial x} < 0, \text{ and similarly for } \frac{\partial h}{\partial y} \tag{32}$$

A stability analysis yields the following requirement:

$$\Delta T_m \leq \frac{\sqrt{2\Delta x^2}}{C} \tag{33}$$

(assuming $\Delta x = \Delta y$)

The advantage of this method is that it does not rely on any particular expression for q_x and q_y. However, it does require Equation 31 to be satisfied.

3.6.3 Interpolation onto cell faces

For all except the upstream scheme a 2-D interpolation procedure is used to transfer the bed level changes calculated at the cell centres to the respective cell faces. This is defined as follows (see also Figure 2):

Treating x and y directions equally a change in cell u-depth (east cell side) by an amount Δhu_{ij} is given by:

$$\begin{aligned}\Delta hu_{i,j} = \tfrac{1}{4}\Big[\Delta h_{i,j} + \Delta h_{i+1,j} + \tfrac{1}{4}\{\Delta h_{i,j} + \Delta h_{i+1,j} + \Delta h_{i,j+1} + \Delta h_{i+,j+1}\} \\ + \tfrac{1}{4}\{\Delta h_{i,j} + \Delta h_{i+1,j} + \Delta h_{i,j-1} + \Delta h_{i+1,j-1}\}\Big] \\ = \tfrac{1}{4}\Big[\tfrac{3}{2}(\Delta h_{i,j} + \Delta h_{i+1,j}) + \tfrac{1}{4}(\Delta h_{i,j+1} + \Delta h_{i-1,j+1} + \Delta h_{i,j-1} + \Delta h_{i-1,j-1})\Big]\end{aligned} \tag{34}$$

and equivalently for the v-depth (south cell side):

$$\Delta hv_{ij} = \tfrac{1}{4}\Big[\tfrac{3}{2}(\Delta h_{ij} + \Delta h_{i,j-1}) + \tfrac{1}{4}(\Delta h_{i+1,j} + \Delta h_{i+1,j-1} + \Delta h_{i-1,j-1} + \Delta h_{i-1,j})\Big] \tag{35}$$

At the model boundaries estimates to the fluxes need to be implemented in order to avoid inaccuracies due to this interpolation procedure. These errors were minimised by resetting the flux at the boundary to its most appropriate neighbour.

3.6.4 Timescales

There are three important timescales related to the morphodynamic update procedure, which are all associated with the concept of mapping a continuum, in both time and space, onto a discretised domain. Considering time-invariant driving conditions only, these are summarised as follows:

(1) The maximum timestep allowed for stability of the numerical morphodynamic update scheme, ΔT_{m1}. This can be any number between zero and infinity, depending on the scheme. For an unconditionally stable implicit scheme there is no theoretical limit to ΔT_{m1}, to maintain stability, although there is the compensating disadvantage of loss of accuracy at large timesteps. For an explicit scheme there is the familiar CFL condition to maintain stability, which effectively relates ΔT_{m1} to the speed of propagation of features on the bed.

(2) The timescale over which the changes in depth affect the flow to first order, ΔT_{m2}. Bearing in mind that in the model the bed is effectively static over each ΔT_{m1}, whereas in the physical situation the bed is continually changing, errors are introduced since the flows will change over this timescale. This is especially the case when the bed update scheme allows a relatively long ΔT_{m1}. For this case two scenarios exist: the

changes in flow may be to first order only, whereby the fluid *speeds* alter but the same fluid flux is maintained (corresponding to ΔT_{m2}); or the changes may be to second and higher orders, whereby the fluid *velocities* are altered to an extent that requires a full recalculation of the hydrodynamics (corresponding to ΔT_{m3}, see below). Where the flows are affected to first order only over a timescale ΔT_{m2} for time-invariant driving conditions, a continuity correction is sufficient to recalculate the sediment fluxes without re-running the flow model.

(3) The timescale over which the changes in depth affect the flow to second and higher orders, ΔT_{m3}. At this timescale a full recalculation of the hydrodynamics is required. This timescale is difficult to predict, but tests by other partners in the MAST G6M research programme (personal communication) suggest it is many (~50) times ΔT_{m2} for the river outflow test case described in Chapter 4. In this case the continuity correction for updating the flows saves a lot of computing effort.

However, there are other limits on how long the bed changes can be extrapolated. For example, the flow must be recalculated at least on the timescale of the hydrodynamic forcing, ie the duration of a wave condition or tide. Another timescale is that required for the flow to reach a steady state, for steady driving forces, i.e. the time it takes for transients in the model to be removed. If the flow is still reacting to a change in the forcing or bed levels it may not be reasonable to assume velocities are constant throughout ΔT_{m2} or ΔT_{m3}.

3.7 Dynamic linking shell and mode of operation of PISCES

Having developed each particular module and interface of PISCES, it remained to link them together in one overall shell in order to automate the whole model. Using the UNIX environment a Bourne shell was written to link the modules in the manner presented in Figure 1. To run the model the user specifies the start and stop times of the required simulation, and this information, together with the elapsed run time is stored in temporary files accessible by all the necessary modules.

A typical simulation involves the following stages of operation. The procedure begins with the generation of steady, initial flow conditions according to tidal, wave, or wind forces or any combination of these over an immobile bed. These hotstart fields are stored in a master directory as the main starting conditions. All runs of PISCES start from these initial conditions.

From the hotstart field the morphodynamic integration is initiated by specifying the duration of the first morphodynamic timestep, based on experience. Hereafter the morphodynamic timestep consistent with a stable solution of the bed update equation is calculated. The current module is integrated forward in time for the duration of this morphodynamic timestep, whereafter the sediment transport is calculated according to the average flow conditions over this timestep. (For test cases with time invariant driving conditions the ultimate flow field at the end of the morphodynamic timestep could be used, provided sufficient time has elapsed to allow transients to be removed from the model). The morphodynamic update module is then called to recalculate the bed level based on the sediment transport fluxes and the morphodynamic timestep. The new morphodynamic timestep is then recalculated according to the latest

conditions, and the elapsed simulation time is updated. This loop is continued until the total simulation time is reached.

For the wave module the elapsed time is needed since the wave parameters may change during a simulation, whereas for the current module both the elapsed time and the morphodynamic timestep are required, and for the morphodynamic module only the timestep is required.

4 Application of the model

Development of the model was undertaken by testing various isolated schemes of increasing complexity, where the true behaviour of the system is either well understood or has been studied in detail. As the flow and wave modules have been extensively employed in other studies these tests concentrated on mobile bed applications. Initial tests comprised (a) the steady-state development of a plane channel under unidirectional flow without waves, (b) 1-D and 2-D development of a sand dune in a channel under unidirectional flow without waves, and (c) more complex coastal applications of a wave driven current field in the vicinity of a river mouth, and wave driven currents in a semicircular bay.

As a result of collaboration with other European institutes under the MAST G6-M programme, an intercomparison of model results for the river outflow and the semicircular bay test cases was undertaken.

4.1 Free surface flow over a flat bed in a channel

4.1.1 Introduction

The first test of PISCES comprised the simple case of free-surface flow over a plane, level sandy bed. In the case of a rigid bed, steady, subcritical flow conditions give rise to a sloping free-surface with the depth gradually decreasing downstream. This results in increased velocities and corresponding increased sediment transporting potential in the downstream direction. These flow conditions over a mobile bed should result in removal of sand in the downstream direction until uniform depth, and hence velocity distribution is obtained.

4.1.2 Model layout

The model area represented a channel 1.0km long, 10.0m (unit cell) wide and a uniform 10.0m deep with a regular square grid of size 10.0m. Boundary conditions comprised an upstream discharge boundary with an equivalent input velocity (depth-averaged) of 1.0m/s and input depth 10.0m, and a specified downstream elevation boundary, which was in this case set to a constant 0.0m (relative to initial mean water level). The roughness length and coefficient of eddy viscosity were set to 0.05m and 1.0m^2/s respectively, and the bed was composed of 0.2mm sand.

4.1.3 Generation of the initial conditions

Steady initial flow conditions over an immobile bed were generated after about 0.5 hours of simulation time. The horizontal distribution of the bed, the free-surface and the velocity field are presented in Figure 3 indicating a uniformly sloping free-surface, and corresponding velocity distribution that increases linearly in the downstream direction. An assessment of the results files

indicates that the sediment flux field also increases in the downstream direction, as expected.

4.1.4 Mobile bed simulation

Having generated the initial conditions, the full mobile bed simulation was started. The final bed configuration and hydrodynamic fields, shown in Figure 3, indicated that the model was working correctly. Erosion had occurred over the length of the channel to give a bed slope of the same magnitude as the free-surface slope, so that the total water depth was constant. There was therefore no velocity gradient and hence the sediment flux field was uniform, and no further bed level changes took place.

4.2 1-D sand dune in a channel

4.2.1 Introduction and model layout

The channel design described in Section 4.1 was adjusted for the second test case; that of a 1-D sand dune in a channel. The initial bed comprised an initially sinusoidally shaped (in profile) sand dune with peak height 1.0m and base width 140.0m. The flow conditions were as before, viz, input water depth of 10.0m and velocity of 1.0m/s giving input and peak Froude numbers of 0.1 and about 0.12 respectively.

Two tests were carried out; one including the bed slope effect in the sand transport relation, and one with this effect left out. In each case the simulation represented the evolution of a single sand dune on a sandy bed of grain size 0.2mm under steady unidirectional flow. The bed was assigned a roughness length of 0.05m and the coefficient of eddy viscosity was $1.0m^2/s$.

4.2.2 Without bed slope effect

Steady initial flow conditions over an immobile bed were generated after about 0.5 hours of simulation time, after which the mobile bed runs were initiated. The model was run for a period of 150 hours. During this period the updated bathymetry was stored every 10hrs for further postprocessing. Morphodynamic timesteps were of the order of 6hrs. The evolution of the model bathymetry over the 150hr period at 10-hour intervals is presented in Figure 4.The main features to note include a general steepening of the lee side of the dune, and elongation of the upstream side, and maintenance of the initial peak bedform height. An exact analysis of the bed evolution using the method of characteristics indicated that, for the physical conditions simulated, a 'shock' should form after about 130hrs. (Here the term 'shock' is defined as the condition when the horizontal location of the top of the dune coincides with the base of the dune). Clearly, the model does not simulate the shock capture well, but the fact that the model remains stable after the time of expected shock formation indicates that the bed evolution scheme is robust. In reality, the generation of a shock front on a sandwave would be limited by the effect of gravity, which would tend to smooth out bed gradients either by limiting the sediment flux, or by avalanching of the bed once a critical internal angle was reached.

4.2.3 *Including bed slope effect*

The test was repeated including the bed slope effect in the sediment transport relation, all other aspects being identical. The results, presented in Figure 4 show a tendency for the dune to reduce in height and elongate over the simulation period. As one would expect, the bed is generally smoother as the sediment transport gradients are reduced.

4.3 Conical sand dune in a channel

4.3.1 *Introduction and model layout*

Having established that the model was giving sensible results for a 1-D dune in a channel (essentially a problem in one horizontal direction), this test was extended to that of a conical dune in a channel (a problem in two horizontal dimensions). The same parameter settings as before were specified, viz, an initially sinusoidally shaped (in profile) sand dune, but now circular in plan, with peak height 1.0m and base width 60.0m, on a sandy bed of grain size 0.2mm. Unidirectional flow conditions were specified with input water depth of 10.0m and velocity (depth-averaged) of 1.0m/s, roughness length 0.05m and coefficient of eddy viscosity of 1.0m^2/s. The effect of the Coriolis force was neglected, and the effect of the bed gradient was not included in the sand transport relation.

The model covered an area some 600m square with a regular square grid with size 10.0m. The initial bathymetry and initial physical conditions are shown in plan in Figure 5. Boundary conditions comprised an upstream discharge boundary and a specified downstream elevation boundary, in this case set to a constant 0.0m (relative to initial mean water level). No-flow conditions were set on the side boundaries.

4.3.2 *Generation of the initial conditions*

Steady initial flow conditions over an immobile bed were generated after about 1 hour of simulation time. A vector plot of the initial flow field, and a contour plot of the u-velocity distribution are presented in Figures 6 and 7. Occupying only 10% of the total depth, the hill provided little obstruction to the flow field; the streamlines were more or less parallel and the v-velocity component was only of the order of 0.01m/s. The u-velocity increases over the hill by about 5-6%, with the maximum just upstream of the peak of the hill, and viscous forces gave rise to increased velocities on either lateral side of the hill. Also, a small, but significant reduction in speed occurred upstream and downstream of the hill as a result of interaction between the bed and the free-surface. This interaction tended to lower locally the water elevation over the peak of the dune, and likewise raise it both upstream and downstream of the dune.

Based on these steady flows the sediment transport field was calculated, and is presented in vector form in Figure 8. The associated rates of bed level change are shown in Figure 9. As with the flows, the sand flux vectors are more or less parallel, increasing over the hill. Deposition was predicted in the lee, as well as well upstream of the hill, with erosion of the upstream face and further downstream.

4.3.3 *Mobile bed simulation*

Having generated the initial conditions, the full mobile bed simulation was started. The model was run for a period of 100 hours. During this period the updated bathymetry was stored every 2.5hrs for further postprocessing.

Morphodynamic timesteps were of the order of 6hrs, but this was truncated in most instances to the 2.5hr storage interval. The evolution of the model bathymetry over the 100hr period after 25, 50 and 100 hours is presented in Figure 10 and also in isometric projection in Figure 11.

The results from the model indicate a number of complex features associated with the flow in the vicinity of the hill. The main sand hill is advected downstream, in a similar manner to the 1-D dune. However, in this 2-D case the amplitude of the dune is reduced (even without the bed slope effect included) and the bedform also appears to propagate laterally.

The evolution of the main hill is presented in Figure 12. The hill propagates both downstream and laterally at a constant speed, with an apparent point source upstream of the initial disturbance. The main dune expands into a star shape initially, but as the evolution continues the pattern becomes more complex. This star-shaped behaviour was investigated using the method of characteristics and with a numerical model by De Vriend (1987), and also computationally by Duplex and Peltier (1990). In each case this lateral spreading of the dune was identified as a result of interaction between the bed and the pressure field (in this case the free surface). The sediment flux vectors indicate clearly that the behaviour is not as a result of sand being transported laterally.

This spreading out is equivalent to the radial spreading of a surface wave from a point source but in this case there is superimposed on this motion the additional advection of the feature downstream. De Vriend (1987) calculates the angle of spreading of the bed feature, α from the initial location of the point source, relative to the central streamline according to:

$$\tan\alpha = \frac{3T_u\sqrt{3}}{9T_u - 8T_h} \tag{39}$$

where T_u and T_h are the non-dimensional terms given by:

$$T_u = \frac{U}{q_t}\frac{\partial q_t}{\partial U} - 1 \tag{40}$$

$$T_h = \frac{h}{q_t}\frac{\partial q_t}{\partial h} - 1 \tag{41}$$

The celerity of the bed along the streamline, c_0, is given by

$$c_0 = (T_u - T_h)\frac{q_t}{h} \tag{42}$$

and in the lateral direction, c_1, by

$$c_1 = T_u\frac{q_t}{h} \tag{43}$$

For the power law relation for the sand transport given by Equation 8 and used in this simulation, T_u and T_h reduce to :

$$T_u = \frac{U}{(U-U_{cr})}(n-1) \tag{44}$$

$$T_h = -1 \qquad (45)$$

(Here, U is the streamwise velocity, U_{cr} is the critical speed for sediment transport, q_t is the streamwise sediment flux, and h is the bed level, as before).

From the model results the following values were obtained:

- $U = 1.05$ m/s
- $U_{cr} = 0.42$ m/s
- $n = 3.4$
- $q_t = 5.9 \times 10^{-4}$ m^3/m/s (allowing for pores)
- $h = 9.1$ m

which yield theoretical values of:

- $\alpha = 25°$
- $c_0 = 3.3 \times 10^{-4}$ m/s
- $c_1 = 2.5 \times 10^{-4}$ m/s.

From the bedform evolution (Figure 12) the following values were estimated:

- $\alpha \approx 27°$
- $c_0 \approx 2.2 \times 10^{-4}$ m/s
- $c_1 \approx 1.5 \times 10^{-4}$ m/s.

This indicates that the lateral spreading angle is in good agreement whereas in both cases the apparent celerities according to the model are smaller, though of the correct order of magnitude. This discrepancy may be attributed to the spatial averaging which is inherent in the numerical model as a result of the discretisation onto a gridded domain. (The values from the model given above refer to the peak of the bedform, whereas the morphodynamic module calculates "net" erosion or deposition within each grid cell, which is uniform over that particular grid cell).

Other important features associated with this dune advection problem include the generation of at least two more dunes upstream of the main one. These are formed as a result of the interaction between the bed and the free surface elevation as described above. In balance with the elevation field, the flow field exhibits slight deceleration just upstream of the bump and acceleration downstream, and results in the observed areas of accretion and erosion. As one upstream dune is formed it also interacts with the flow field, and in a similar manner gives rise to another dune upstream of this one. In this way a single feature can relatively quickly give rise to a series of disturbances on the bed.

Test cases such as these provide a valuable tool for understanding the fundamental behaviour of relatively simple situations. Furthermore, by the systematic checking of cases where the solution is known, greater confidence in the model is achieved, so that the morphodynamic behaviour of more complex coastal situations can be reliably investigated.

4.4 River outflow into a straight coastline

4.4.1 Introduction

During this first year of development of PISCES, allied research under the EC-funded MAST G6M research programme involving an intercomparison exercise between participating institutes for specified idealised test cases was proposed. This exercise gave an ideal opportunity for further testing of the model, as well as the mutual benefits of the exchange of ideas and methods between the MAST partners.

The test case described here is the simulation of the bathymetric evolution of a coastal area incorporating a river mouth, under the action of large waves, over a four day period. The entire model bed comprised 0.25mm grain size sand.

The 75m wide river discharged a constant volume of 150 cumecs into a steady wave-driven current field. This current field resulted from 2m H_{rms} waves propagating shorewards from an initial direction of 30° to the coast.

As PISCES is developed on a 2-D horizontal flow model, the effects of density variations between the river outflow and the ambient seawater were not simulated in this case.

4.4.2 Model layout

The initial bathymetry represented a uniformly sloping beach at an angle of 2%, from the coastline to a depth of 13.5m. The slightly deeper river channel extended out perpendicularly from the coast. The model covered an area of about 800m seawards and 1600m along the coast. This bathymetry was supplied on a regular 15m grid for all the modules. The model area is shown in plan in Figure 13 and in isometric projection in Figure 14.

For the wave module the offshore boundary had a prescribed wave height and direction with the parameters as given above. For the current module the offshore boundary had a prescribed elevation (which in this case was set to zero relative to still water level). The top (west) boundary also had an elevation boundary with the tidal contribution set to zero, but also included an estimate of the water level setup as described in Section 3.4.1. The bottom (east) boundary had a prescribed discharge boundary according to a calculation of the wave-driven currents, based on the local wave height field, and assuming longshore uniformity, as described in Section 3.4.1. The northern boundary had a no-flow condition except at the river entrance where there was a prescribed discharge boundary based on the river flow conditions given above.

The effect of including the effects of the waves at the model boundaries is highlighted in Figures 15 and 16, which show the steady flow conditions obtained from the model. If no corrections are applied (Figure 15), spurious flows occur at the top elevation boundary because the water level setup is not represented, and at the bottom discharge boundary because the wave driven currents are omitted. By Including these corrections (Figure 16) the flow field in the vicinity of the boundaries is much improved.

4.4.3 *Generation of the initial conditions*

The current model parameters available for adjustment include the bed roughness and the diffusion coefficient. The bed roughness tends to affect overall velocities while the diffusion coefficient affects the lateral shear, and hence the scale of eddy structures. In this simulation the roughness length and coefficient of eddy diffusivity were set to 0.05m and 1.0m^2/s respectively. The effect of the Coriolis force was not simulated.

Initial conditions were generated by running the wave and current modules interactively over an immobile bed. Linking between these two modules was in the form of wave driving forces and wave orbital velocities from the wave module to the current module, and the elevation field (in order to define the total depth) from the current module to the wave module. After a period of about 6hrs simulation time a steady current field had been reached and the sediment transport field was calculated. Initial fields of the wave heights, wave orbital velocities, wave breaking stresses, currents, sediment fluxes and associated rates of bed level change are presented in Figures 17 to 23.

The waves propagated shorewards with slight shoaling to a water depth of about 7m, where they began to break, generating relatively large current-driving forces. Refraction generally changed the wave propagation direction towards the coastline normal.

The wave breaking forces generated a longshore current with a peak in the breaker zone of about 1.0 m/s. Where the river discharge met this wave-driven current field, a complex flow pattern was predicted, resulting in the deviation of the river flow westwards. A gyre was formed on the western side of the river in the shallower water and this gave rise to relatively large easterly currents adjacent to this part of the coast. As a result of the complicated water level setup pattern in the vicinity of the river mouth the flows in the river were fastest on the western side.

The vector plot of the sediment transport field on the initial bathymetry indicated peak longshore fluxes of the order of 4kg/m/s, coinciding with the region of fastest velocities. As the flux field away from the river flow was uniform along the streamlines there was no potential for accretion or erosion in these areas. Around the river mouth the flux field was more spatially variable, resulting in a complex pattern of erosion and deposition. The main response of the model was to predict strong accretion just outside the river mouth, and corresponding erosion within the river due to the local acceleration of the flow. Where the river flow was entrained into the ambient longshore current a pattern of alternating accretion and erosion was predicted. The magnitude of the predicted bed level changes was high, with peak rates of the order of one metre per day.

4.4.4 *Mobile bed simulation*

Having generated steady initial conditions, the full mobile bed calculations were started. The model was run for the simulation period of 4 days. During this period the updated bathymetry was stored every three hours for further postprocessing. When necessary, truncation of the timestep occurred at the end of each three hour period. An example of the calculation of the morphodynamic timestepping over the first 24 hours is presented in Figure 24. Timesteps were initially of the order of 15 minutes, gradually increasing over the 4 day simulation period to about 20 minutes. This increase was not monotonic, however, and the timestep was occasionally reduced by locally

active areas in shallow water, particularly associated with the large scale accretion just offshore and to the west of the river mouth. The evolution of the model bathymetry over the 4 day period at 18 hour intervals and the final bed configuration is presented in Figures 25 and 26.

Results of the simulation indicate the formation of long sandwave-like features that were generated near the river mouth, as a result of spatial variations of sediment flux caused either by the river flow, or due to the deeper water in the river channel. These sandwaves propagated quickly down the coast, almost reaching the end of the model in the 96 hours simulated (equivalent migration rate ~ 8 metres/hour). Closer to the river mouth the river channel was made narrower by rapid accretion on the west side and was diverted to the east. Also, spit-like promontories were formed on either side of the river mouth and were slowly extended offshore. In this way the model exhibits examples of both mobile features (e.g. sandwaves), and static (e.g. spit, delta) type formations.

The updated bathymetry, wave height and flow fields after 4 days are presented in Figures 27 to 31. As expected, the wave height fields reflect the local bathymetry as a result of wave breaking, and as such exhibit a much more complex distribution of wave driving forces than for the initial bathymetry. The flow pattern is also distorted according to the bed, but the main features of the flow associated with the entrainment of the river current by the ambient wave-driven current persists. The updated sediment fluxes and associated rates of bed level changes highlight the disturbance to the bed downstream of the river mouth, whereas upstream of this area the bed is largely undisturbed.

4.4.5 Acceleration of the solution for steady problems.

To run the full 4 day sequence as described above required a real-time duration of the order of 3 days. This was in part due to the flow and sediment transport calculations which required time-sharing of the DAP computer with other users. However, these are by far the most time-consuming modules in cpu time, as well as elapsed time. For these applications based on time-invariant driving forces it was recognised that for a large proportion of the flow simulation the flow conditions modelled were not changing, and the model was simply integrating a constant solution in time. To investigate the speeding up of the simulation a convergence test was devised whereby if the flow conditions at all grid points had not changed within a specified tolerance the solution was assumed to be steady and the flow model was exited. This convergence test was carried out on the three main variables of u- and v-velocity and free-surface elevation at every active model cell and after every (hydrodynamic) timestep.

Two tests were carried out, with tolerances of 0.5% and 5%. The final bed configuration and an assessment of the morphodynamic timestepping for the first 24 hours (for comparison with Figure 24) for the test with a tolerance of 5% are presented in Figures 32 and 33. Elapsed times for the 4 day simulation were of the order of 2 days for the test with 0.5% tolerance, and 24hrs for the test with 5% tolerance, due to the vast reduction in time spent in the current module (Figure 33). This method of accelerating the solution gave rise to a broadly similar bed configuration in both tests, indicating that the method did not affect the solution unduly. Furthermore, it indicates that the sediment transport processes in the simulation are dominated by the large scale advection processes, and that small "errors" in the flow field (due to lack of convergence) were not significant.

4.4.6 *Effect of the bed slope*

The 4 day simulation was repeated after inclusion of the effect of the bed slope in the sediment transport relation, as described in Section 3.5. For this sensitivity test the convergence test acceleration was employed as described above, with a convergence tolerance of 5%. The final bed configuration is presented in Figure 34, and should be compared with that shown in Figure 32 in order to identify the effect of the slope term. As expected, the bed is generally smoother since the bed gradients are reduced due to the higher sediment transports downslope. An animation of the 3 hourly stored bed levels was undertaken, and monochrome stills of the bathymetry are presented in Figure 35. This highlights the large bed level changes in the vicinity of the river mouth and the sandwave features that are shed from this area and propagated downstream.

An intercomparison of these results with those from the other main institutes from the MAST G6-M research programme was carried out (de Vriend et al, 1993). The bed evolution presented here was a lot more dynamic than those of the other participants, which has been largely attributed to the different sediment transport predictions for this wave dominated test case. Such sensitivity highlights the need for a greater understanding of the behaviour of the sediment transport field in coastal systems.

4.4.7 *Alternative bed update scheme*

The 4 day simulation was repeated using the alternative bed update scheme described in Section 3.6.2. This test gave much the same final bed configuration, shown in Figure 36, as that in Figure 34, but the morphodynamic timesteps were significantly longer in this case, resulting in an elapsed-time duration for the simulation of the order of 12 hours. This represents a realistic turn-around time for the test, and provided the results are reliable will enable more thorough testing of other aspects of the morphodynamic model.

4.5 Semicircular bay

4.5.1 *Introduction*

A second intercomparion exercise under the MAST G6M research programme was undertaken for the case of the bathymetric evolution of a coastal area incorporating a small semicircular bay under the action of 0.6m H_{rms} waves over a 36 hour period. The bed comprised 0.2mm grain size sand. Tidal variations were not included.

Physical model tests were carried out on this particular test case layout at EDF-LNH (Péchon, 1985), and results from this study, in the form of net bed level changes were available for comparison with the numerical model results. However, the numerical model tests were carried out at prototype scale.

4.5.2 *Model layout*

The bathymetric data was supplied in digital form on a regular 4m grid. The model covered an area some 280m long and 240m wide, resulting in a model grid comprising 63 cells by 77 cells. The initial bathymetry represented a small bay in a uniformly 3% sloping section of otherwise straight coastline, aligned at an angle to the model grid. The bay incorporated a shallow shelf at a depth of 2.5m before shelving more steeply (bed gradient 9%) offshore to another shelf at a depth of 5.5m. The model area is shown in plan in Figure 37 and in isometric projection in Figure 38.

For the wave module the offshore boundary had a prescribed wave height as given above, in a direction normal to the offshore boundary. (In the physical model tests the offshore boundary was the wave paddle).

For the current module no boundary information was required since the model represented a confined basin without tidal level variation. All sides of the model were no-flow boundaries, representing the sides of the wave basin.

4.5.3 Generation of the initial conditions

The current model parameters available for adjustment include the bed roughness and the diffusion coefficient. The bed roughness tends to affect overall velocities while the diffusion coefficient affects the lateral shear, and hence the scale of eddy structures. In this simulation the roughness length and coefficient of eddy diffusivity were set to 0.05m and 1.0m^2/s respectively. The effect of the Coriolis force was not simulated.

Initial conditions were generated by running the wave and current modules interactively over an immobile bed. Linking between these two modules was in the form of wave driving forces and wave orbital velocities from the wave module to the current module, and the elevation field (in order to define the total depth) from the current module to the wave module. After a period of about 3 hours real time simulation a steady current field had been reached and the sediment transport field was calculated. Initial fields of the wave heights, wave orbital velocities, wave breaking stresses, currents, sediment fluxes and associated rates of bed level change are presented in Figures 39 to 44.

The contour plot of wave heights indicate shoaling due to the relatively steep offshore bed gradient. The orbital velocity field highlights the refraction within the bay, concentrating the wave energy to the sides of the bay. Wave breaking is evident at a depth of about 2m, resulting in quite strong current-driving forces (up to 0.02N/m^2) in the shallow waters.

The resulting current flow patterns exhibit a complicated distribution of longshore currents, gyres and return flow from the offshore side of the basin. The main features include a strong longshore current on the east side of the bay, and a large eddy on the western side of the bay, which drives a north-easterly longshore current adjacent to the coast. From the centre of the bay a strong offshore jet, associated with the eastern side of the eddy, drives a counter-clockwise circulation around the deepest part of the basin.

The sediment fluxes (Fig 43) reflect this flow pattern, and the corresponding initial rates of bed level change (Fig 44) indicate two main areas of activity, associated with the two longshore current streams. As a result of this flux distribution, accretion was predicted at the entrance to either side of the bay, with adjacent areas of erosion away from the bay. Peak sediment fluxes were of the order of 0.4kg/m/s and the peak initial rate of bed level change was of the order of one metre per day.

4.5.4 Mobile bed simulation

Having generated steady initial conditions, the full mobile bed calculations were started. The model was run for the simulation period of 36hrs. Morphodynamic timesteps were initially of the order of 30 minutes, gradually increasing over the 36 hour simulation period to about 45 minutes.

Due to the smaller driving forces the bed was much less dynamic in this simulation compared to the river outflow, with the main changes being confined to the breaker zone. The final bathymetry and hydrodynamic and sediment-related fields are presented in Figures 45 to 50. Of particular interest is the fact that the rates of bed level change are a good deal smaller than the initial rates, indicating that for this particular test the bed would be likely to reach a statically-stable configuration within a fairly short period of time.

Figure 51 shows net bed level changes over the 36 hour simulation period, and physical model results from the EDF-LNH Laboratory are presented in Figure 52 for comparison. The results appear to be in broad agreement, with large scale deposition in the bay and erosion on either side. There is also some evidence of similarity in the structure of the deposition in the bay, where the locations of the greatest deposits and also the smaller two areas of deposition to the west agree rather well. The details of the erosional areas, however, are not so well matched.

5 Future developments

A good deal of progress has been made in this first year of the study, resulting in a fully integrated coastal area morphodynamic model that is capable of simulations of relatively simple test cases and timespans of the order of several days. It is intended that work in the remaining part of the study will concentrate on two main areas: further development of the model, and specific operational tests to assess the response of the model.

Future developments will include the following:

Further interaction between the modules; in particular to pass the current field back to the wave module, to incorporate the effects of refraction of waves by a strong current gradient. This development will also require an iterative procedure to allow for the subsequent feedback of waves through to the current field.

All test cases to date have been under steady driving conditions. Inclusion of a tide curve in the current module boundary conditions will be incorporated. This development will have a significant bearing on the morphodynamic module, in particular on the timestepping procedures, which will also require modifications.

A major development will be the incorporation of 3-dimensional processes involving resolution through the vertical. This is especially important in the breaker zone where there are usually strong vertical flow gradients, and in cases of density stratification. The incorporation of wind-generated currents will also require consideration of vertical current resolution.

It is anticipated that work being undertaken in MAST G8M to parameterise the complex processes of (a) seabed wave-current interaction and (b) sediment transport by waves and currents will be incorporated in PISCES when ready.

An important potential application of PISCES is to problems of long-term morphodynamic change (i.e. over years and decades). Even with future improvements to computing power and numerical solution techniques it would not be practical to run PISCES for this length of simulation time. To address

the problem of long-term predictions, new theoretical approaches are needed involving the filtering of processes and input conditions over the shorter timescales. Furthermore, new methodologies for the use of the resulting model need to be established. This major area of investigation is to be the subject of a separate MAFF-funded project.

Testing of the model will include:

An assessment of the sensitivity of the model results to the sediment transport relation. In particular, for the river outflow test case, it has already been observed that qualitatively different results are obtained between PISCES and models at other MAST institutes.

Running a specific test case with time varying wave and tidal conditions.

A range of simple and complex test cases to assess the overall performance and range of applicability of the model.

6 Conclusions

1. During this first year of the full three year study attention has been concentrated on the design and initial testing of an integrated coastal area model, which has been given the name PISCES.

2. Work on the model has comprised the linking together of existing flow, wave and sand transport models, writing a new morphological module, and integration into one overall model.

3. The model is automatic in the sense that for a particular application the simulation starts from the initial conditions and runs for the simulation duration without further intervention. The bathymetry is updated throughout the simulation at variable timesteps calculated according to a robust protocol which maintains numerical stability of the bed levels.

4. To date, testing of the model has been via specific applications with steady forcing conditions, although allocation has been made for future inclusion of time-varying wave and tidal conditions.

5. For the case of a flat bed channel under unidirectional flow, the model was shown to behave sensibly, eroding sediment in the downstream direction until a constant water depth, and hence constant velocity gradient, was achieved.

6. A single sinusoidal sand wave in the same channel was shown to propagate downstream with a steepening lee slope. Although shock conditions could not in principle be reproduced, the near-shock conditions present a severe test of the stability of the bed update scheme. This scheme behaved robustly. Inclusion of the gravity term gave rise to a smoother evolved dune shape, together with a reduction in height as the dune propagated forwards.

7. The dune test case was extended to 2D, where a rather more complicated bed evolution pattern was predicted in this case. The main feature was advected downstream in a similar manner to the 1D case. However, interaction between the bed and the flow field gave rise to an

apparent lateral dispersion of the dune, at a large angle to the main flow direction. The dune also caused the formation of other smaller dunes upstream of the main feature, as a result of modifying the main flow stream.

8. A more complicated test case of a 4 day simulation of a river discharging into a coastal wave driven current field was investigated. This simulation enabled thorough testing of all the modules under steady driving conditions. Results indicated the formation of both static spit-type features and dynamic dune features that were propagated longshore through the model domain. The results also appear to be sensitive to the method of calculation of the sediment transport; a topic that will be investigated further in the remainder of the study.

9. In another coastal application the evolution of a semicircular bay under the action of waves was investigated. This simulation had the advantage of comparison with physical model tests, where the agreement with the results from PISCES was reasonable.

10. Development and testing of the model has been greatly facilitated by the involvement of HR in the MAST-G6M Coastal Morphodynamics research programme. In particular, intercomparisons between participating institutes for the river outflow and the semicircular bay test cases gave valuable insight into problems requiring specific attention.

11. A good deal of progress has been made during this first year. The remainder of the study will concentrate on improvements to the existing modules, and by applying the model to more elaborate test cases. By this means a greater understanding of these complex morphological systems will be achieved, as well as highlighting areas that require further attention.

7 Acknowledgements

The authors gratefully acknowledge the help and advice from R L Soulsby, Dr G V Miles, Dr A J Cooper, G Gilbert and Dr R Hulme at HR Wallingford, and also extend their thanks to colleagues in the MAST G6M collaborative research group for their effort and support.

8 References

Bagnold R A (1966) An approach to the sediment transport problem from general physics. US Geol Survey, Prc paper 4221.

Bailard J A (1981) An Energetics Total Load Sediment Transport Model for a Plane Sloping Beach, J. Geophys. Res. Vol 86 No C11.

Chesher T J (1992) Aspects of long-term morphodynamic modelling. Report SR 306, HR Wallingford (April).

De Vriend (1987) 2DH Mathematical Modelling of Morphological Evolutions in Shallow Water, Coastal Engineering, Vol 11 No. 1

De Vriend HJ, Zyserman J, Péchon P, Roelvink JA, Southgate HN and Nicholson J (1993) Medium-Term Coastal Area Modelling (submitted to Coastal Engineering).

Duplex J and Peltier E (1990) Code TSEF. Numerical method and tests. EDF-LNH Report HE/42/90.44 (in French).

Galappatti R and Vreugdenhil C B (1985) A Depth Integrated Model for Suspended Sediment Transport, J. Hydr. Res. Vol 23, No. 4.

Grass A J (1981) Sediment Transport by Waves and Currents. SERC London Centre for Marine Technology Report FI29, University College, London.

HR Wallingford (1991) Poole Bay Phase II - Hydraulic Study, Report EX 2228.

Nairn R B and Southgate H N (1993) Deterministic Profile Modelling of Nearshore Processes. Part 2. Sediment Transport and Beach Profile Development, Coastal Engineering Vol 19 No 1,2.

Péchon P (1985) Experimental Study of the Littoral Transport and First Comparisons with the Model TRADEF. EDF-LNH Report HE/42/85.05 (in French).

Roelvink J A (1992) Treatment of the Lateral Boundary Conditions in the Case of Wave-Current Interaction. MAST G6-M Report.

Southgate H N (1989) A Nearshore Profile Model of Wave and Tidal Current Interaction, Coastal Engineering, Vol 13.

Southgate H N and Goldberg D G (1989) An Efficient Computational Model for Wave Refraction and Diffraction using Finite Differences, Report SR 213, HR Wallingford (June).

Southgate H N (1991) Initial Plans for a Q3D Morphodynamic Coastal Area Model, HR Wallingford internal report.

Southgate H N and Nairn R B (1993) Deterministic Profile Modelling of Nearshore Processes. Part 1. Waves and Currents, Coastal Engineering Vol 19 No 1,2.

Stive M J F (1986) A Model for Cross-Shore Sediment Transport, Proceedings 20th Coastal Engineering Conference, Taipei, Taiwan, Vol II, pp1550-1564.

van Rijn L C (1984) Sediment transport, part III. Bed Forms and Alluvial Roughness. J. Hydr. Eng, Vol 110, No. 12.

Wild B R (1988) A Numerical Sand Transport Model With Time Dependent Bed Exchange, Report SR 148, HR Wallingford (February).

Figures

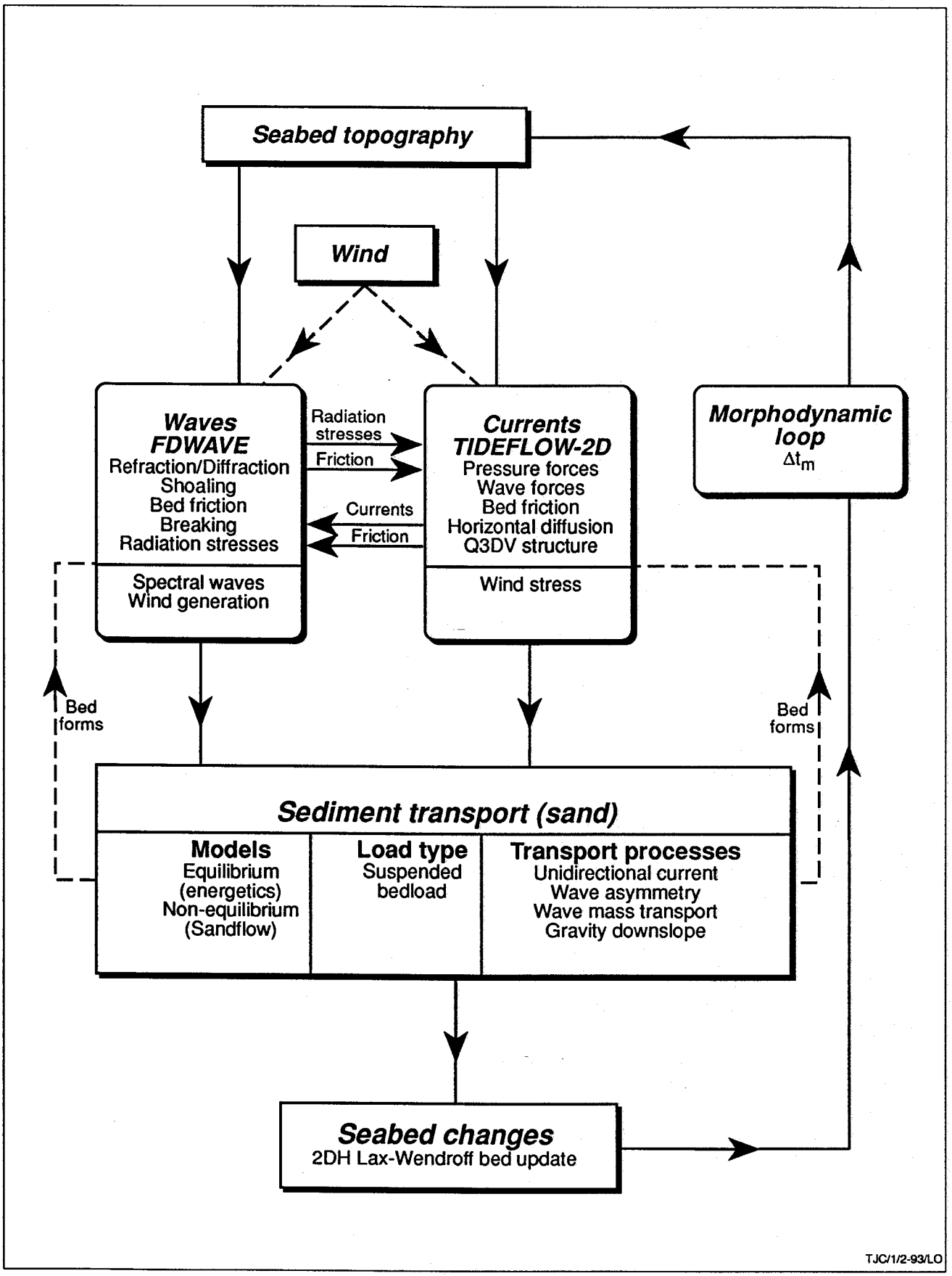

Figure 1 PISCES model structure

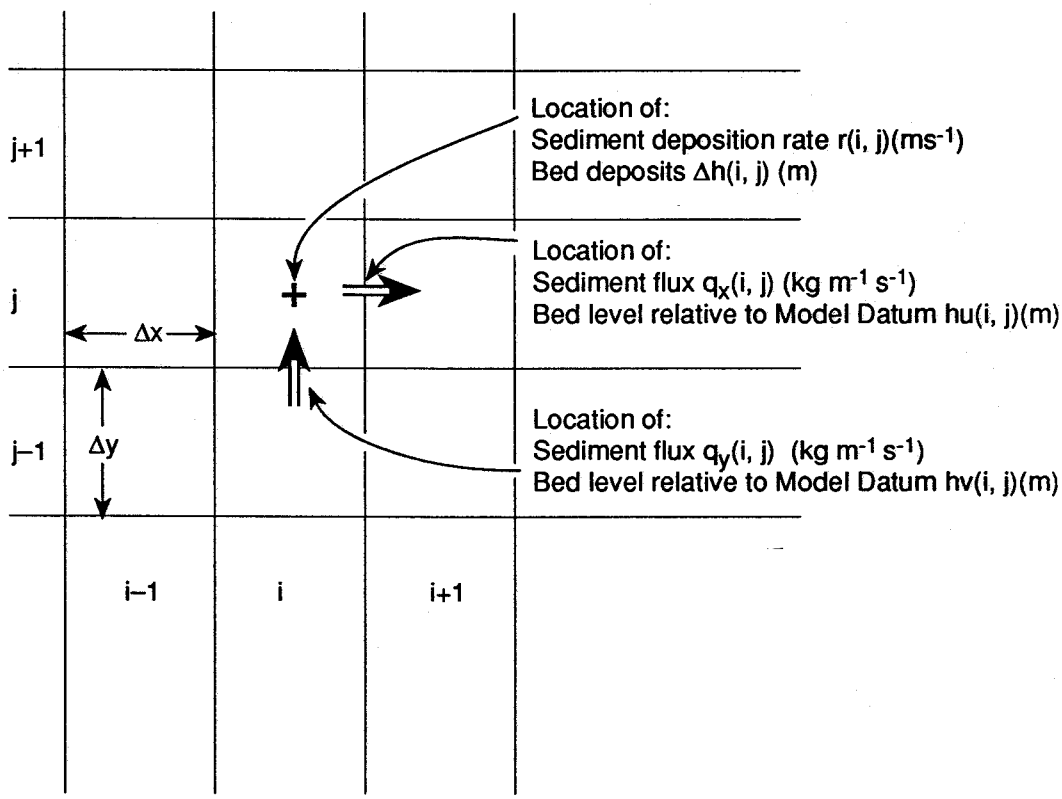

TJC/2/2-93/LO

Figure 2 Definition of sediment fluxes, bed levels and sediment deposition rate at model cell (i, j)

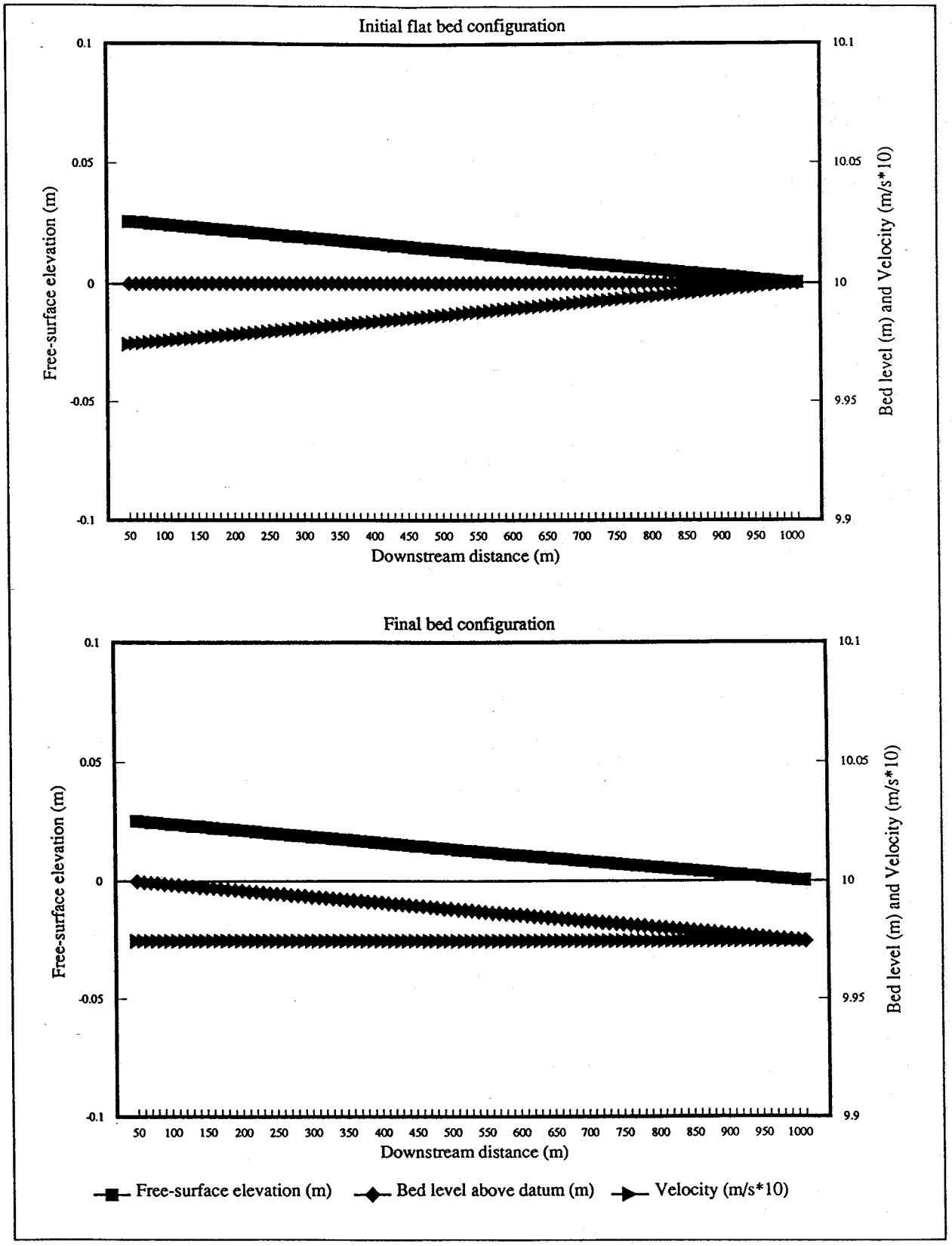

Figure 3 Flat bed channel test case
Initial and final distribution
of bed level and hydrodynamics

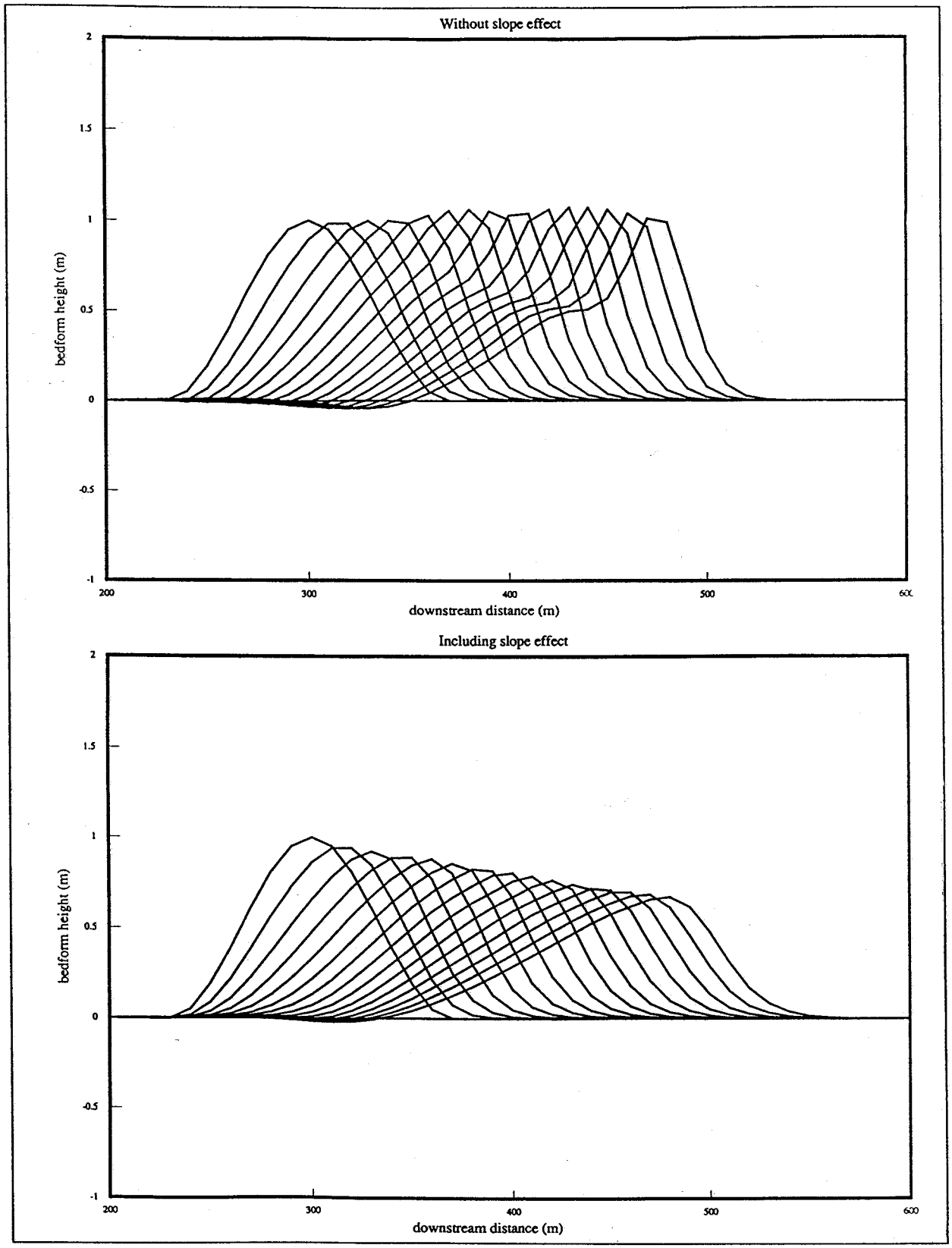

Figure 4 1–D dune test case
Bed evolution over 150 hours
With and without bed slope effect
included in sediment transport relation

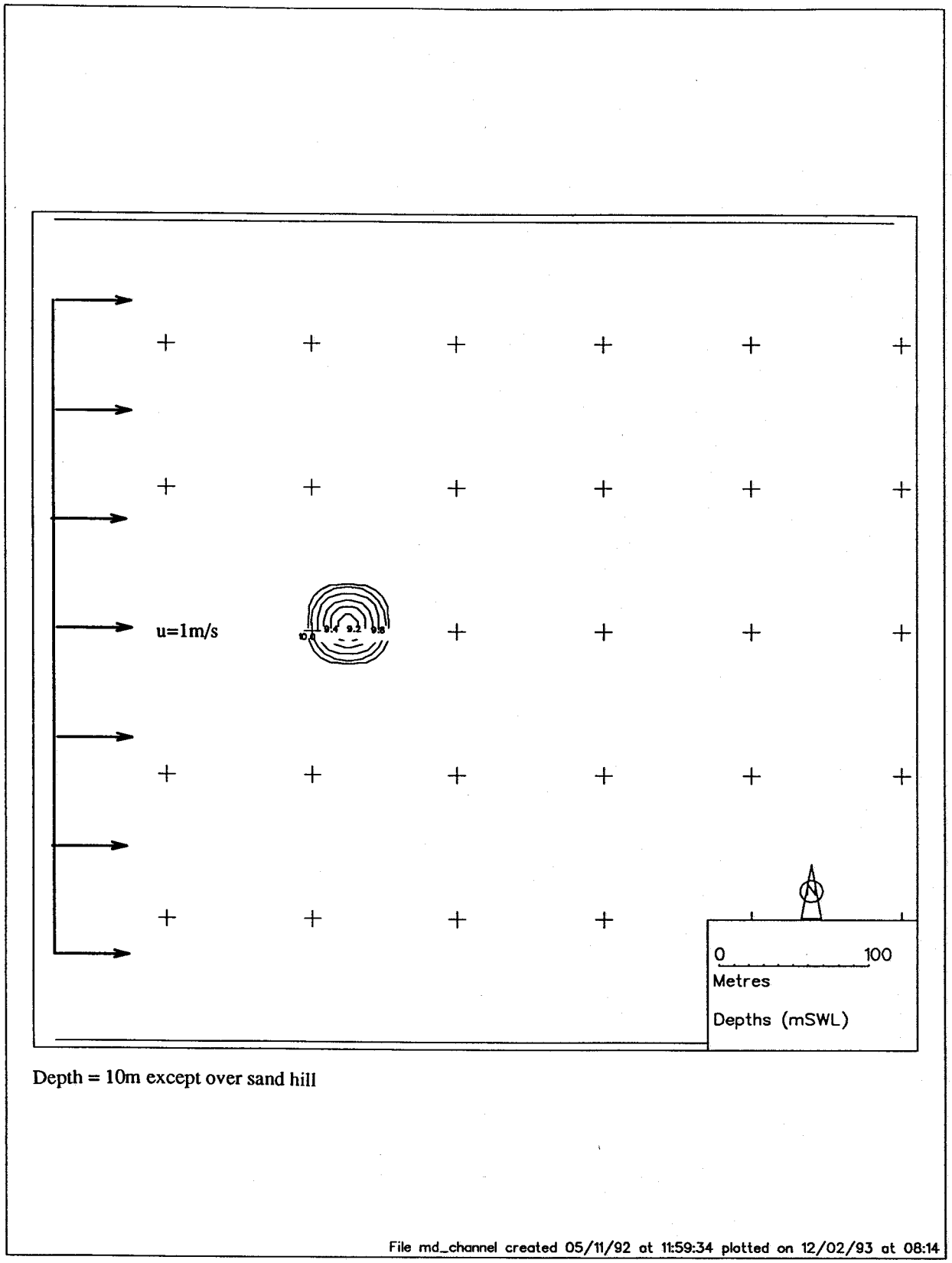

Figure 5 Isolated sand hill test case
Initial bathymetry and test conditions

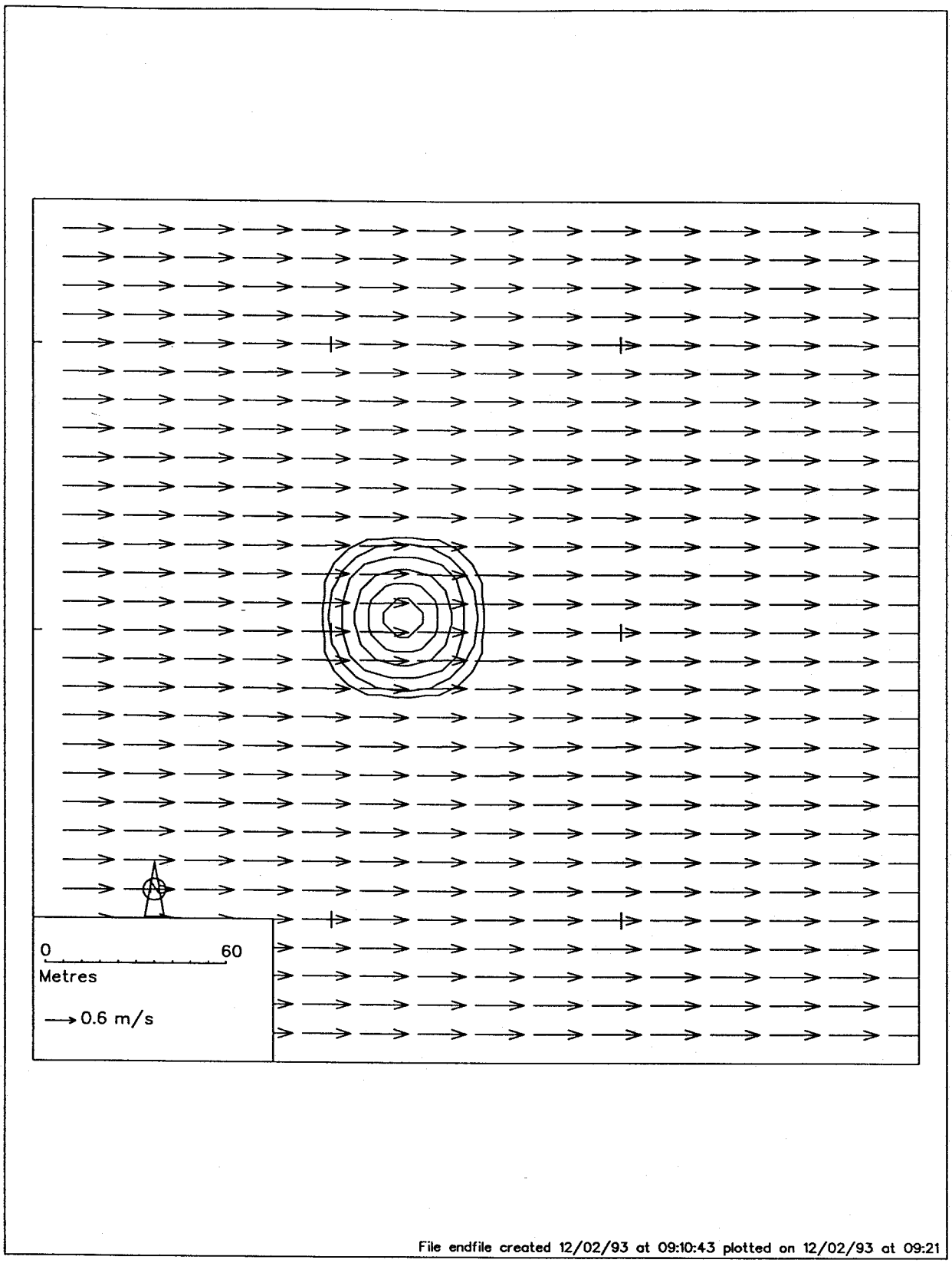

Figure 6 Isolated sand hill test case
Velocity field over initial bathymetry

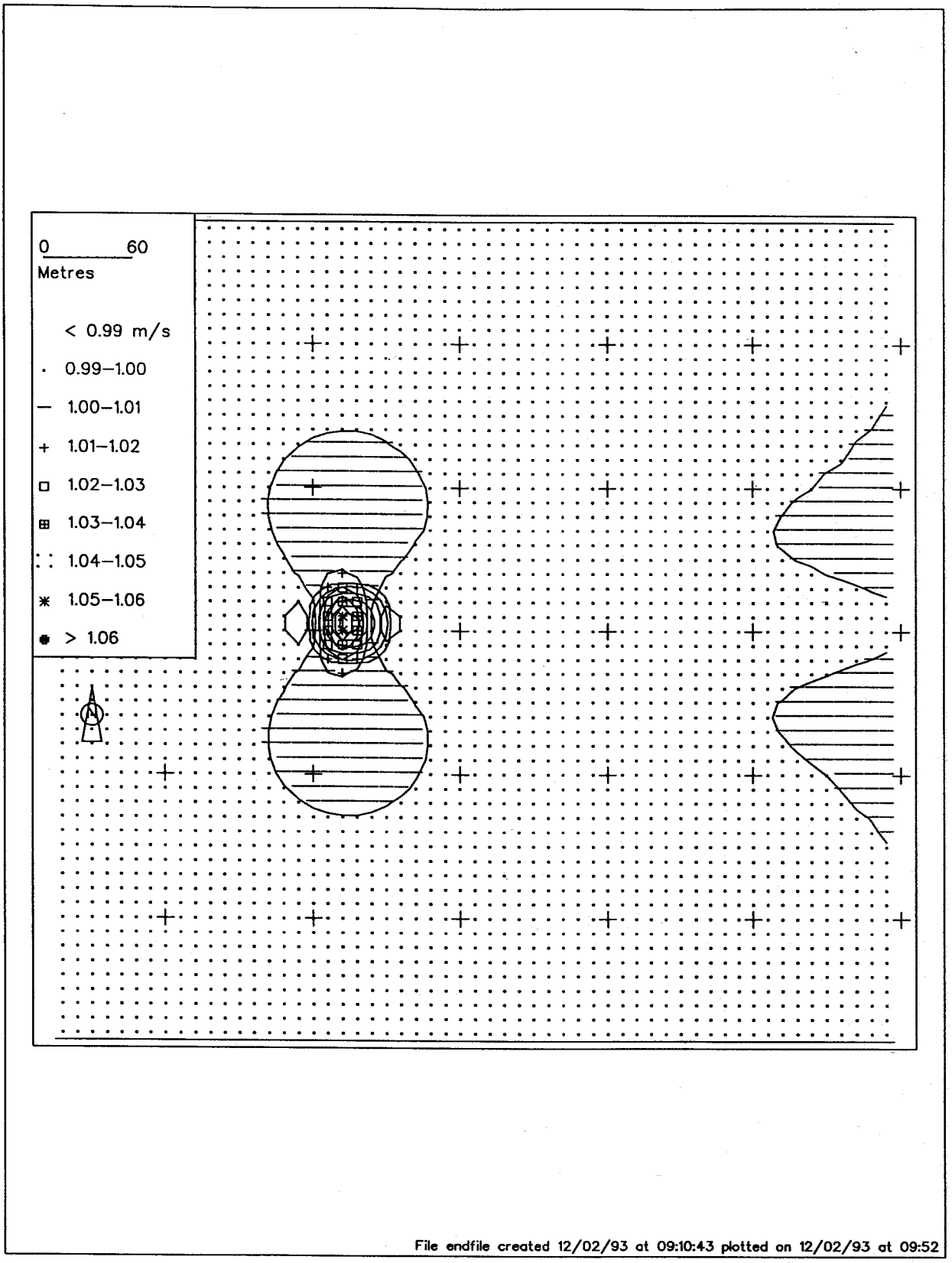

Figure 7 Isolated sand hill test case
U–velocity field over initial bathymetry

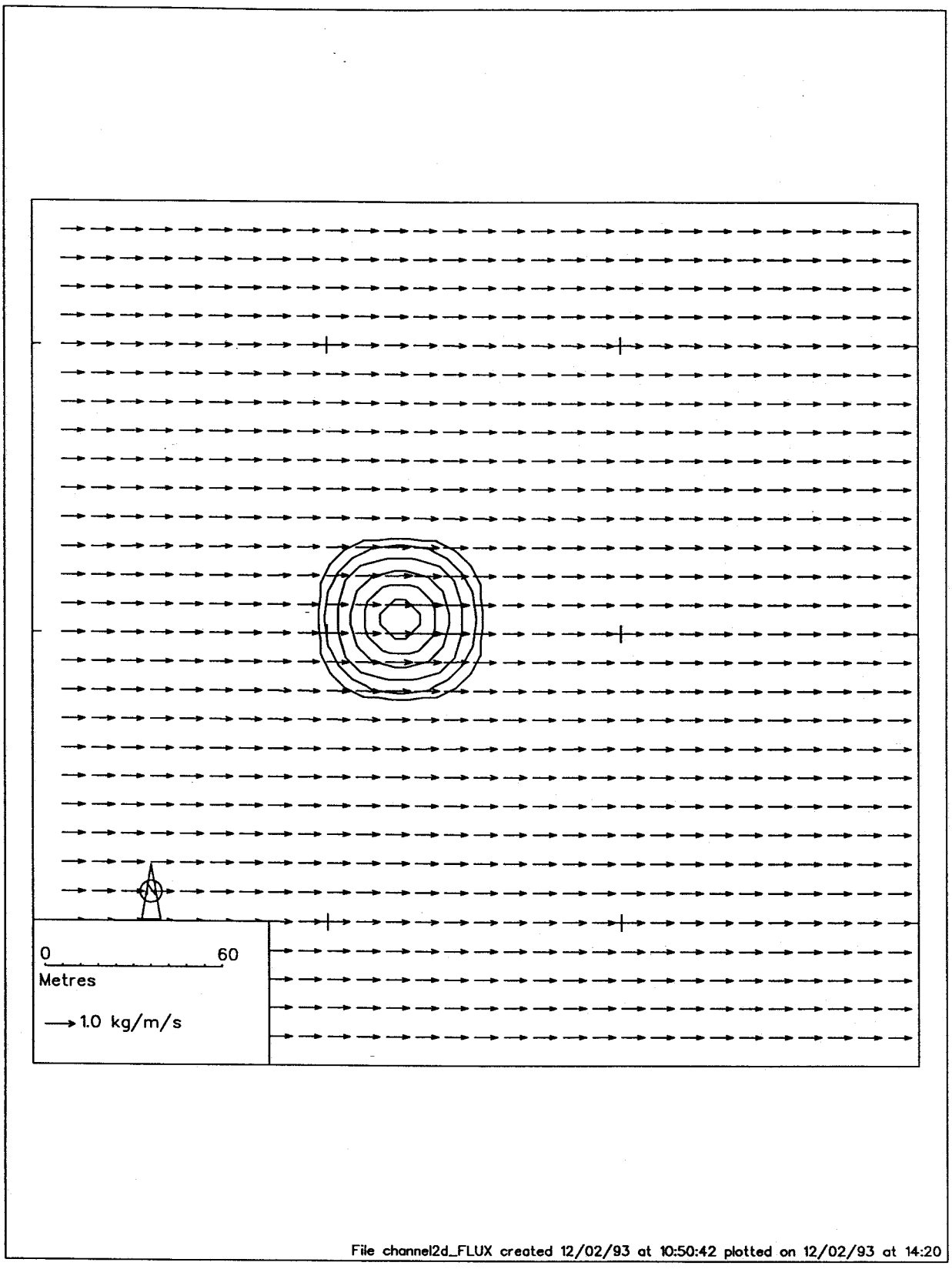

Figure 8 Isolated sand hill test case
Sand transport field over initial bed

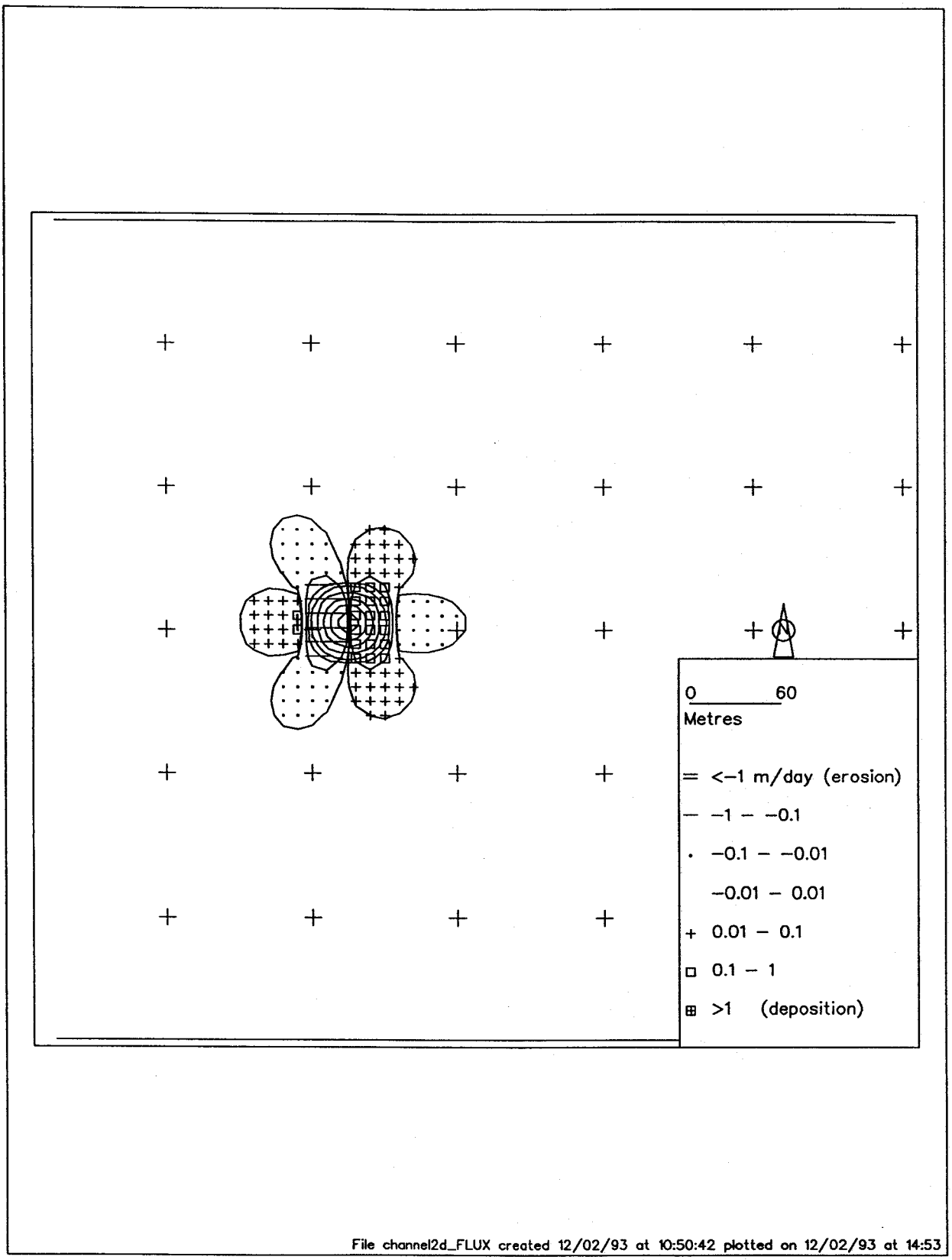

Figure 9 Isolated sand hill test case
Initial rate of bed level change

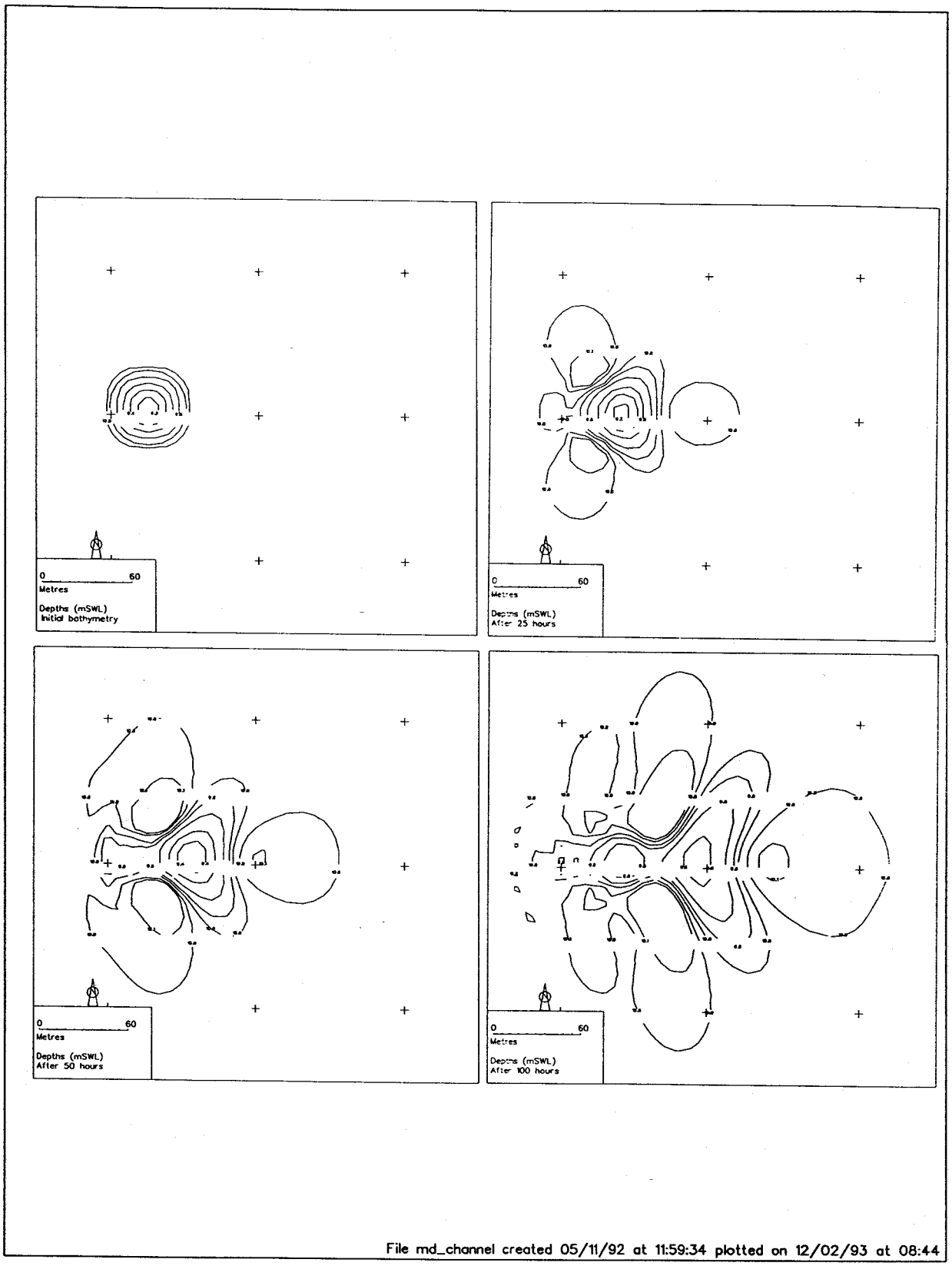

Figure 10 Isolated sand hill test case
Evolution of bedform over 100 hours
Detail of main bedform

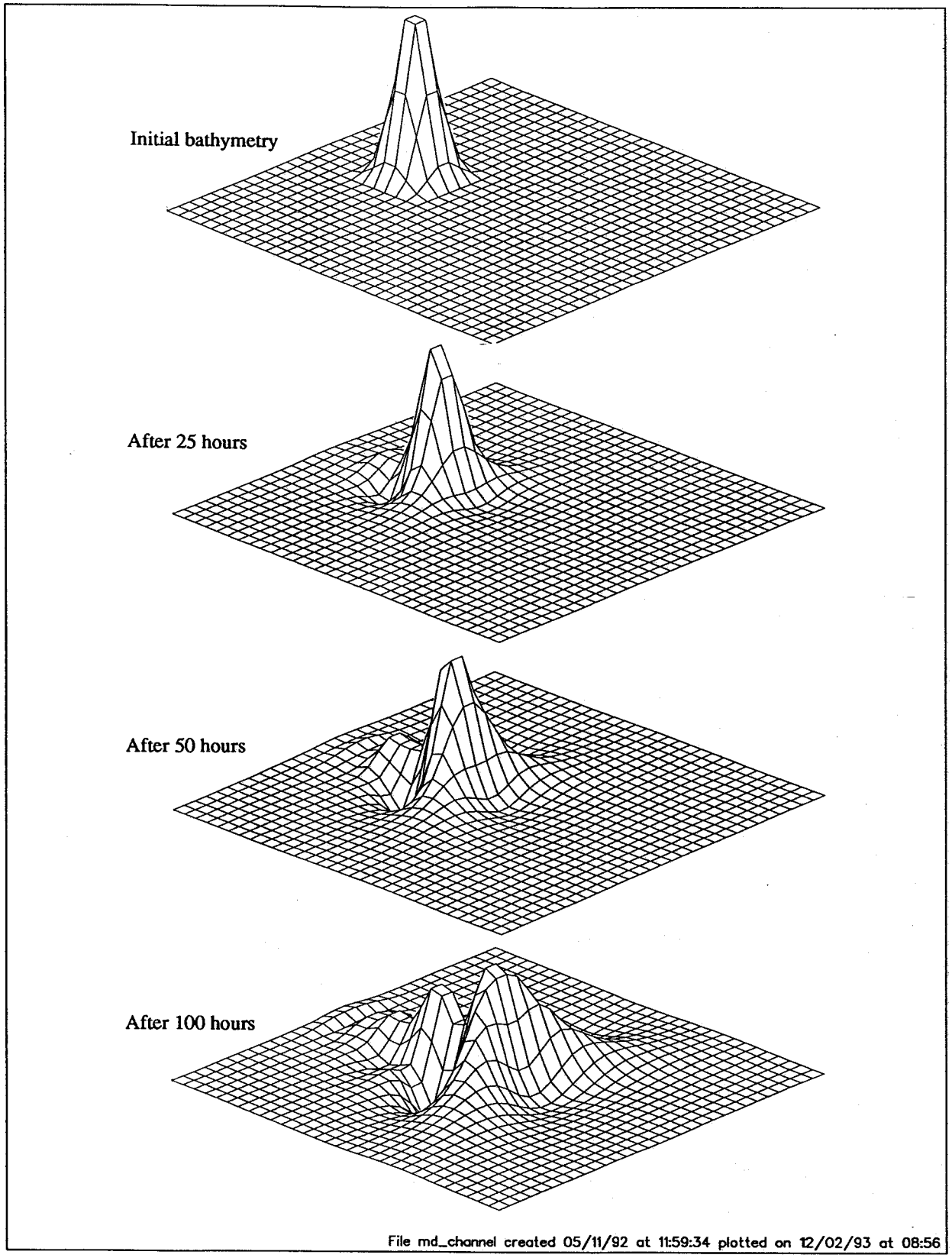

Figure 11 Isolated sand hill test case
Evolution of bedform over 100 hours
Detail of main bedform from SW

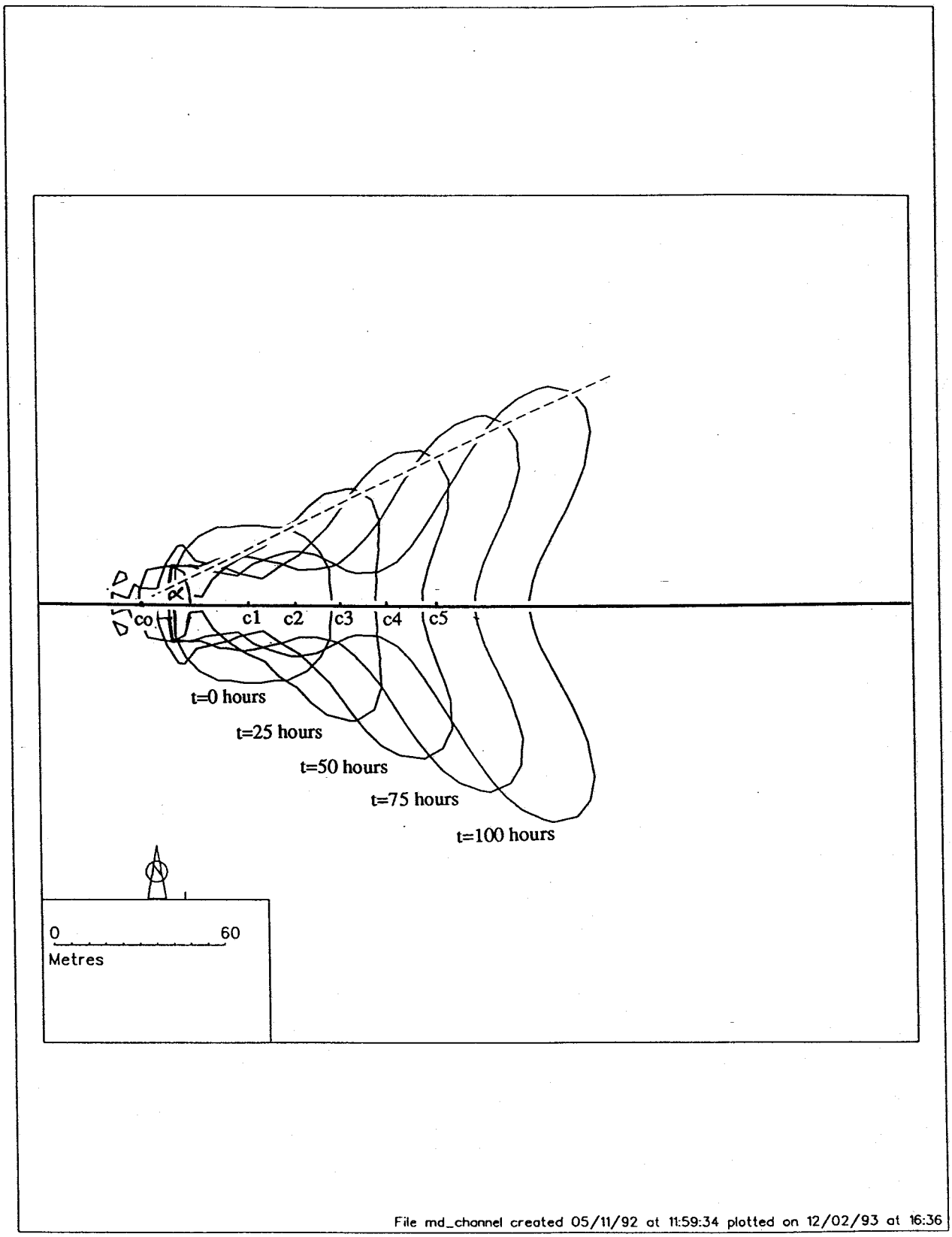

Figure 12 Isolated sand hill test case
Analysis of bed evolution

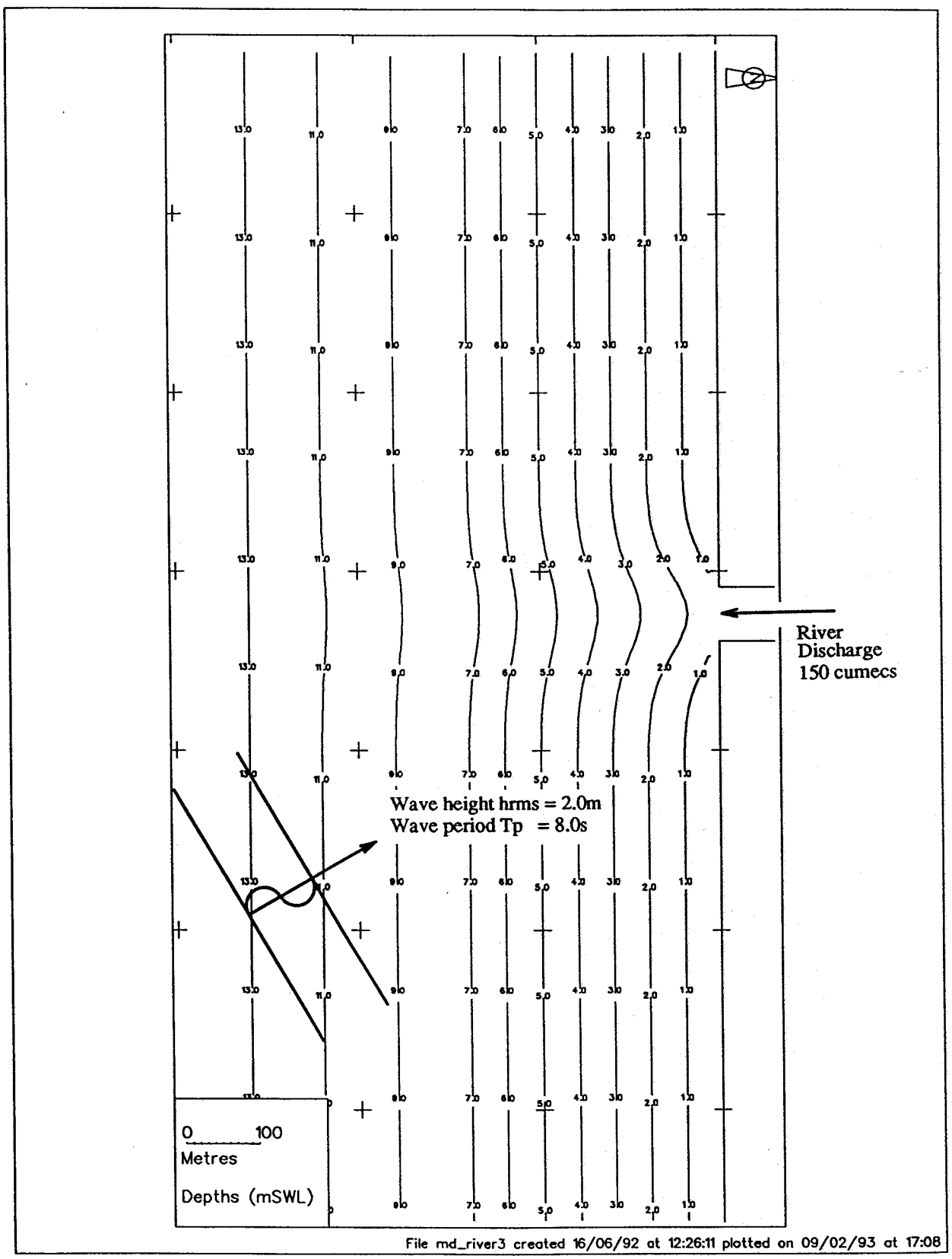

Figure 13 River outflow test case
Initial bathymetry and test conditions

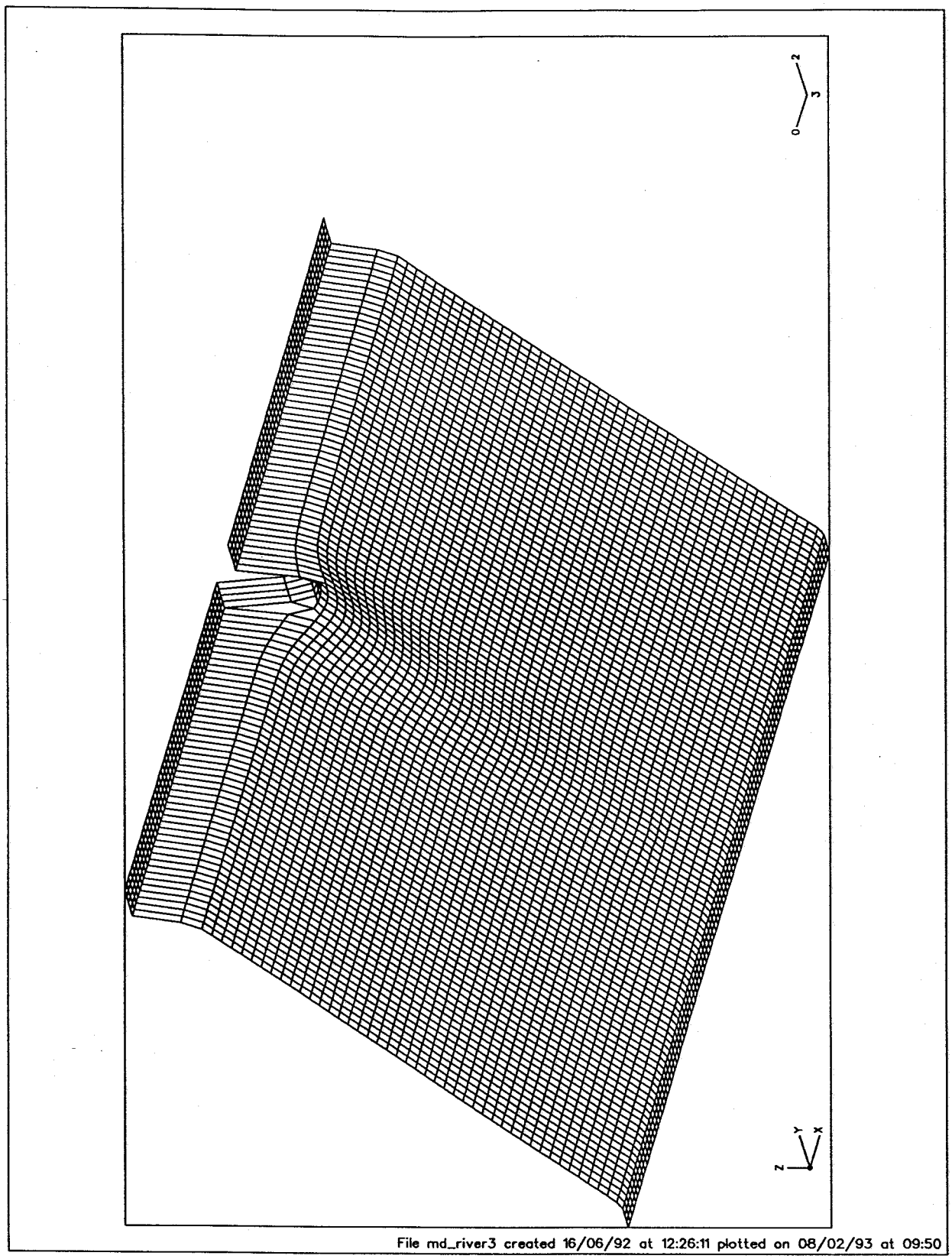

Figure 14 River outflow test case
Initial bathymetry

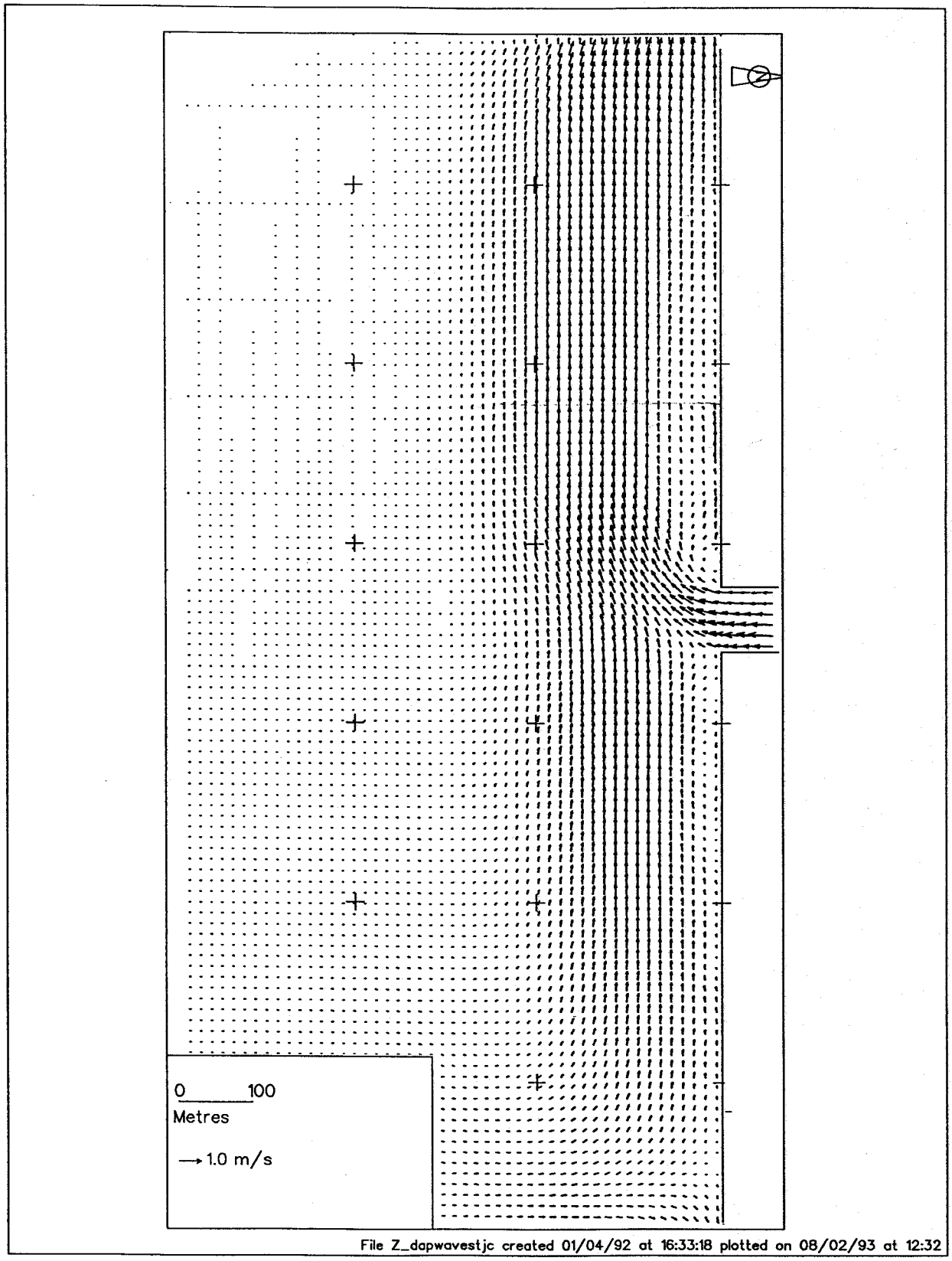

Figure 15 River outflow test case
Velocity field on initial bathymetry
Without corrections to boundaries

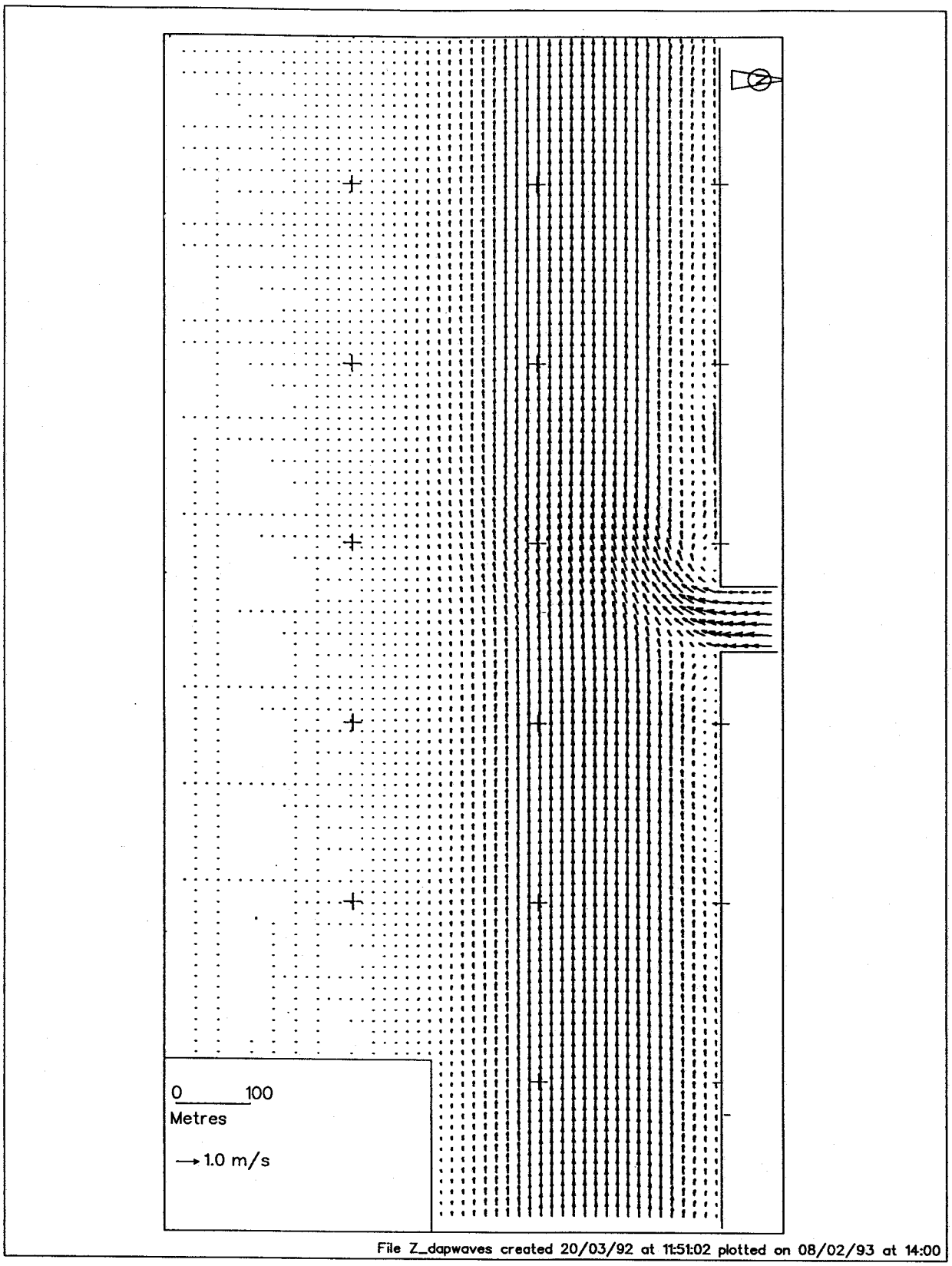

Figure 16 River outflow test case
Velocity field on initial bathymetry
With corrections to boundaries

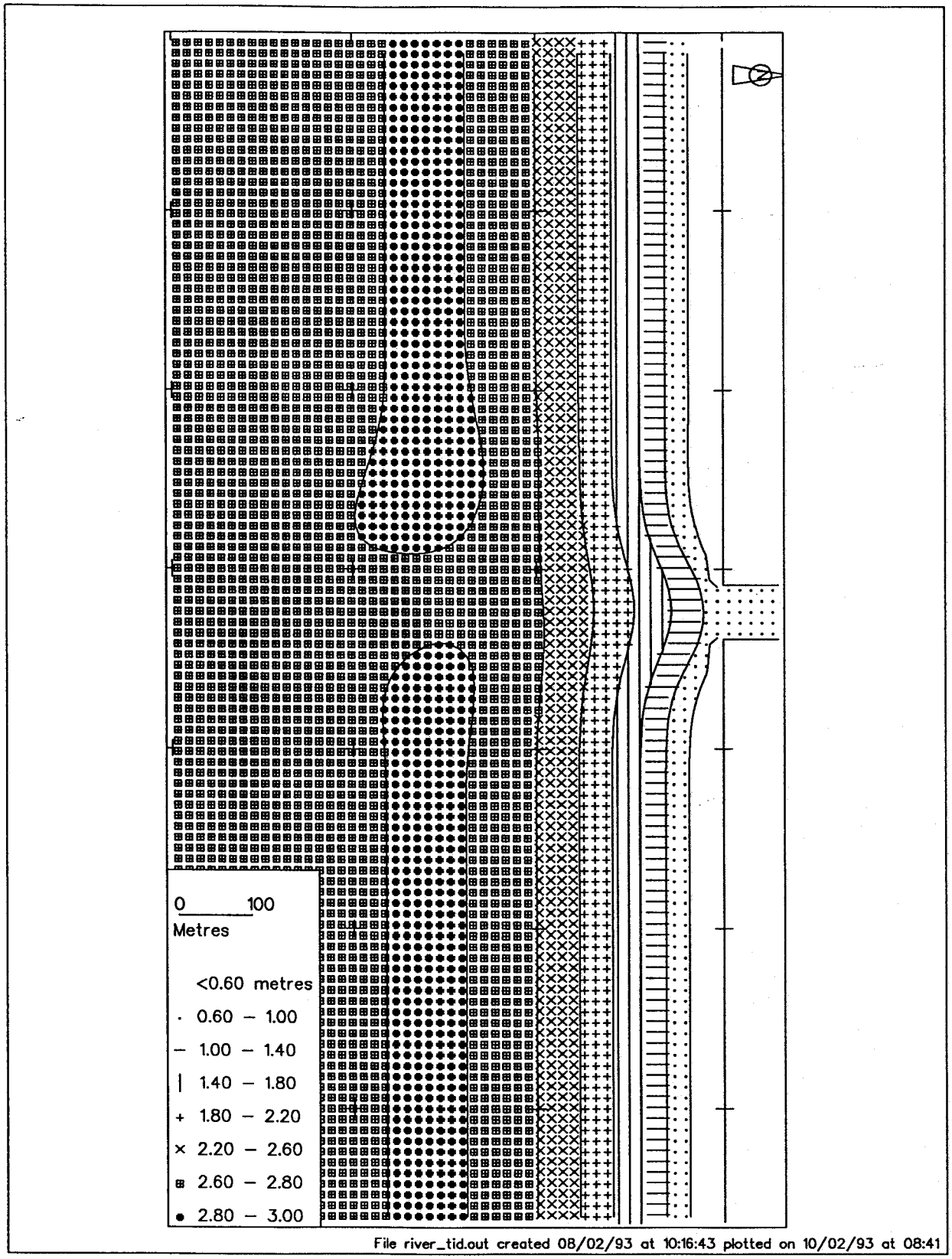

Figure 17 River outflow test case
Wave height (Hs) over initial bathymetry

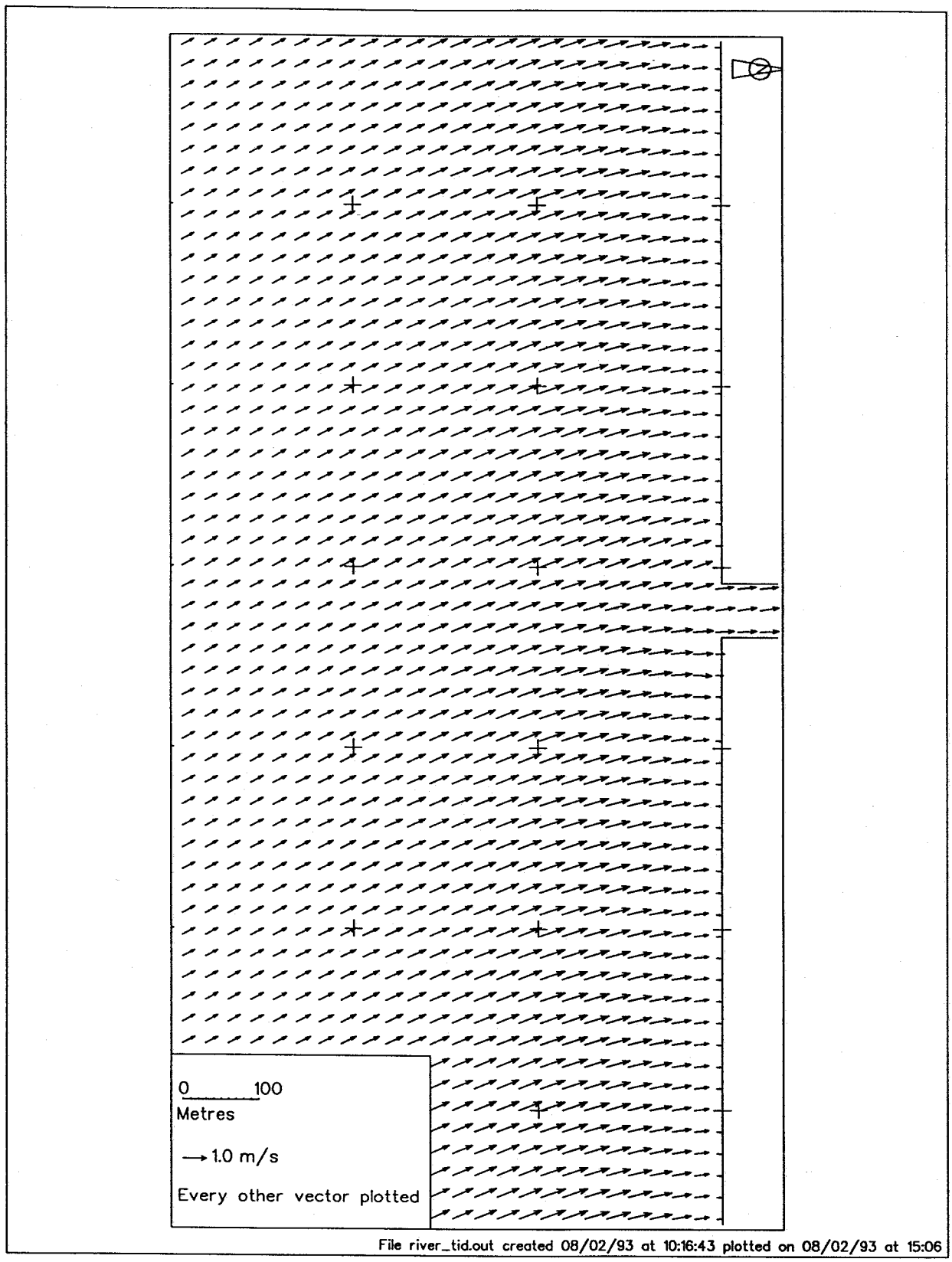

Figure 18 River outflow test case
Wave orbital velocity over initial bed

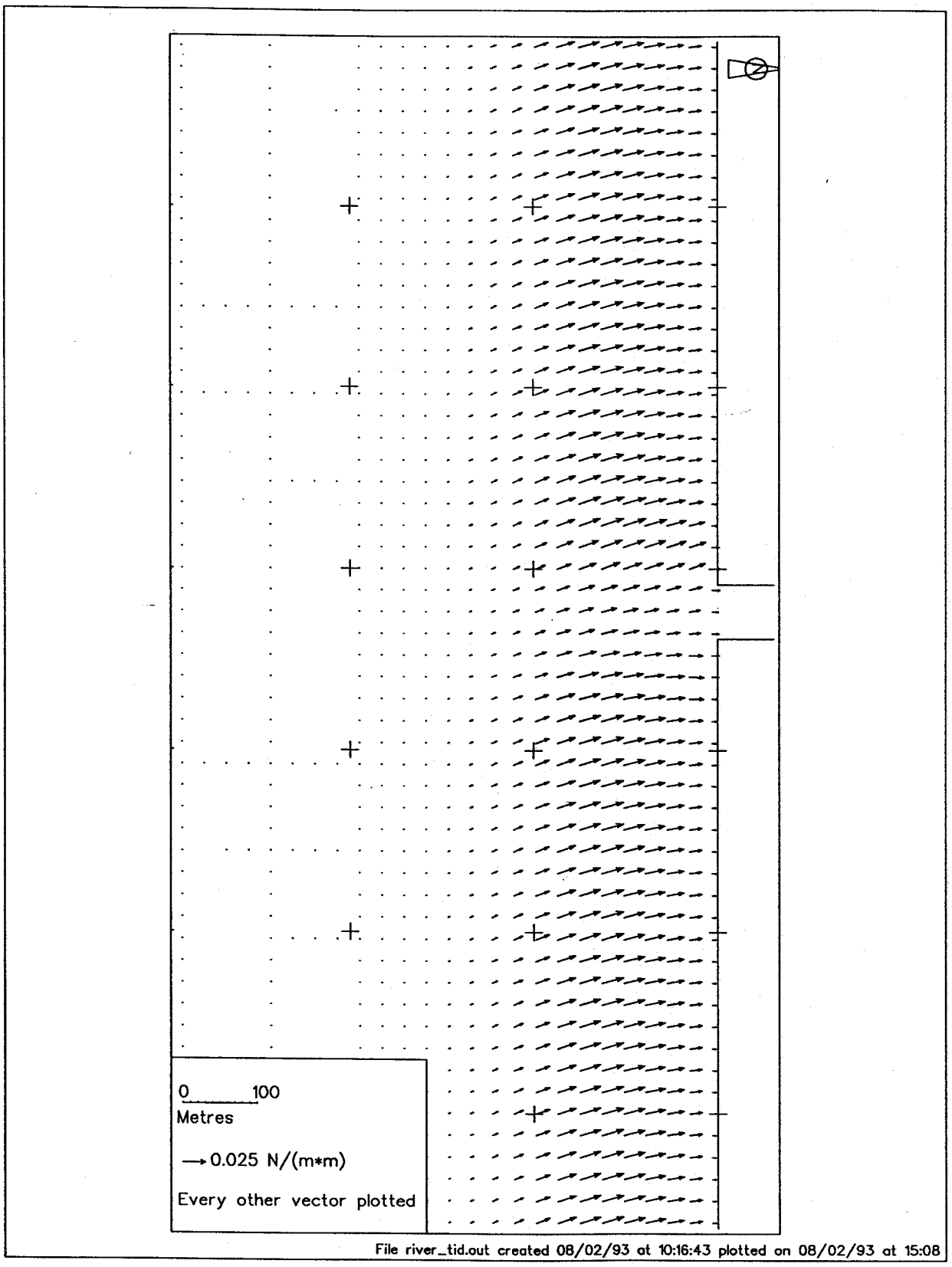

Figure 19 River outflow test case
Wave breaking stress over initial bed

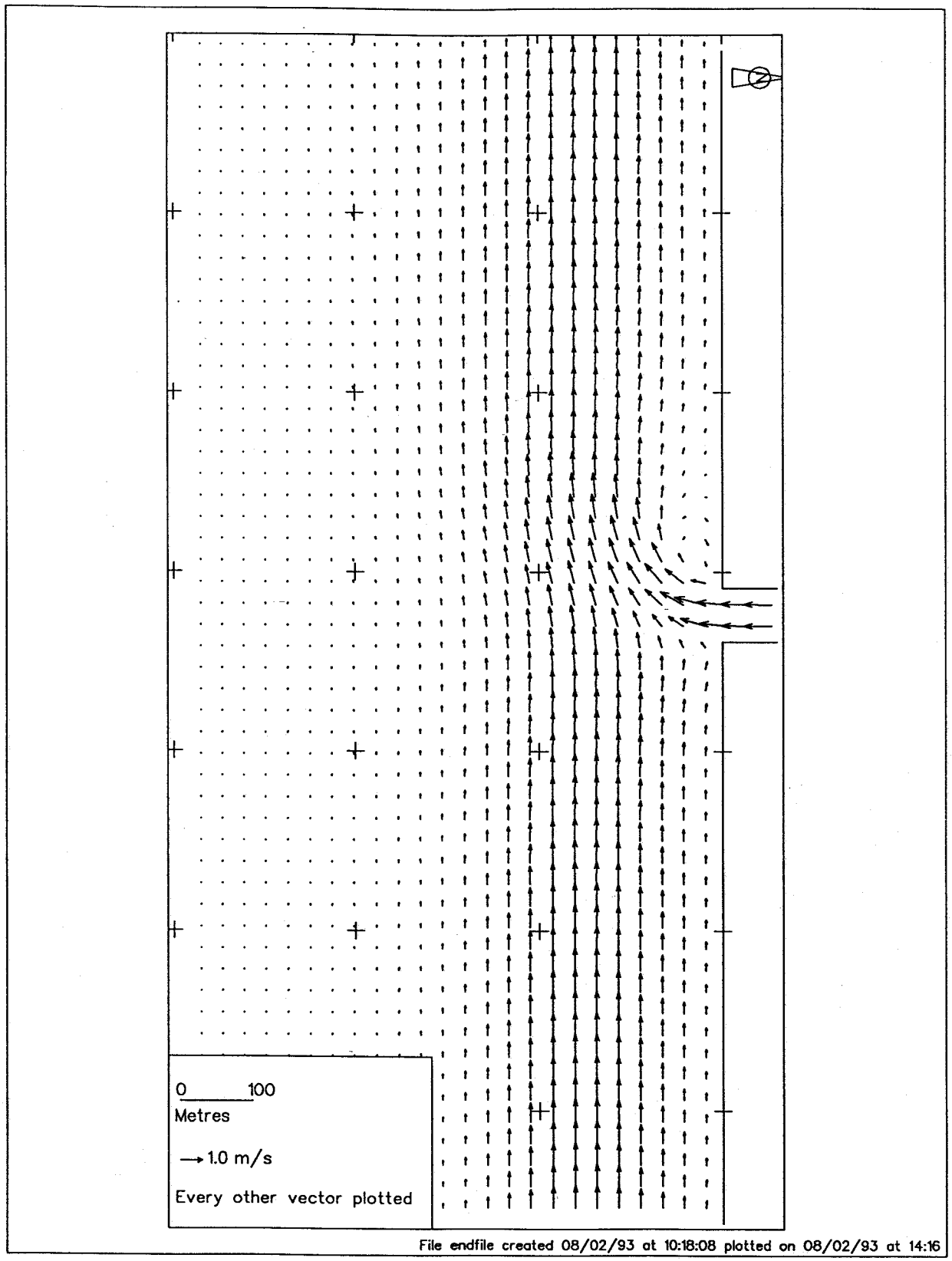

Figure 20 River outflow test case
Velocity field over initial bathymetry

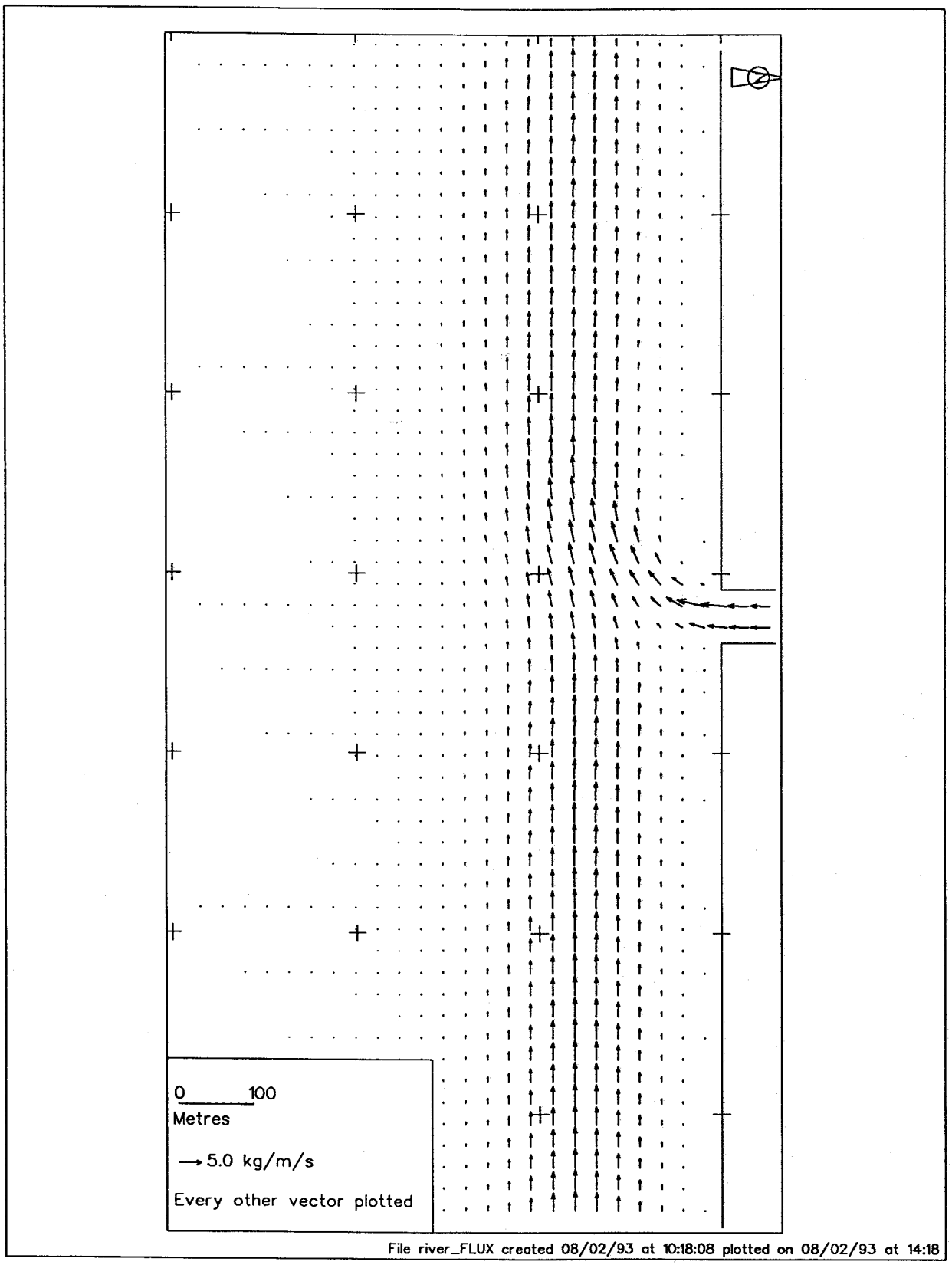

Figure 21 River outflow test case
Sand transport field over initial bed

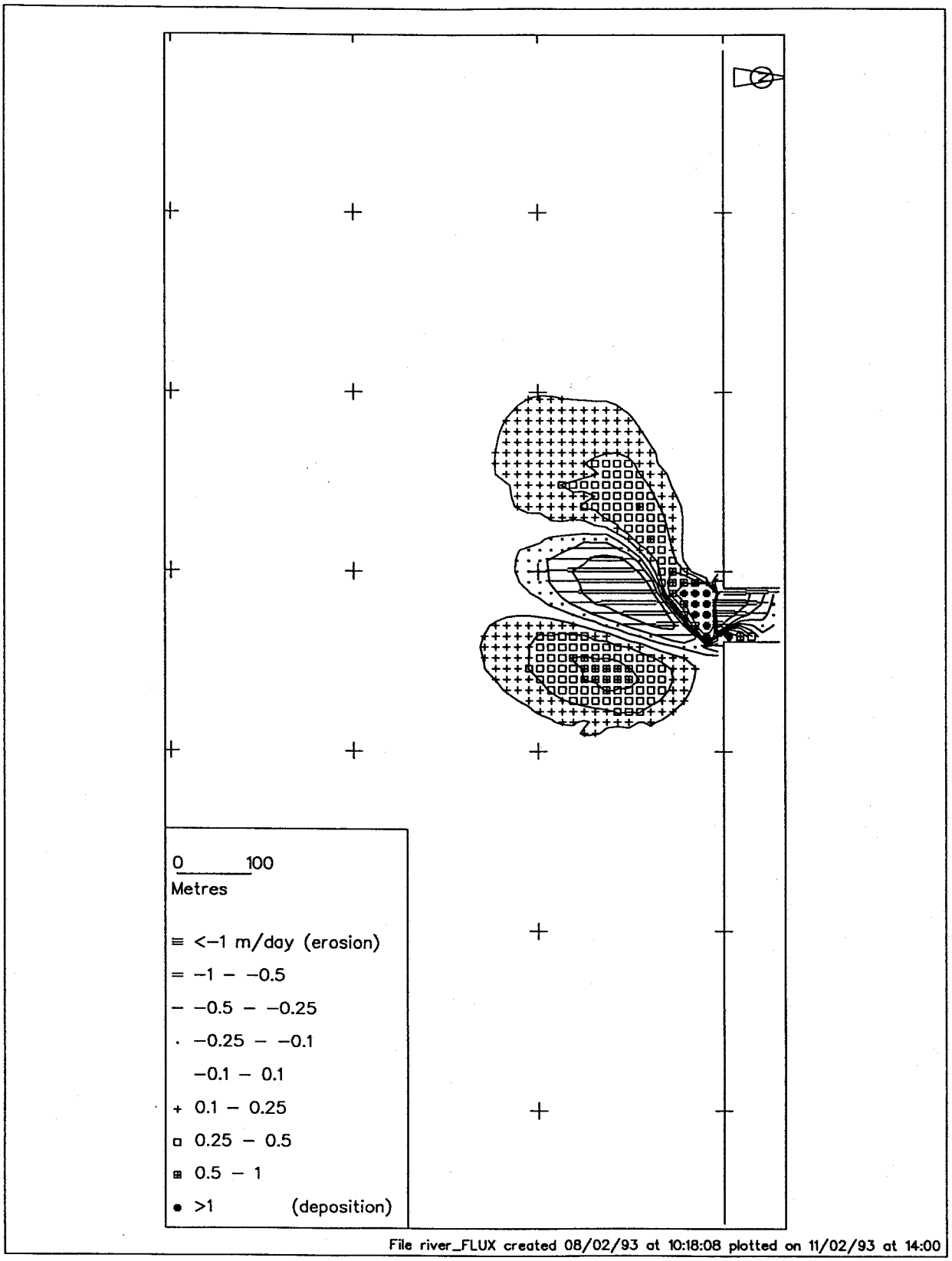

Figure 22 River outflow test case
Initial rate of bed level change

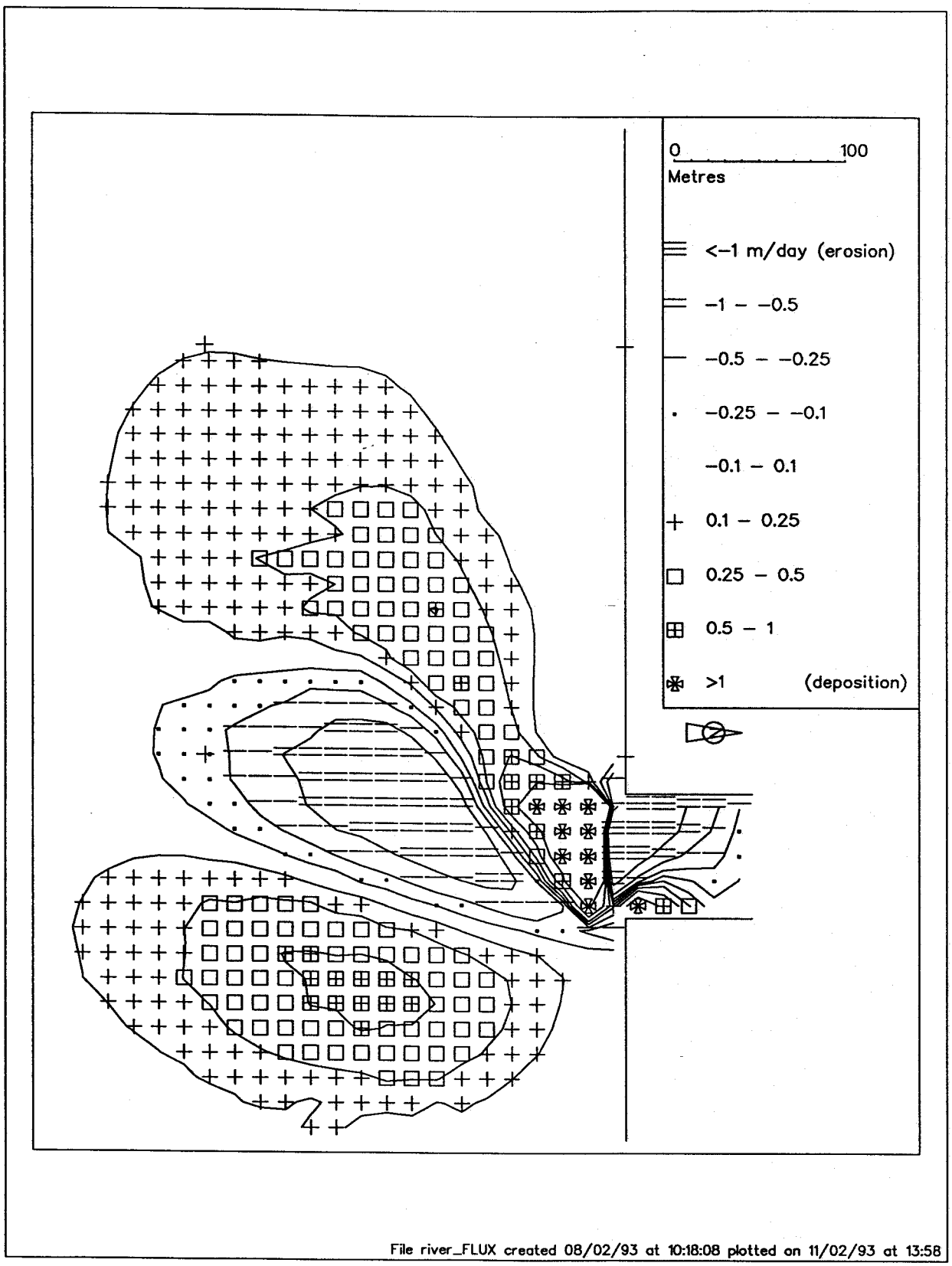

Figure 23 River outflow test case
Initial rate of bed level change
Detail of river mouth entrance

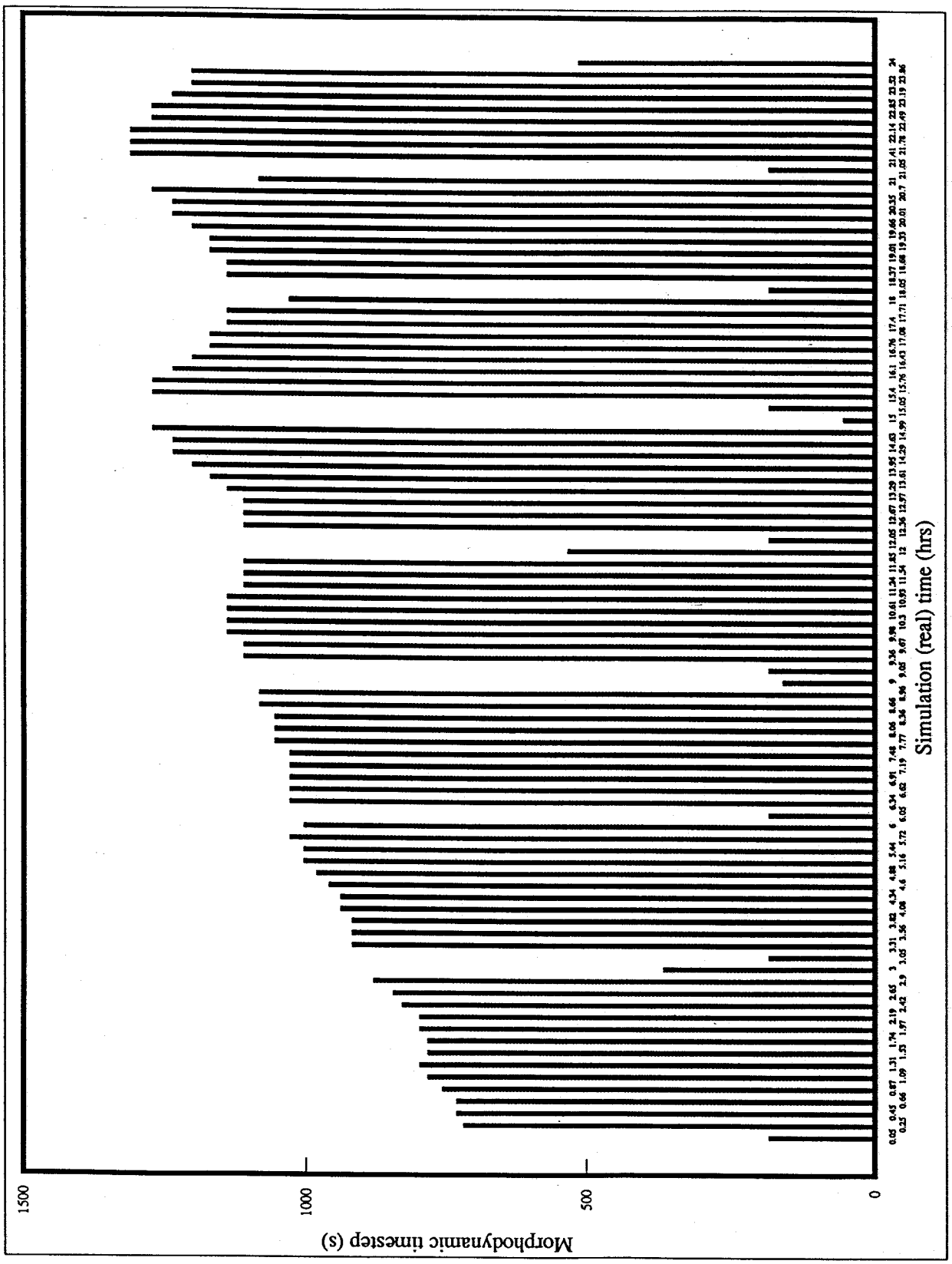

Figure 24 River outflow test case
Example of morphodynamic timestepping

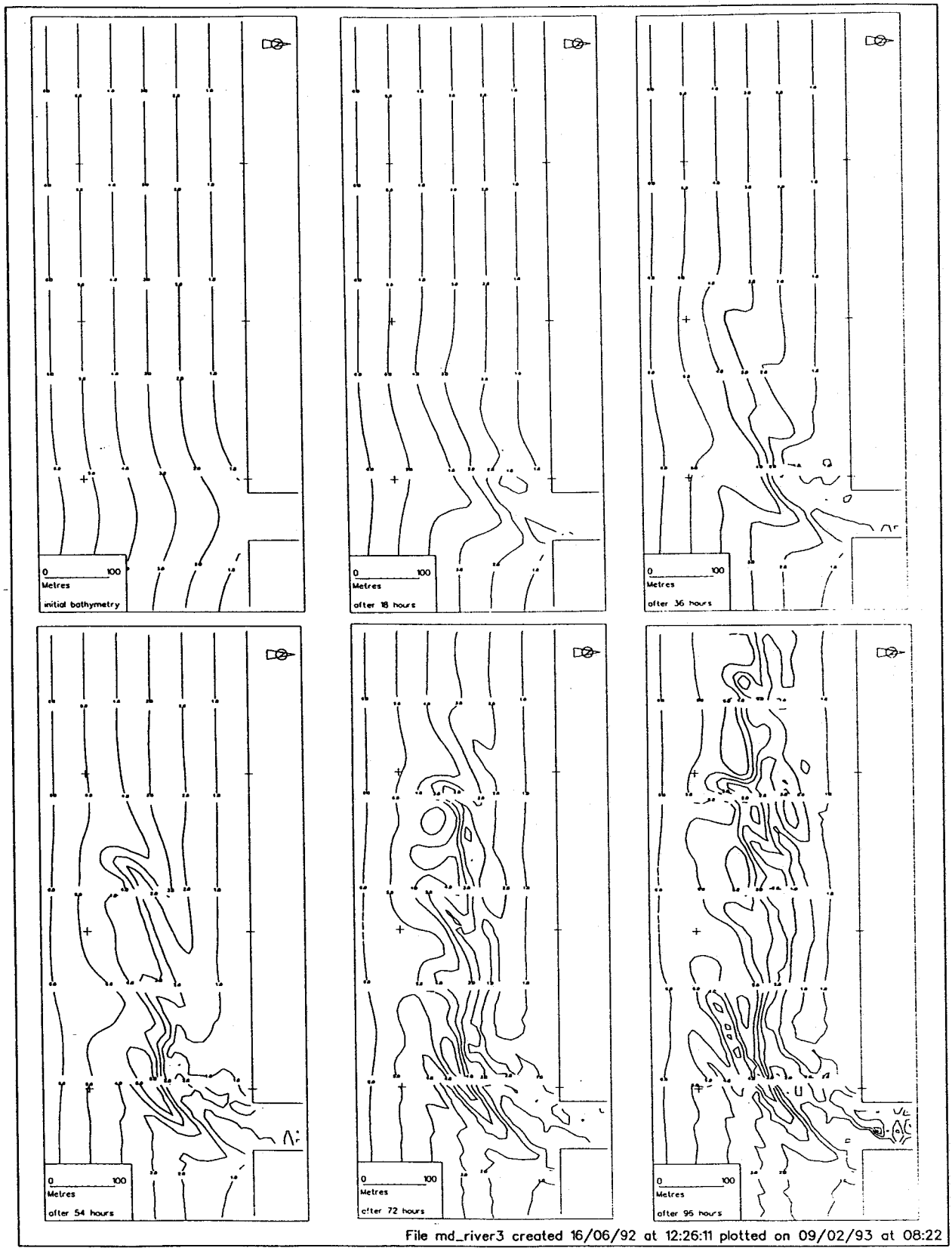

Figure 25 River outflow test case
Detail of bed evolution over 96 hours

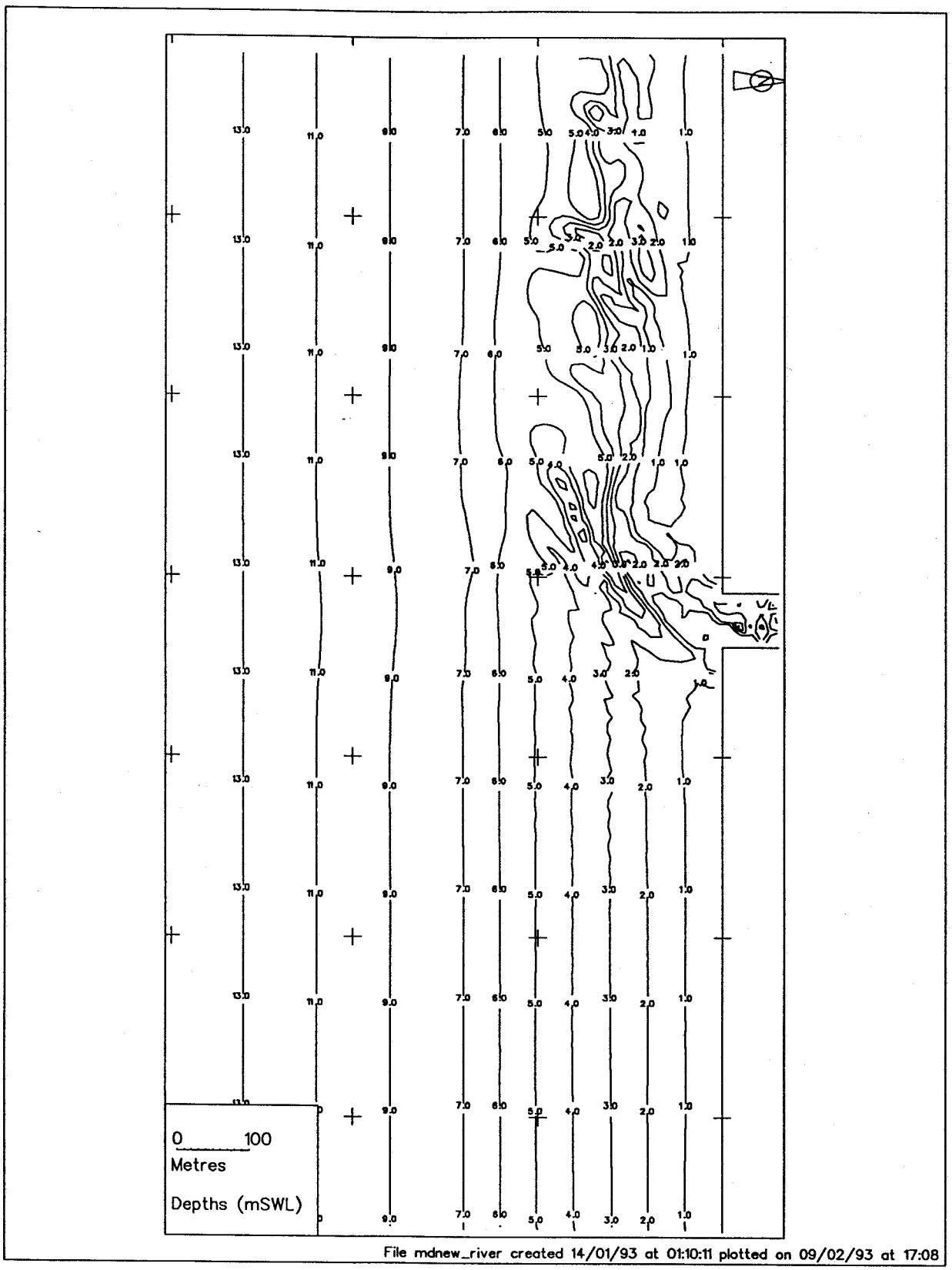

Figure 26 River outflow test case
Bathymetry after 96 hours

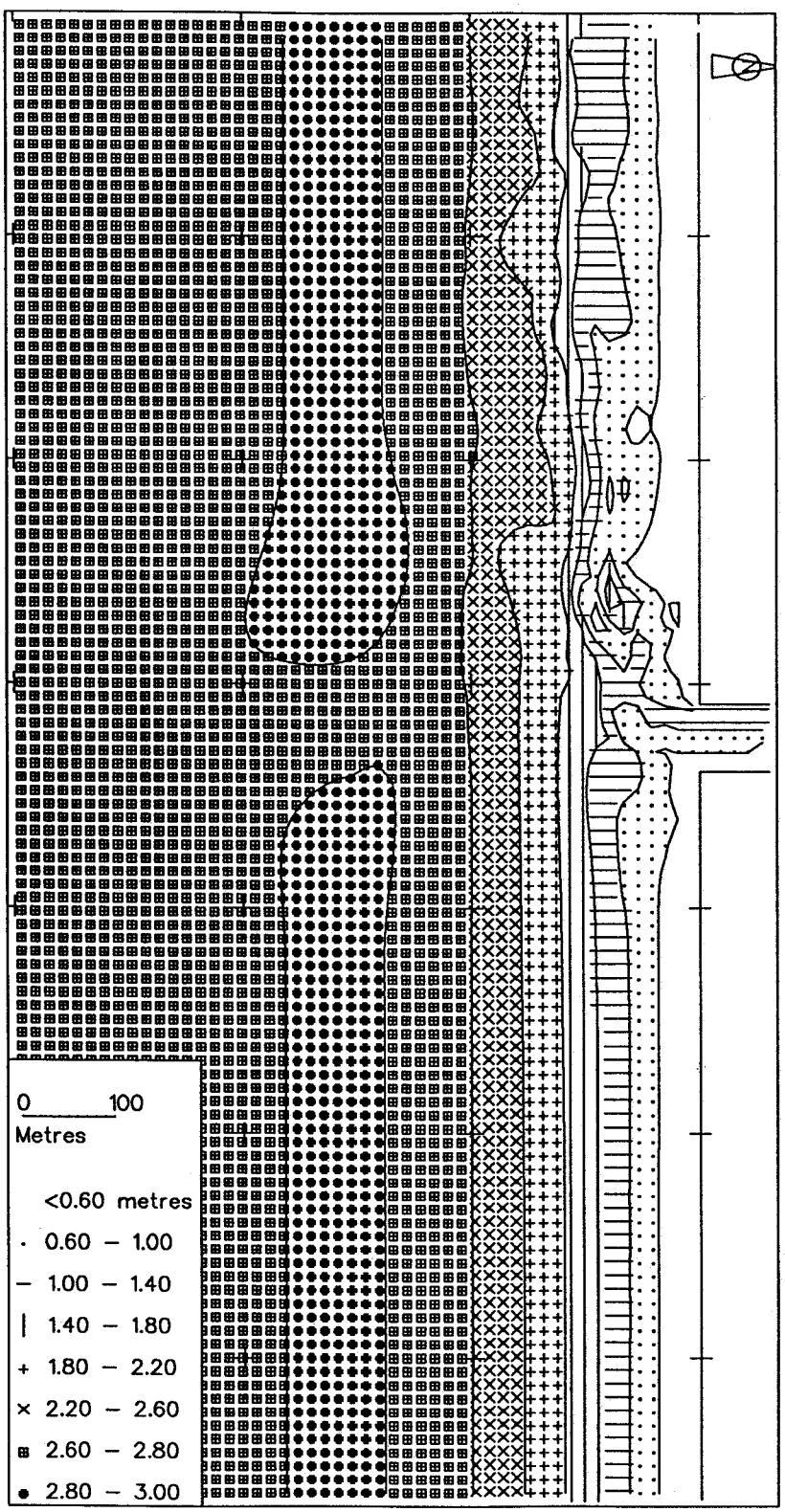

Figure 27 River outflow test case
Wave height (Hs) after 96 hours

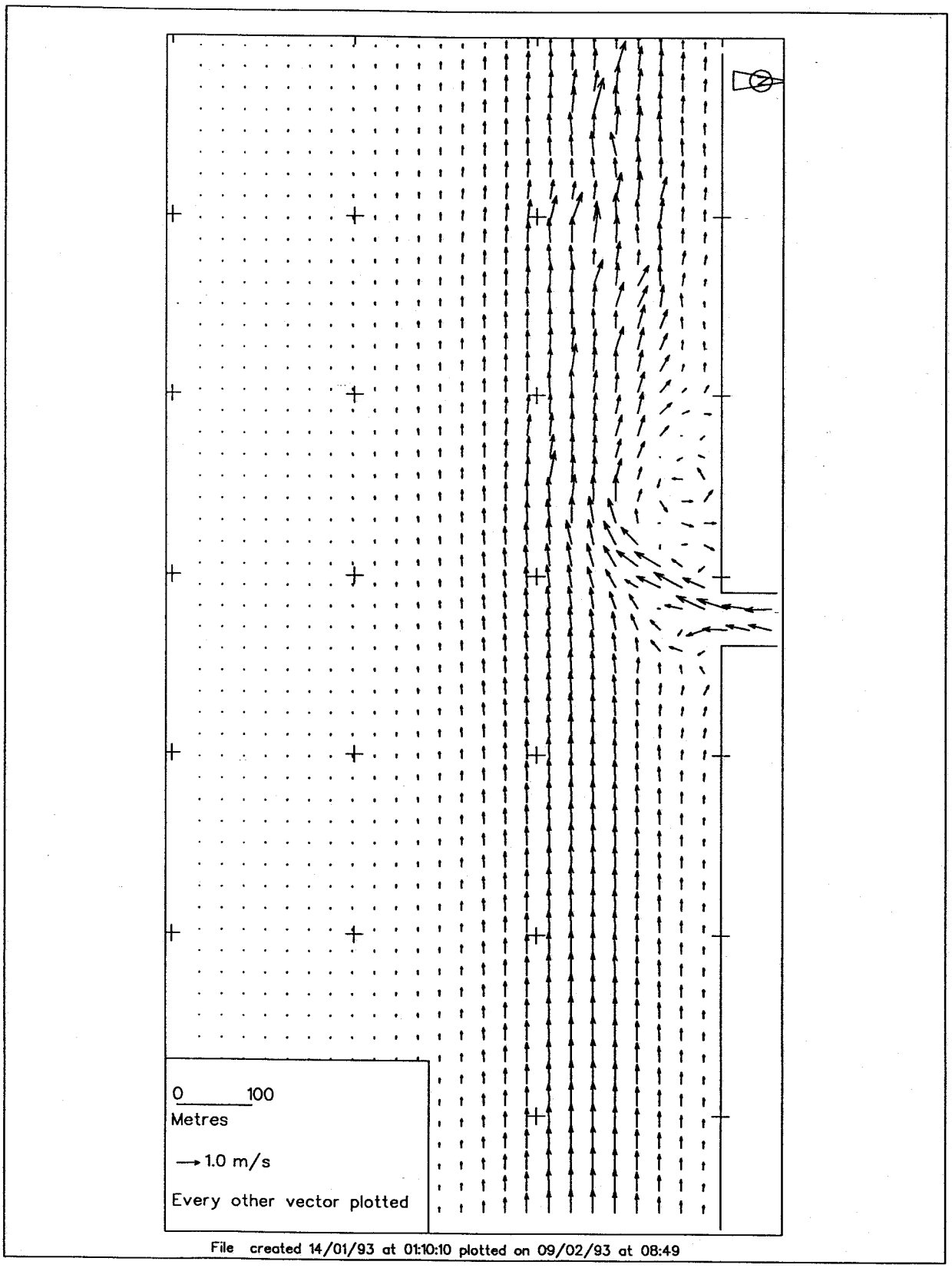

Figure 28 River outflow test case
Velocity field after 96 hours

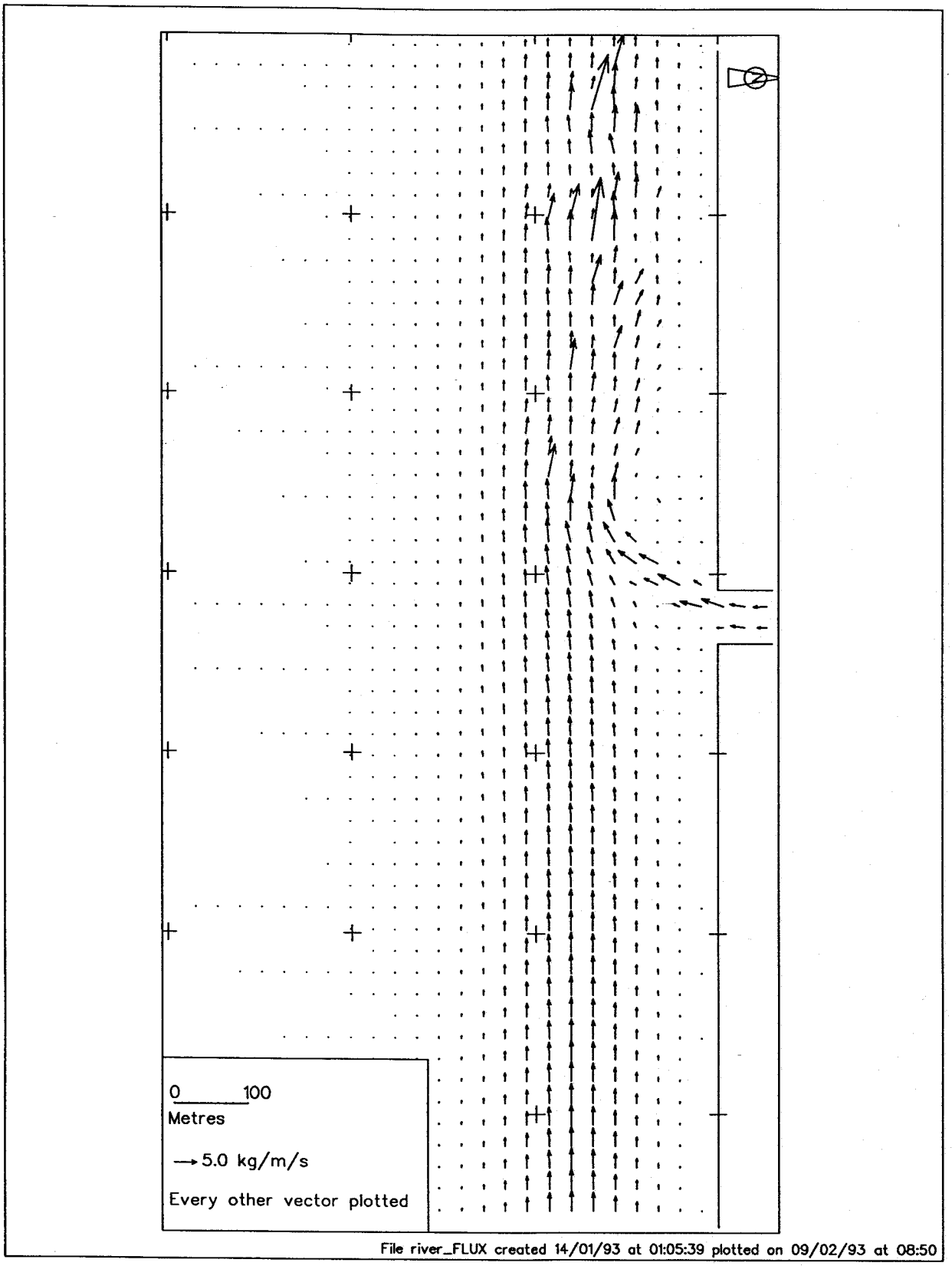

Figure 29 River outflow test case
Sand transport field after 96 hours

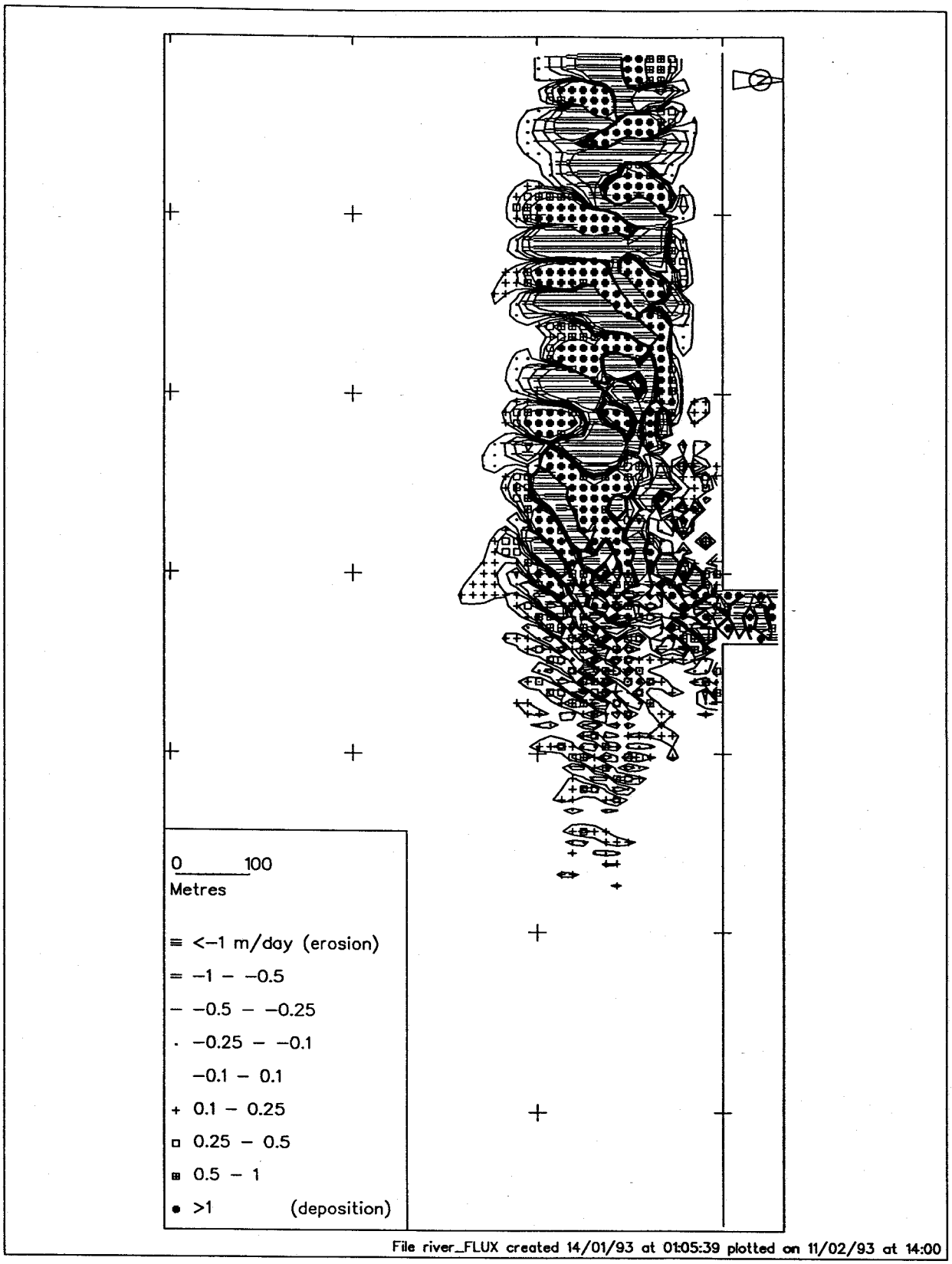

Figure 30 River outflow test case
Rate of bed level change after 96 hours

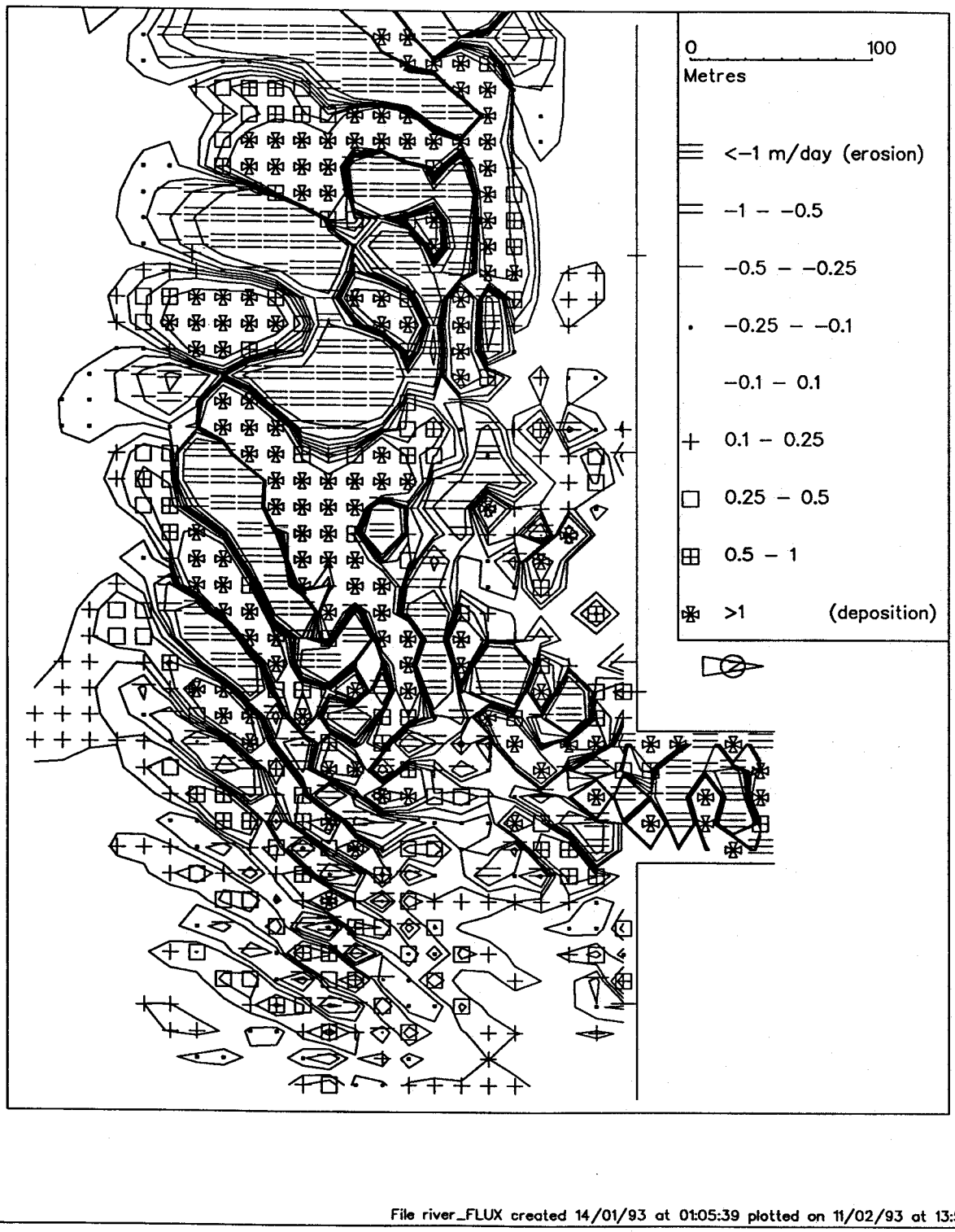

Figure 31 River outflow test case
Rate of bed level change after 96 hours
Detail of river mouth entrance

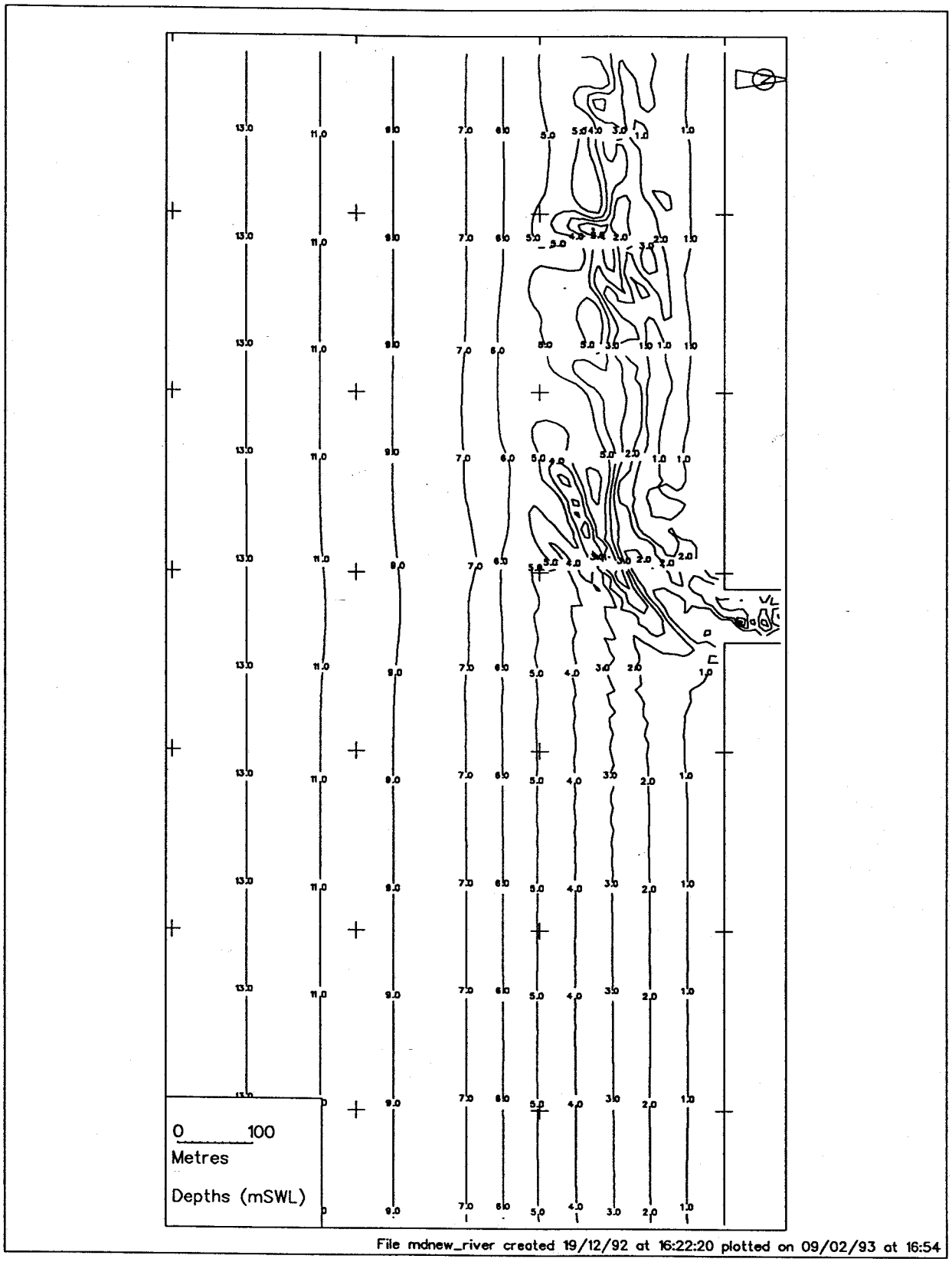

Figure 32 River outflow test case
Bathymetry after 96 hours
With convergence test, tolerance 5%

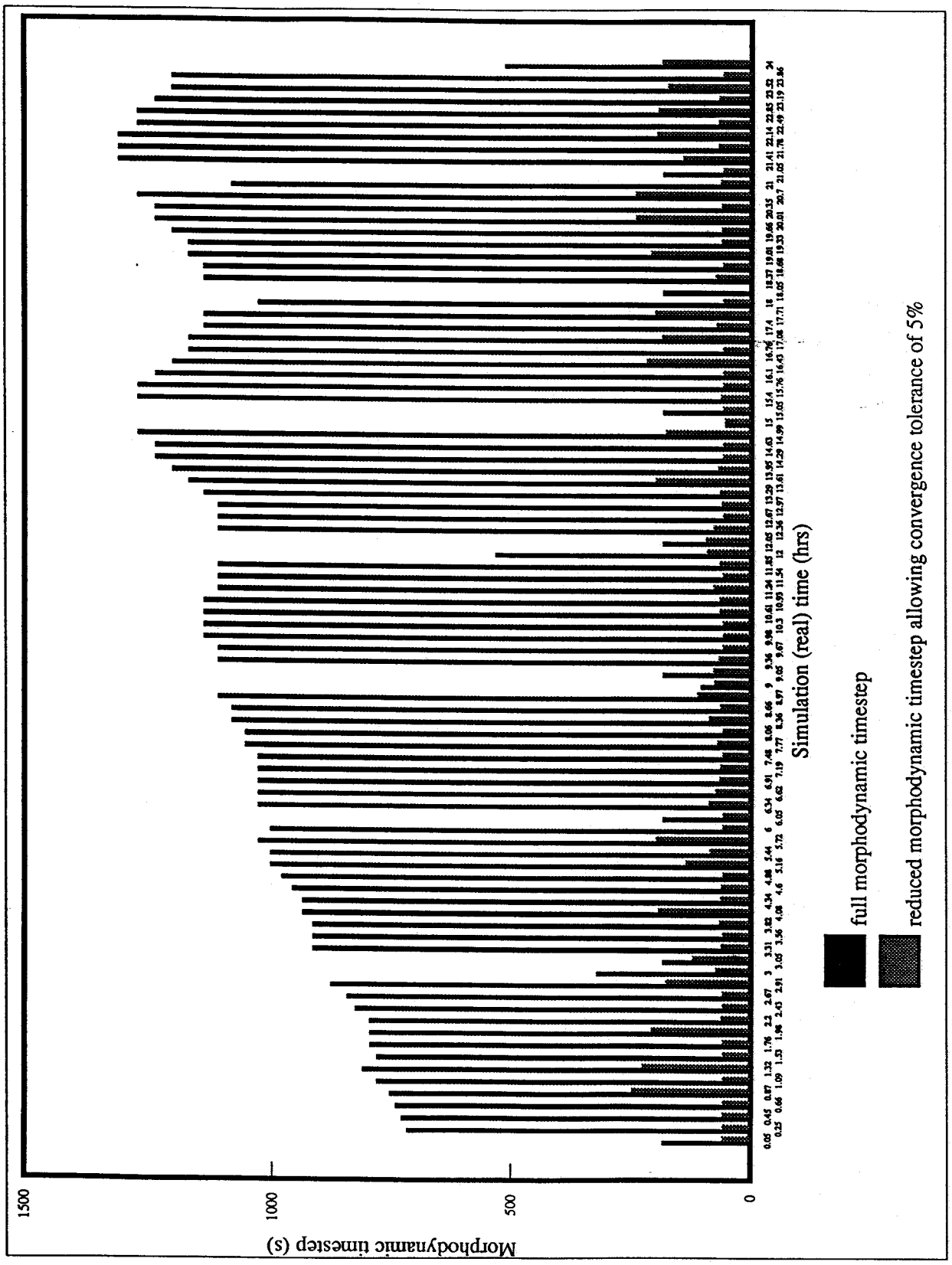

Figure 33 River outflow test case
Example of morphodynamic timestepping with convergence test

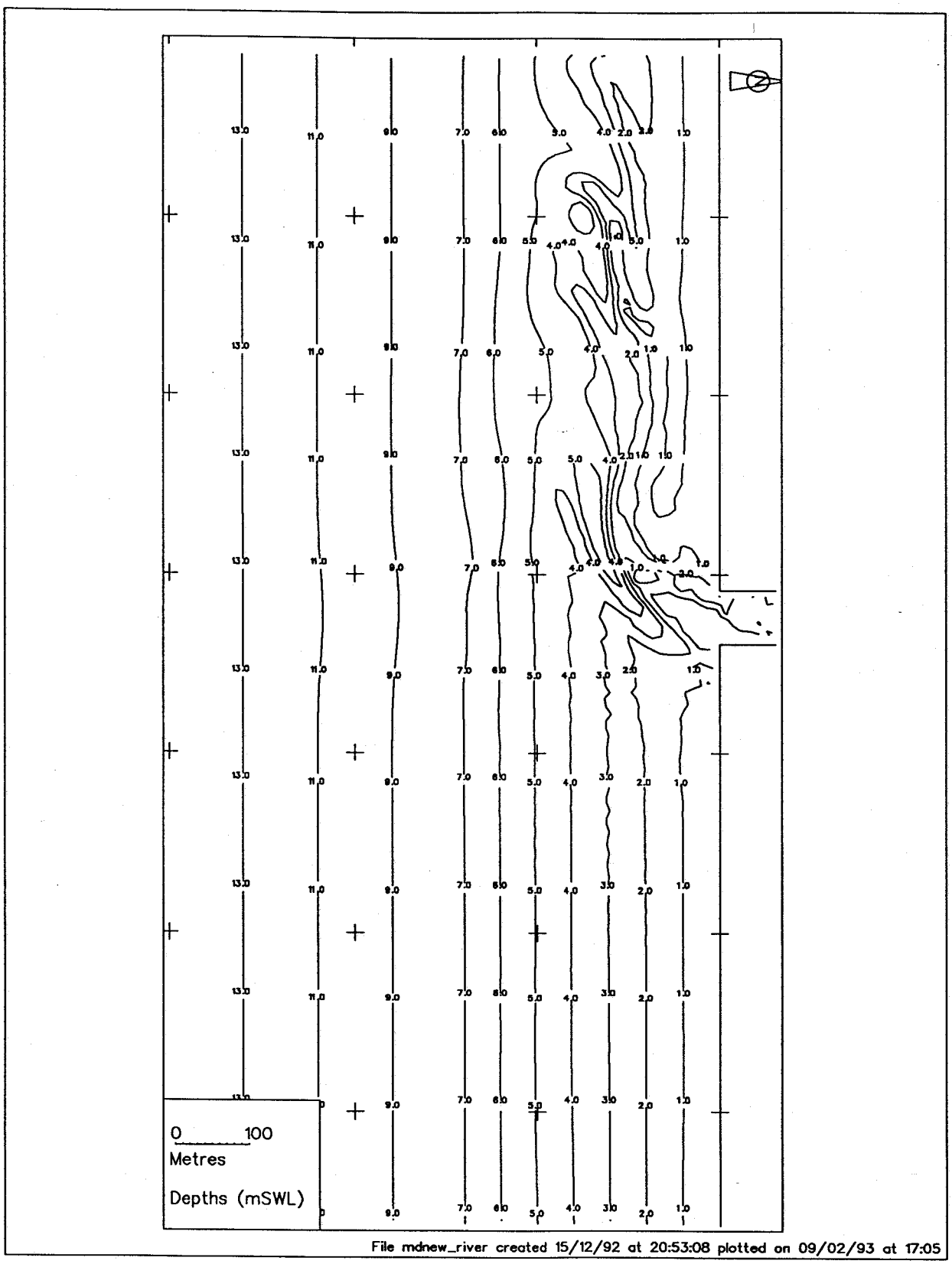

Figure 34 River outflow test case
Bathymetry after 96 hours
Bed slope effect included in sediment transport relation

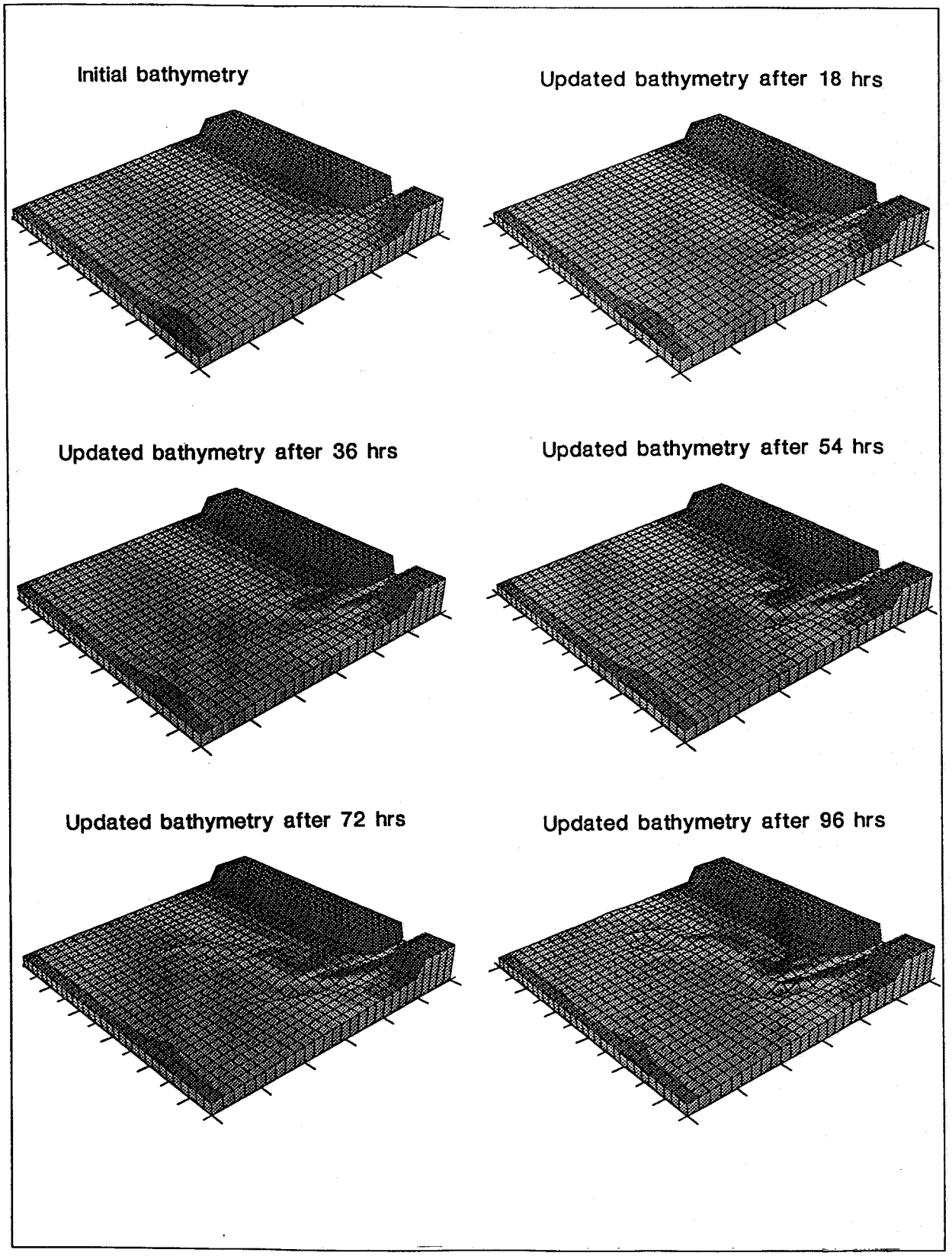

Figure 35 River outflow test case
Schematic of bed evolution over 96 hours
Bed slope effect included in sediment transport relation

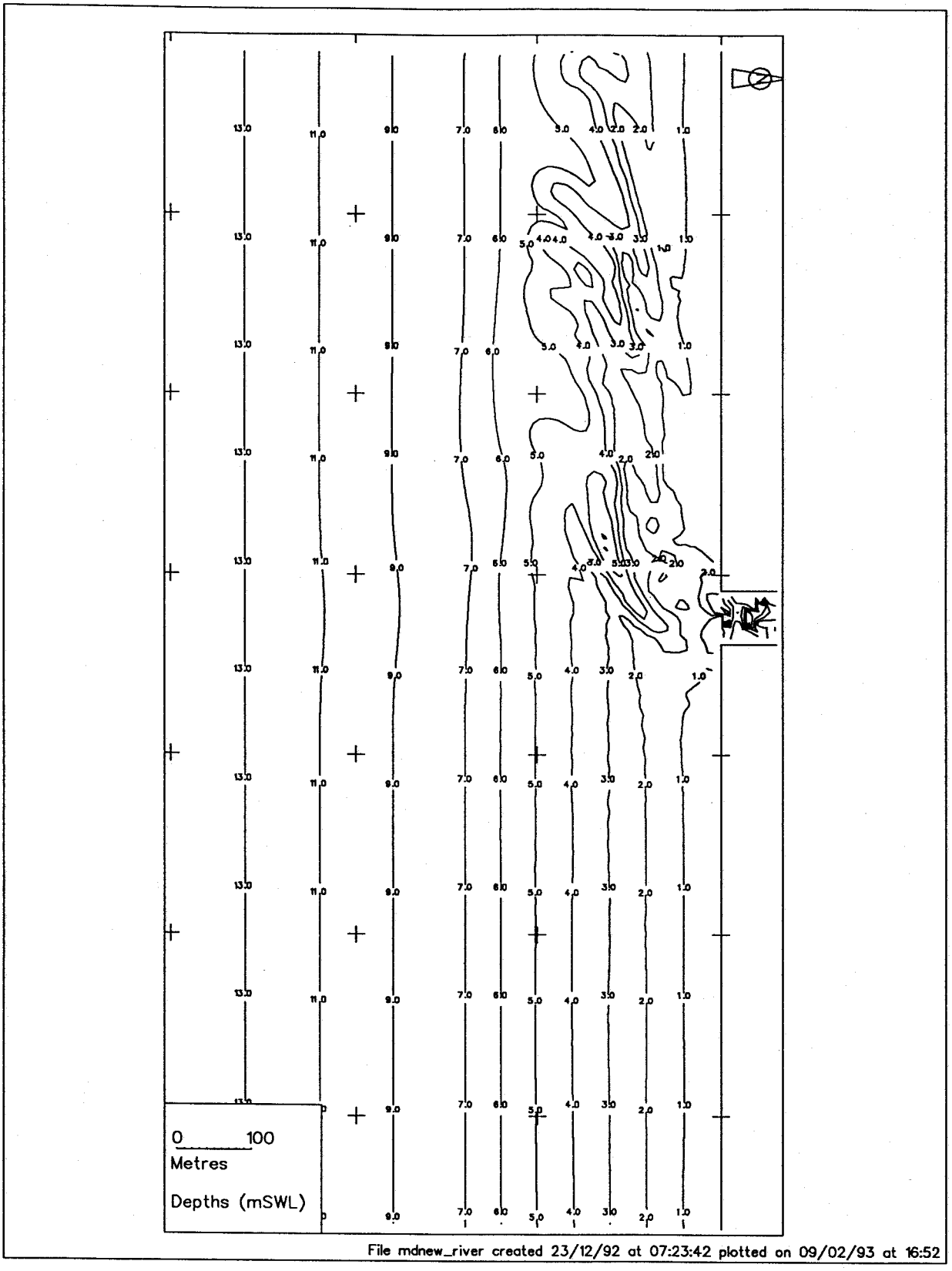

Figure 36 River outflow test case
Bathymetry after 96 hours
With bed slope effects and
alternative Lax Wendroff scheme

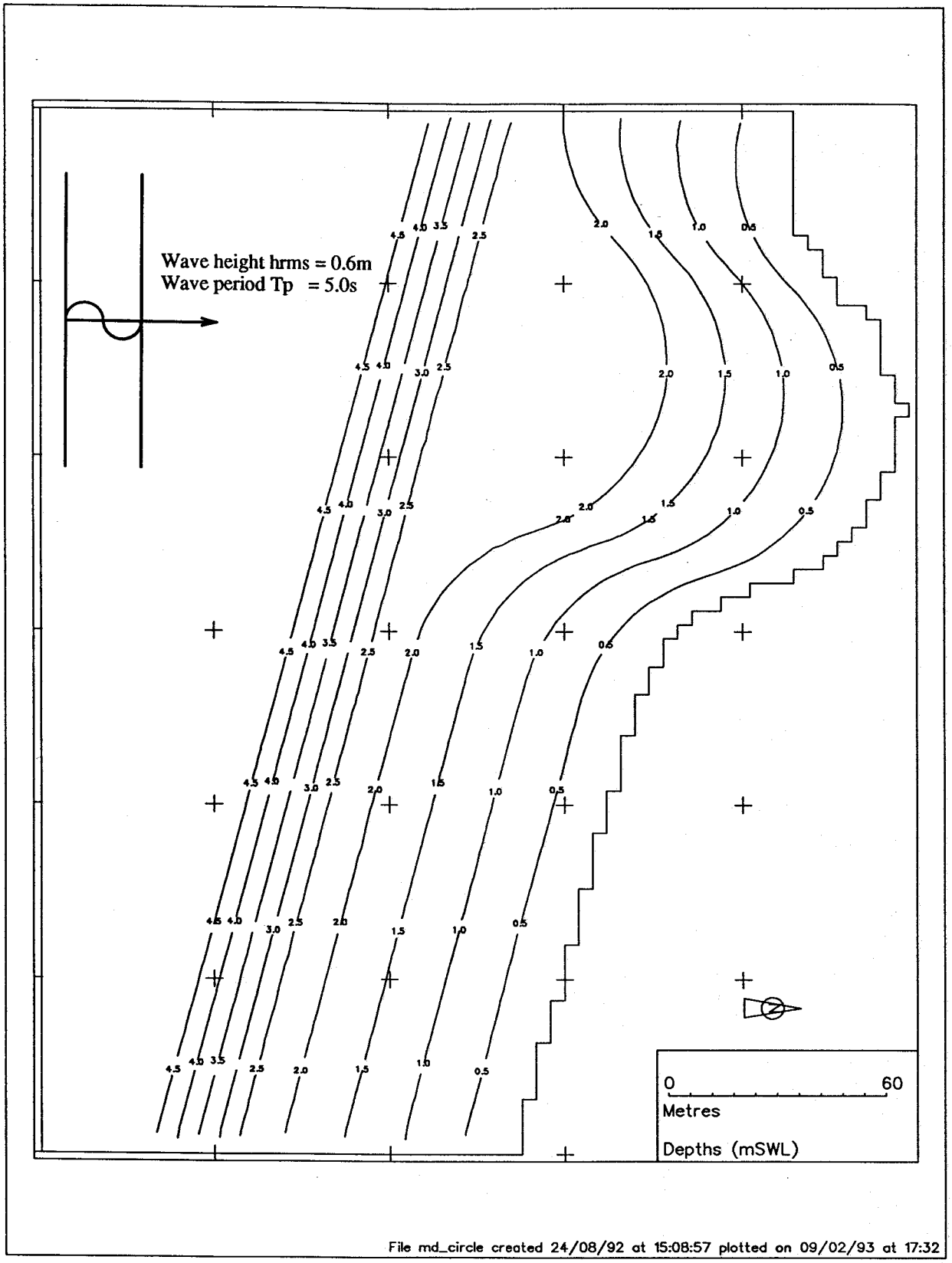

Figure 37 Semicircular bay test case
Initial bathymetry and test conditions

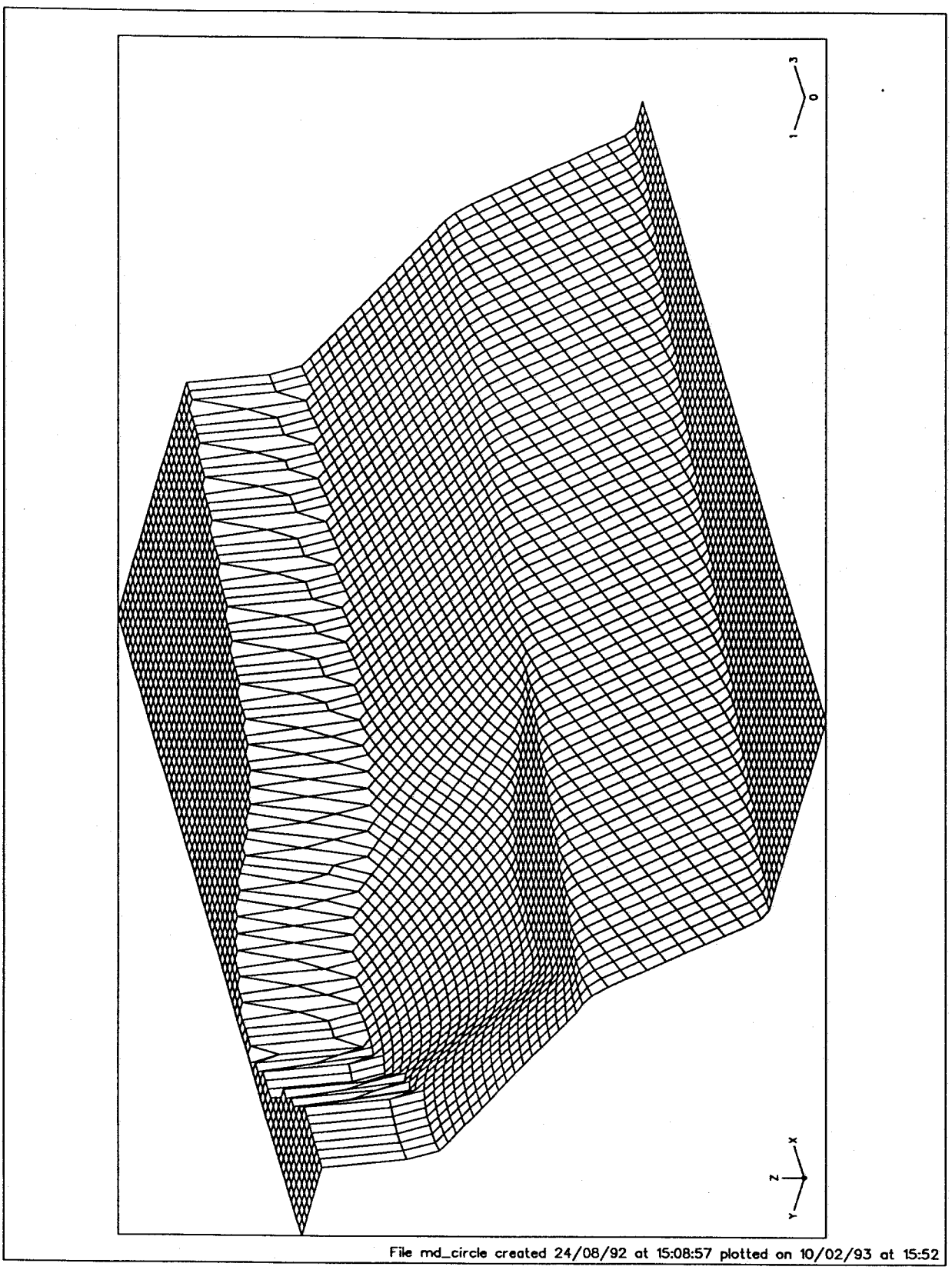

Figure 38 Semicircular bay test case
Initial bathymetry

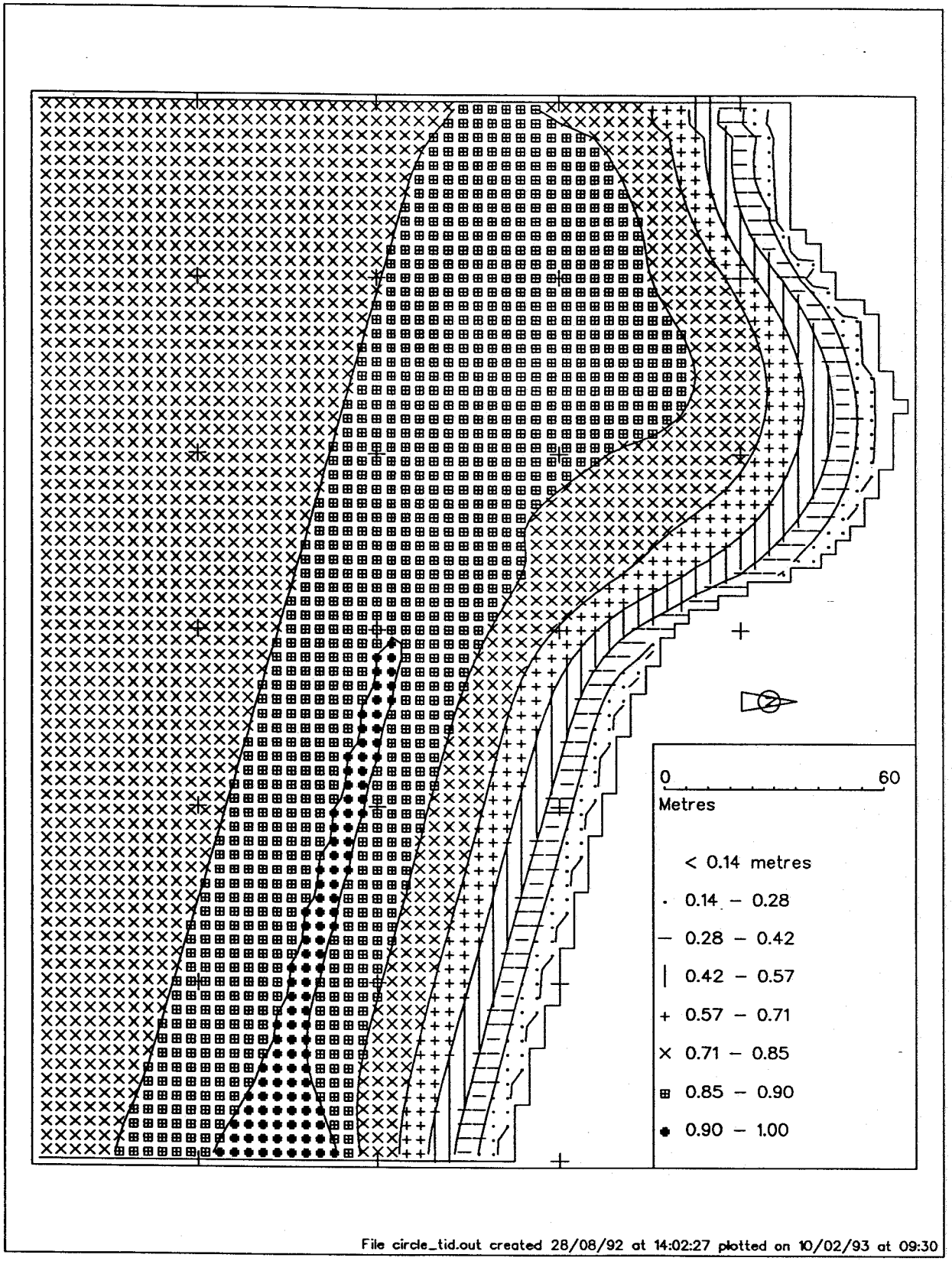

Figure 39 Semicircular bay test case
Wave height (Hs) over initial bathymetry

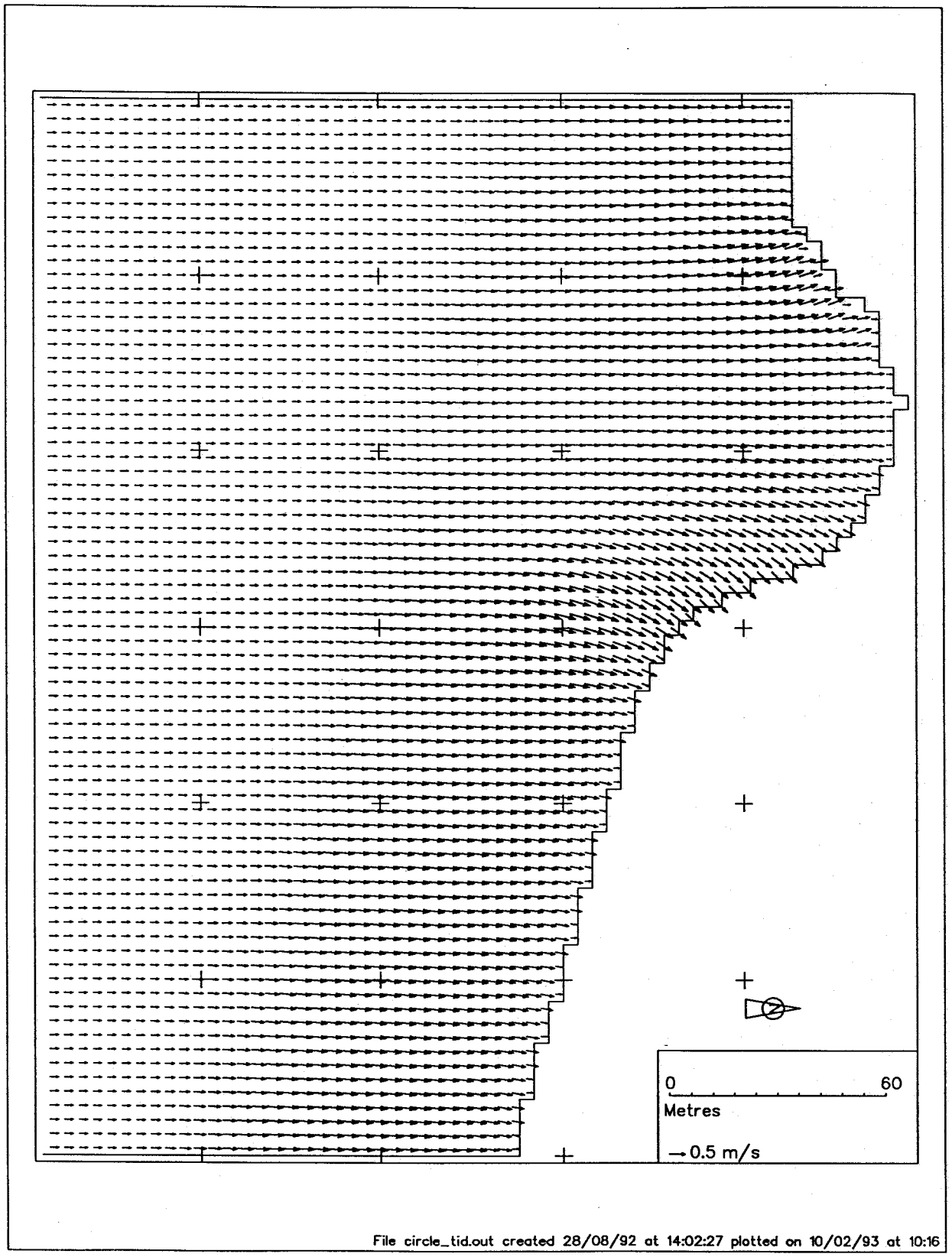

Figure 40 Semicircular bay test case
Wave orbital velocity over initial bed

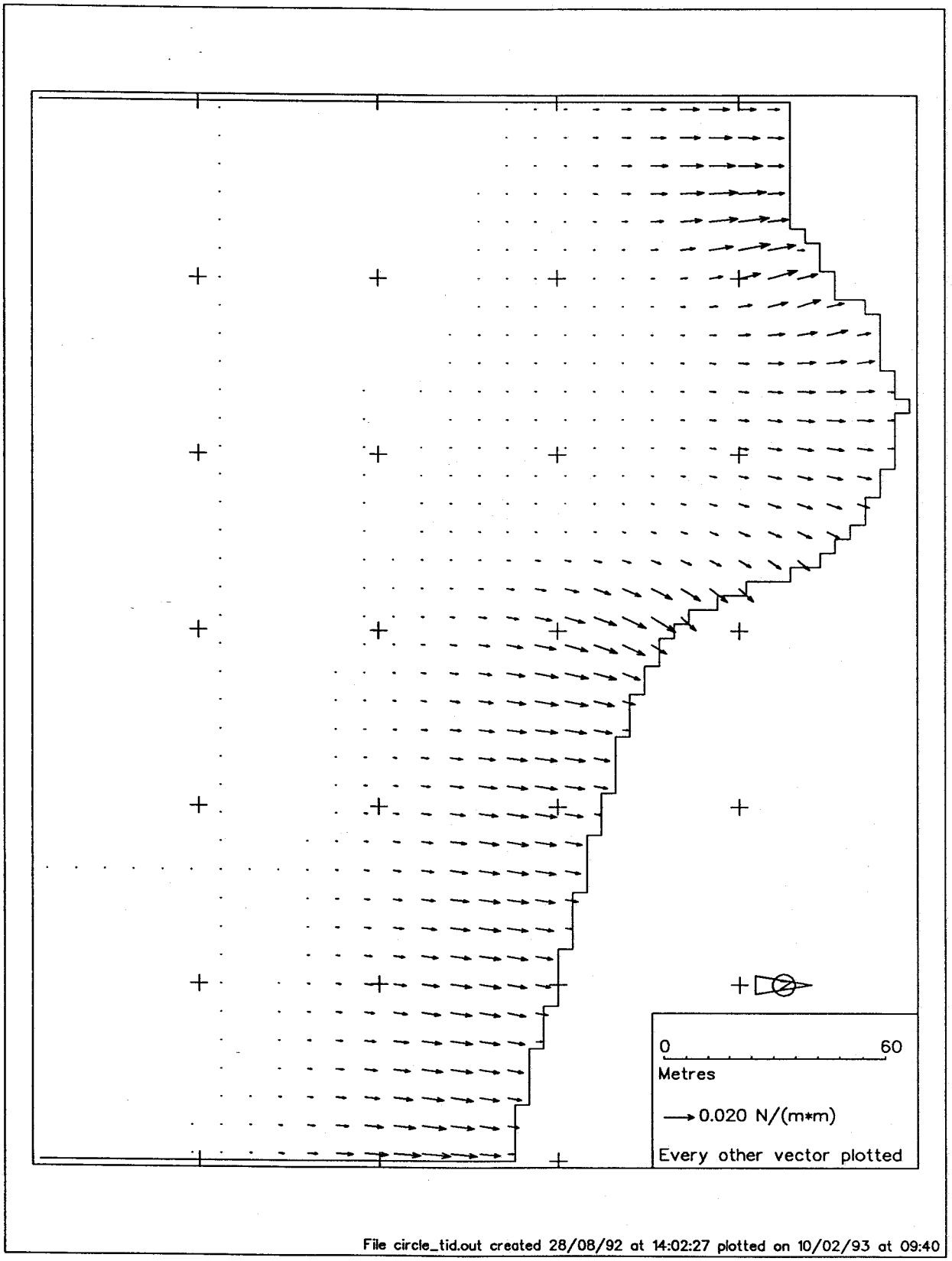

Figure 41 Semicircular bay test case
Wave breaking stress over initial bed

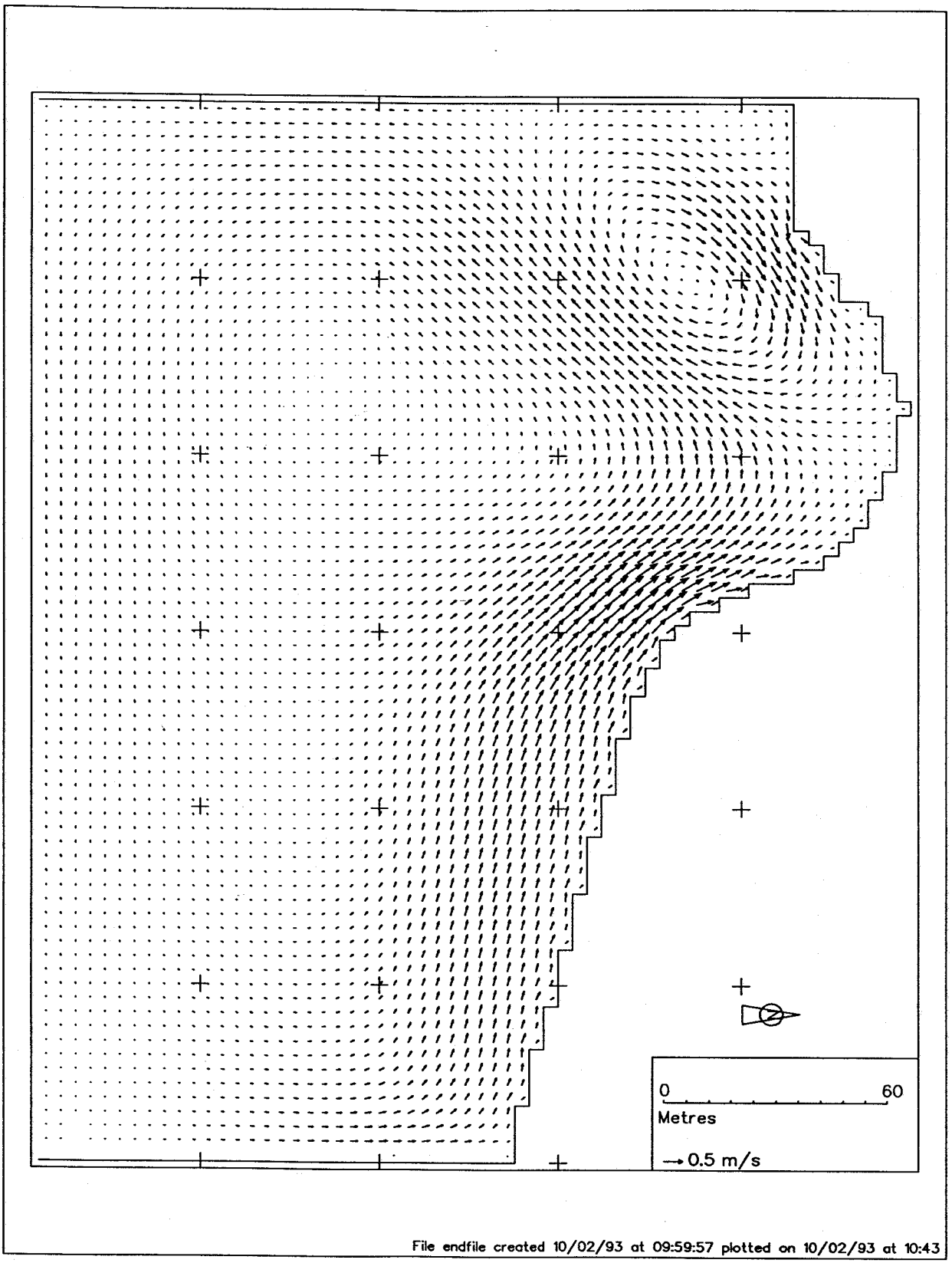

Figure 42 Semicircular bay test case
Velocity field over initial bathymetry

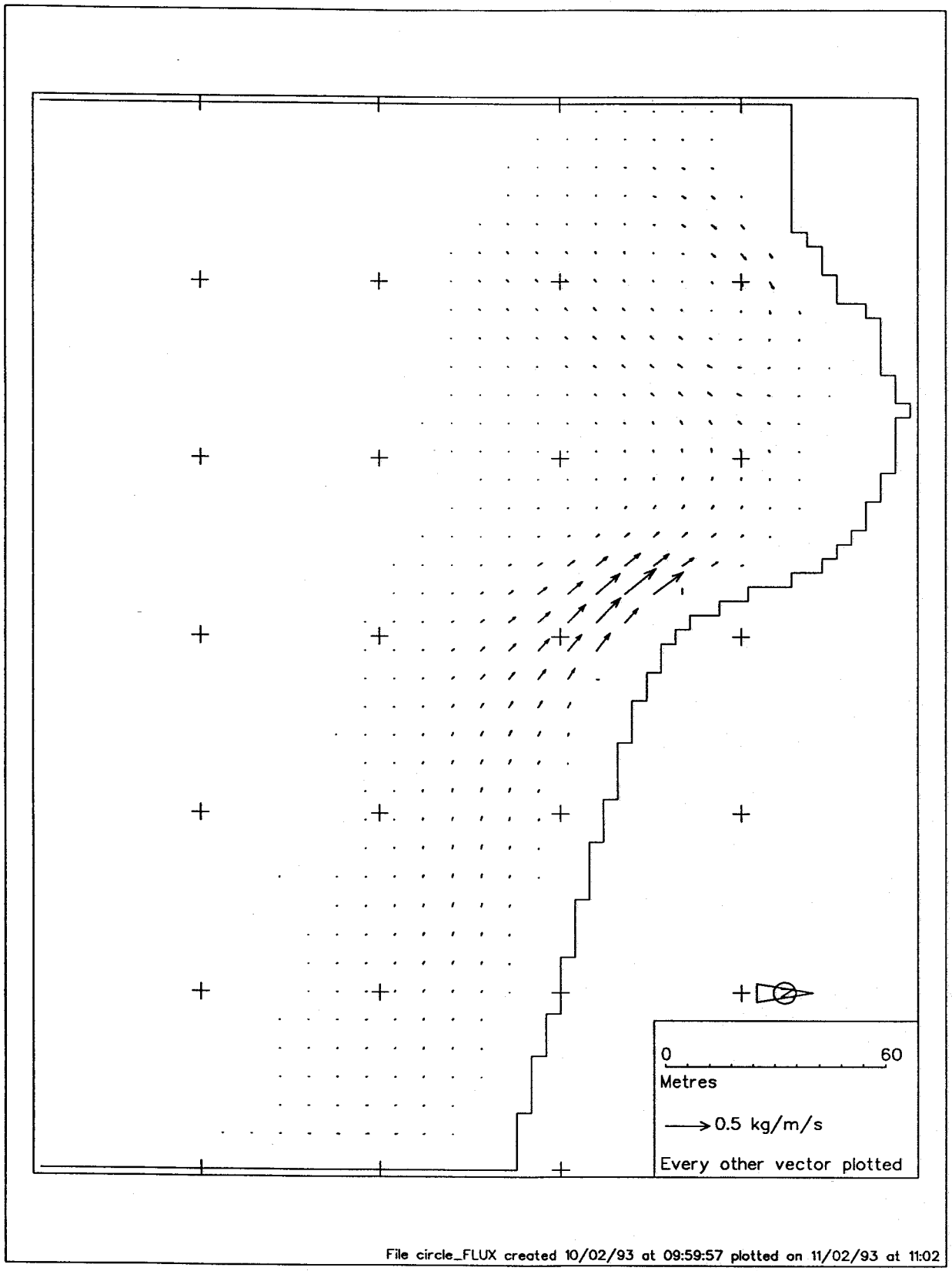

Figure 43 Semicircular bay test case
Sand transport field over initial bed

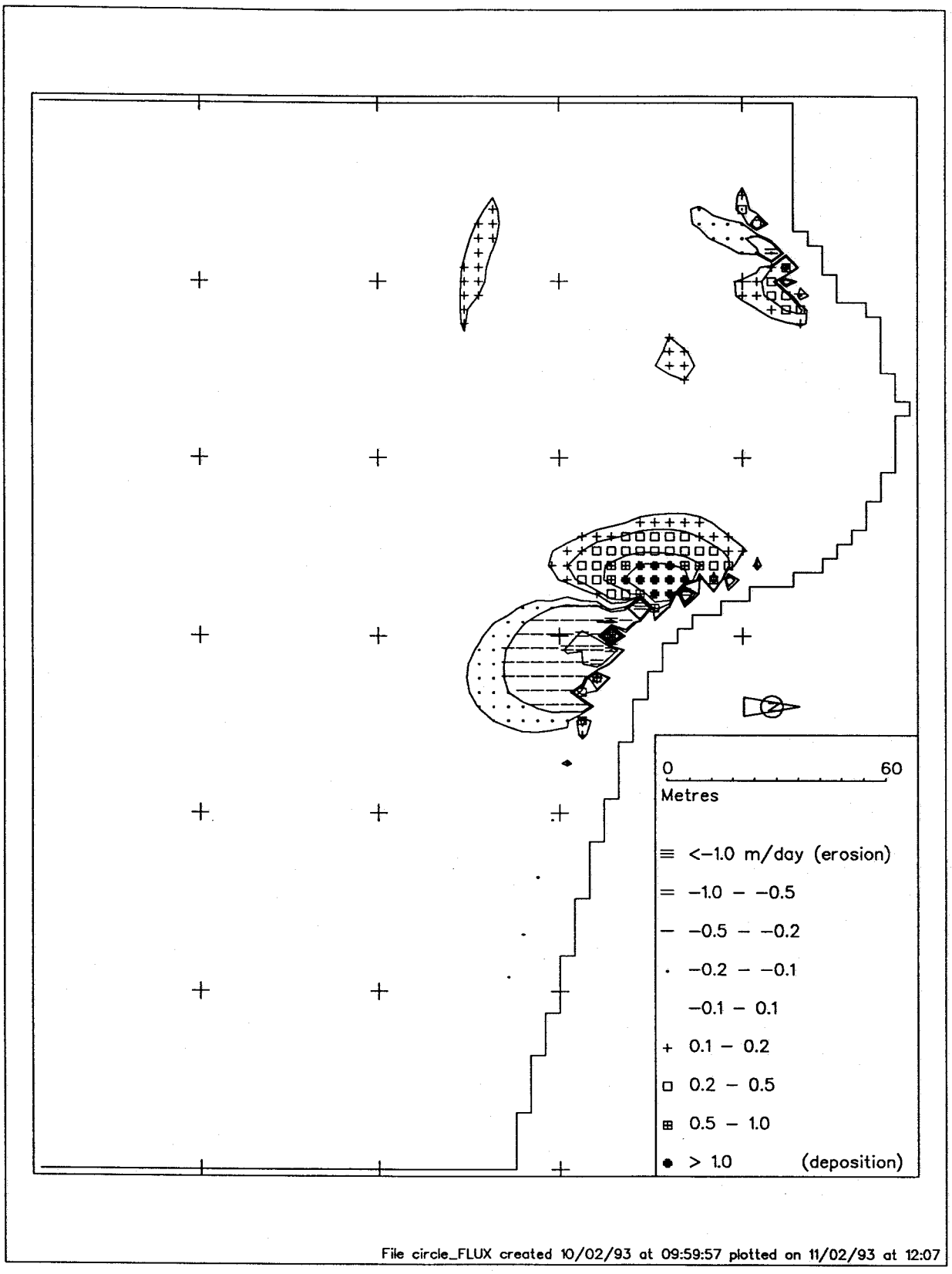

Figure 44 Semicircular bay test case
Initial rate of bed level change

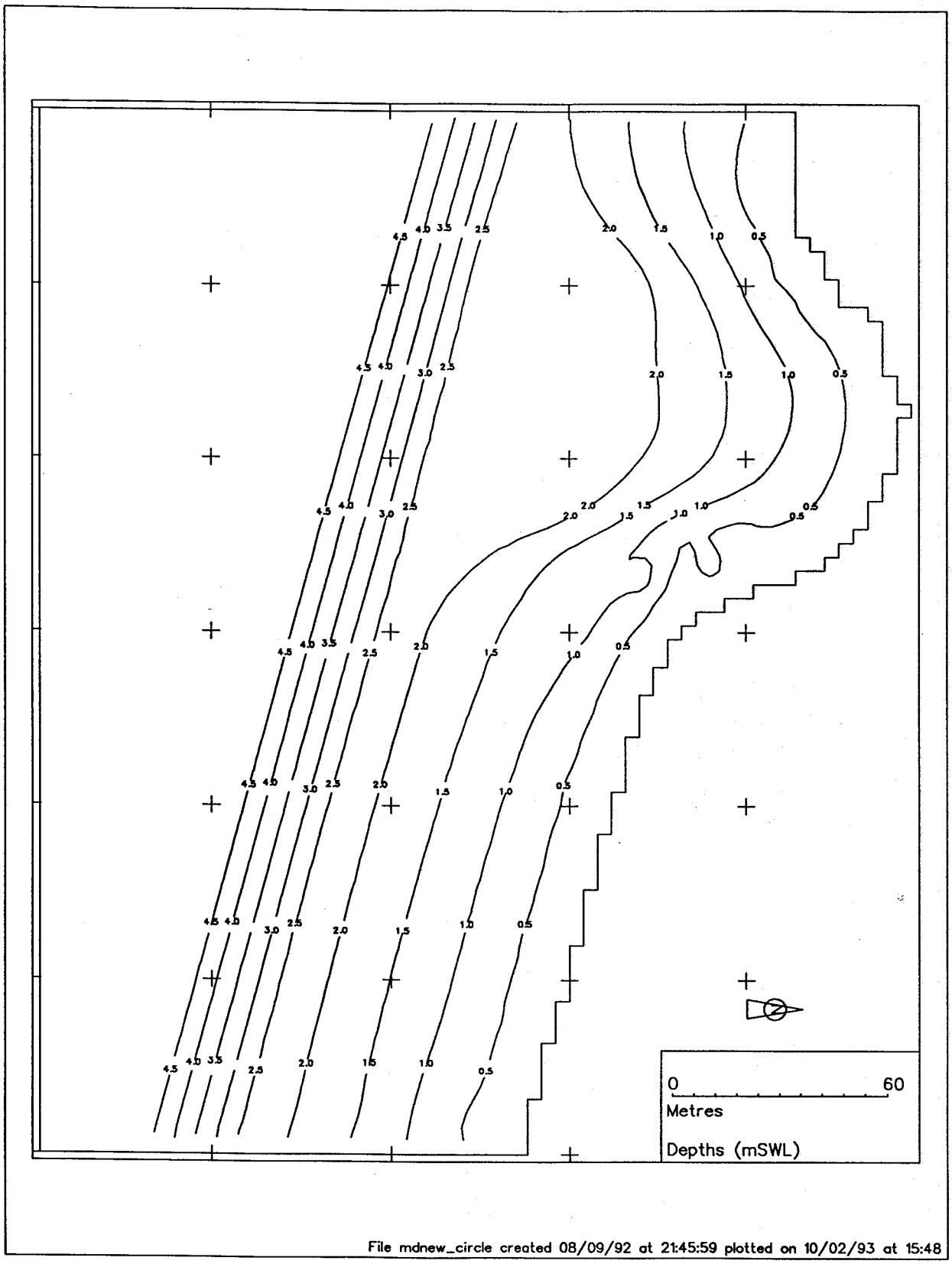

Figure 45 Semicircular bay test case
Bathymetry after 36 hours

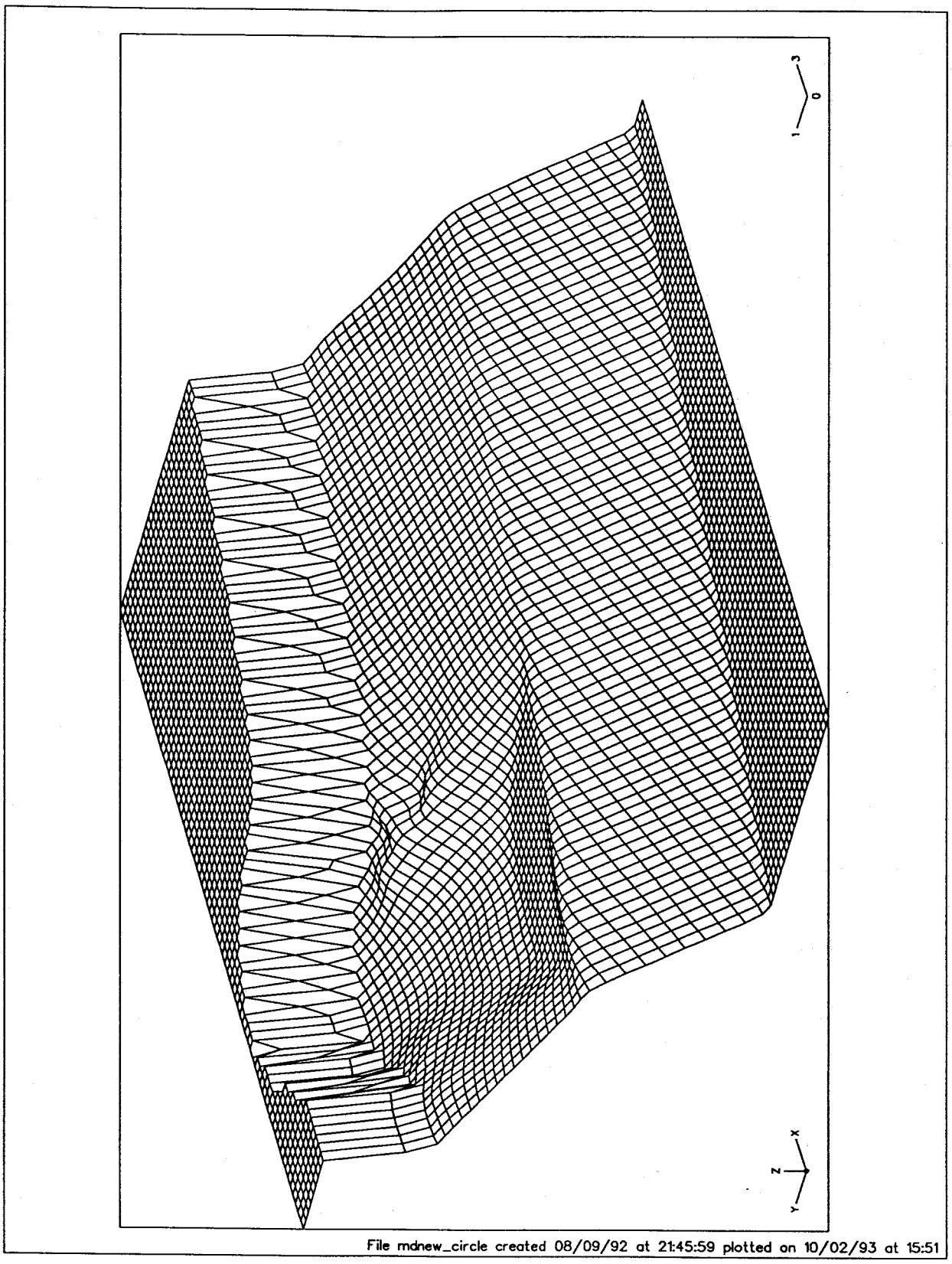

Figure 46 Semicircular bay test case
Bathymetry after 36 hours

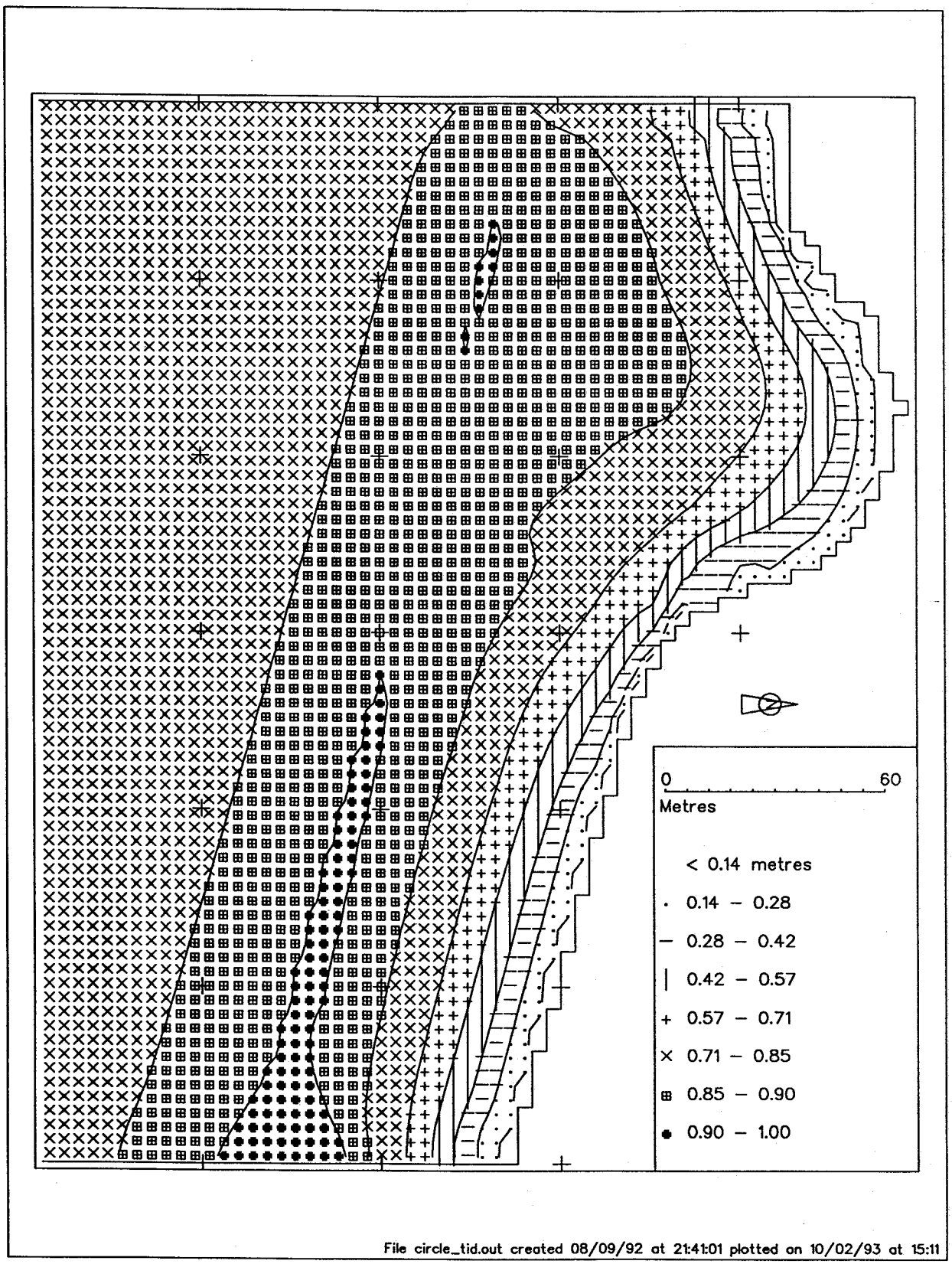

Figure 47 Semicircular bay test case
Wave height (Hs) after 36 hours

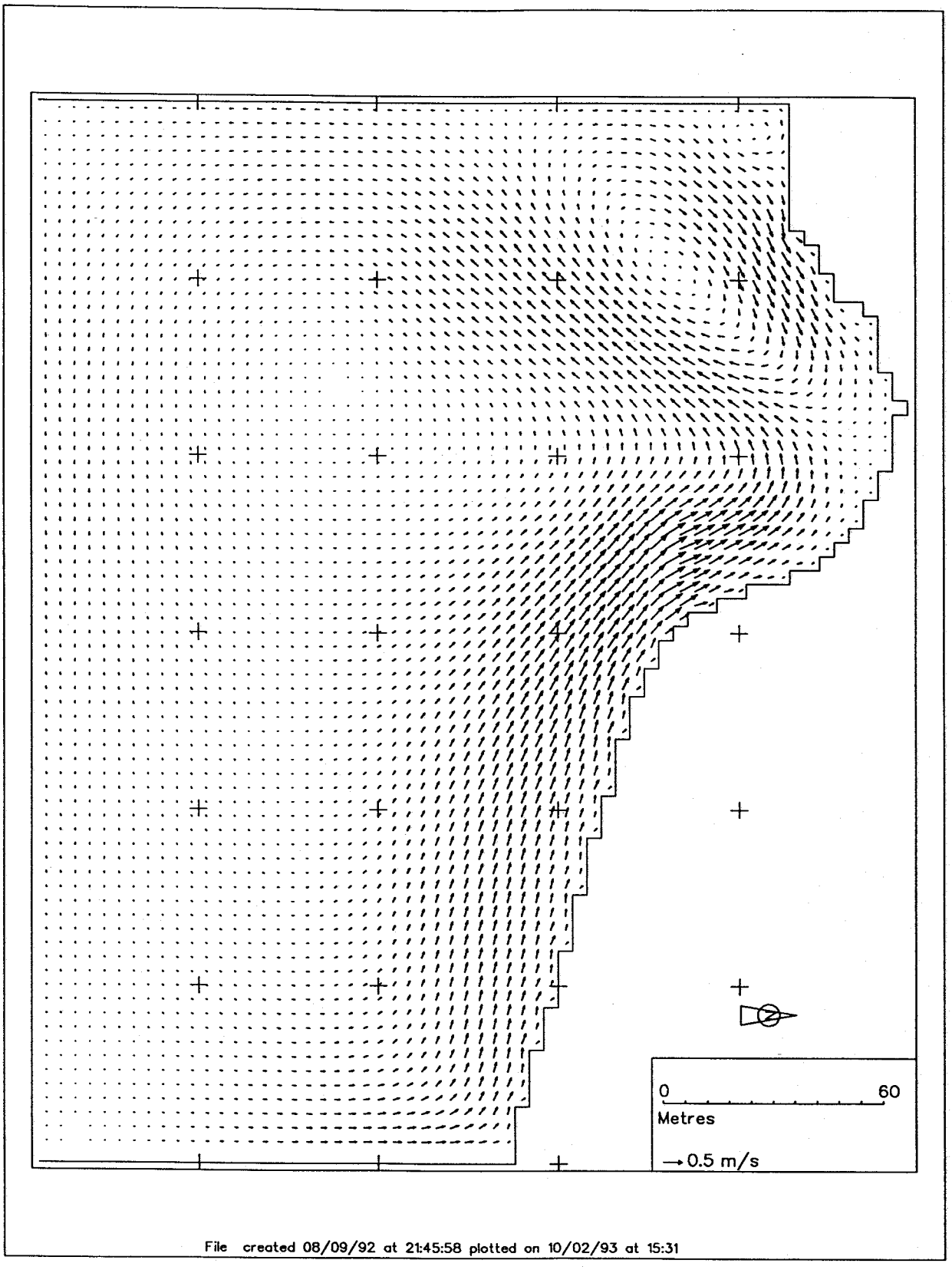

Figure 48 Semicircular bay test case
Velocity field after 36 hours

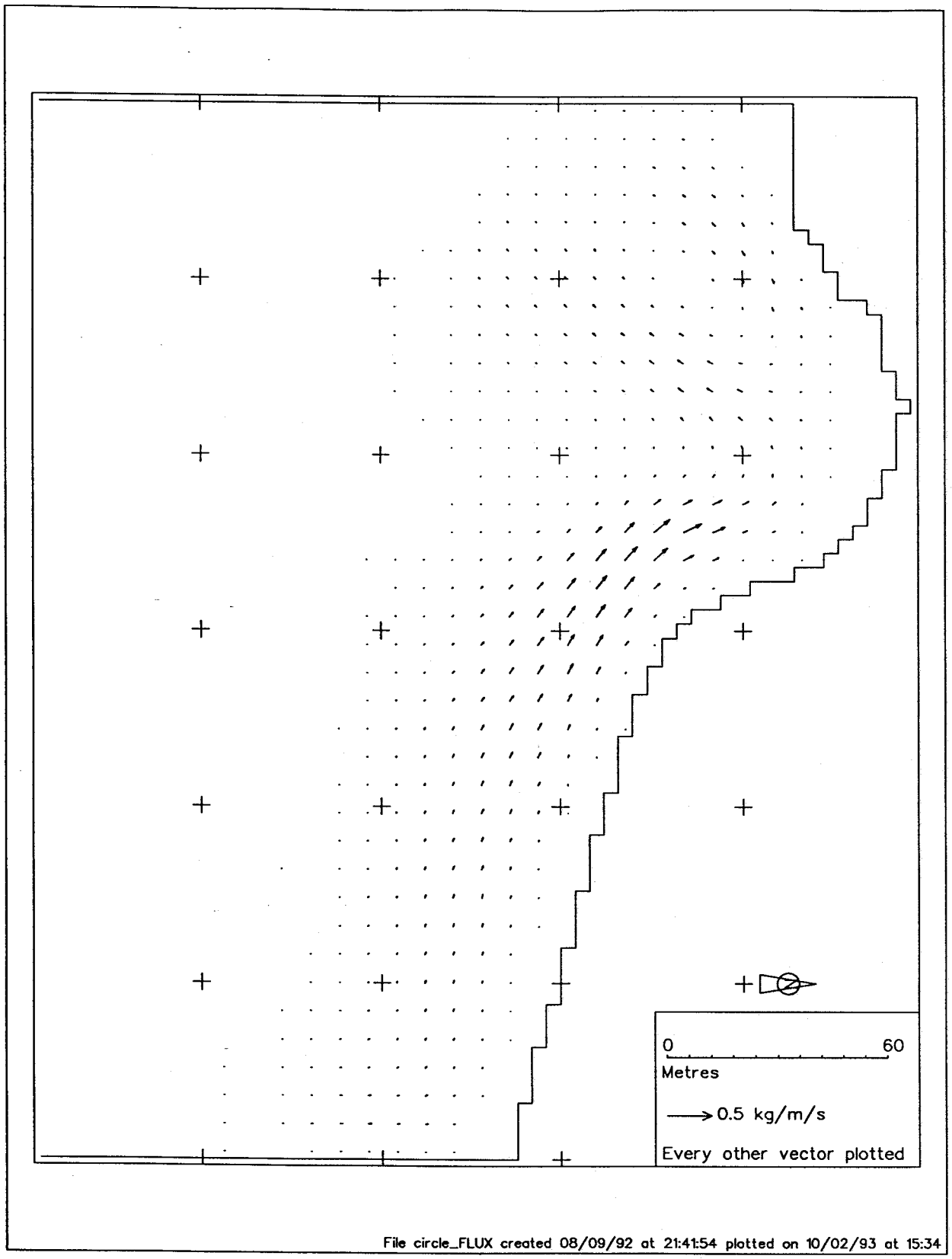

Figure 49 Semicircular bay test case
Sand transport field after 36 hours

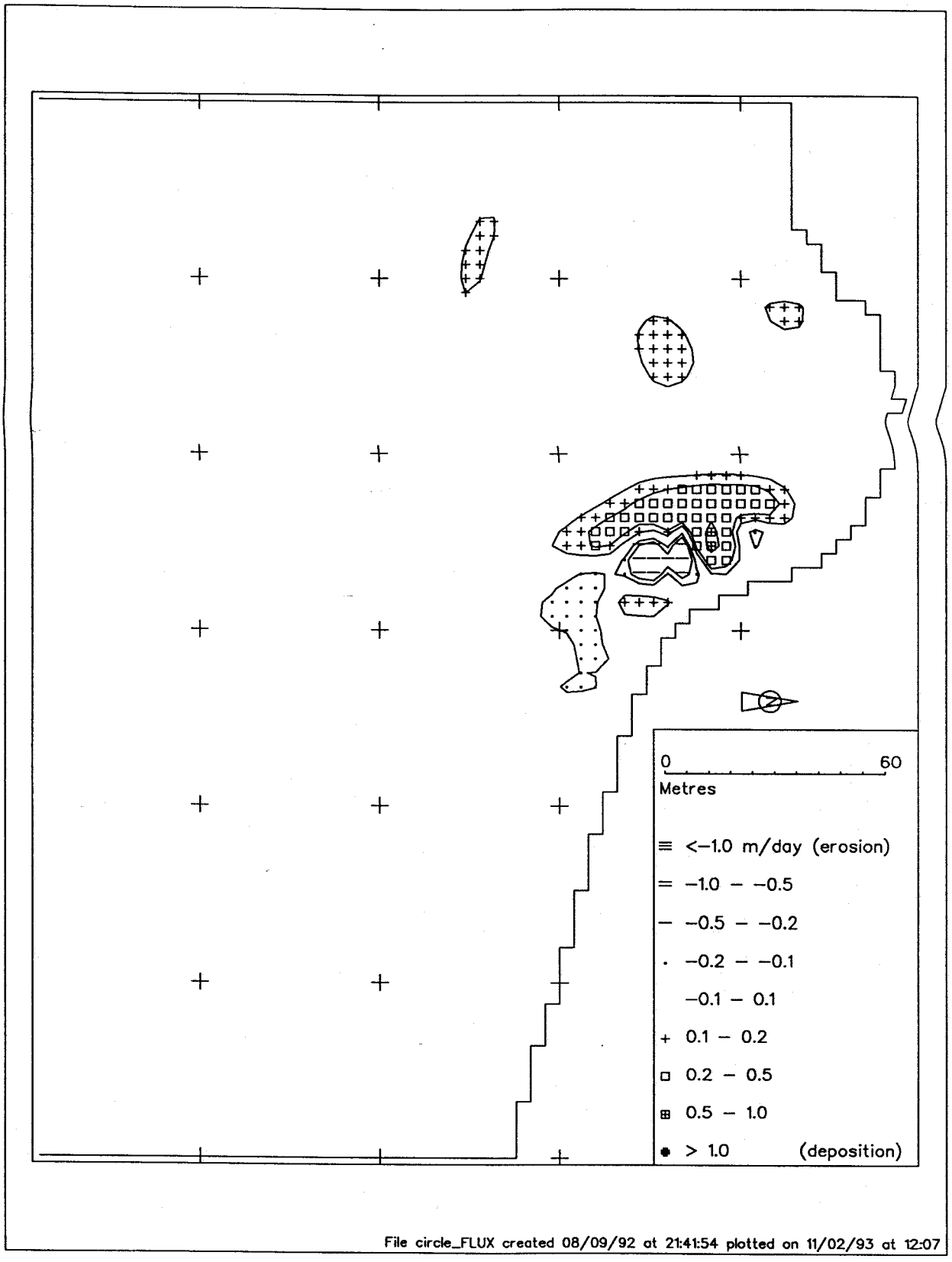

Figure 50 Semicircular bay test case
Rate of bed level change after 36 hours

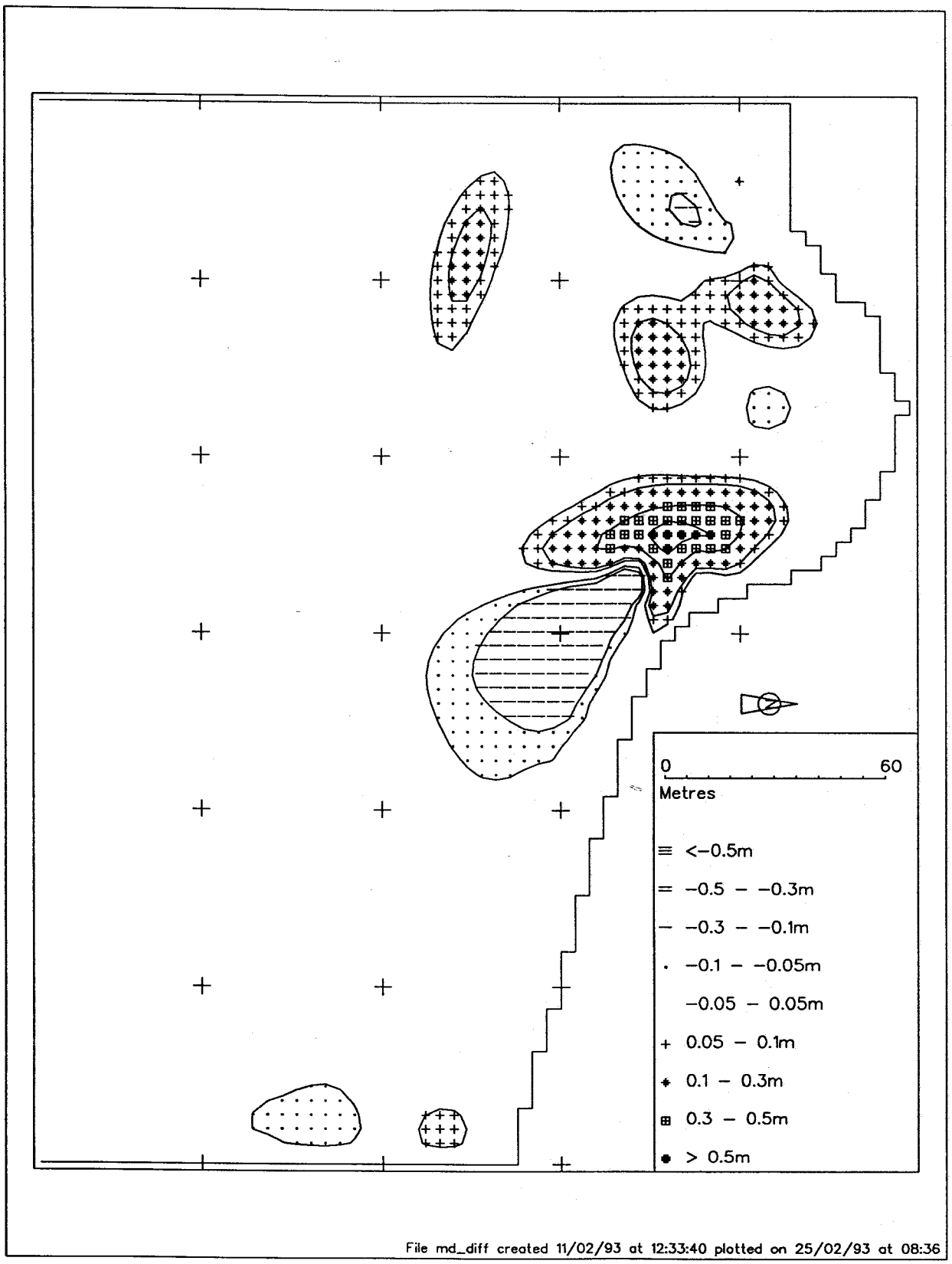

Figure 51 Semicircular bay test case
Bed level changes over 36 hours

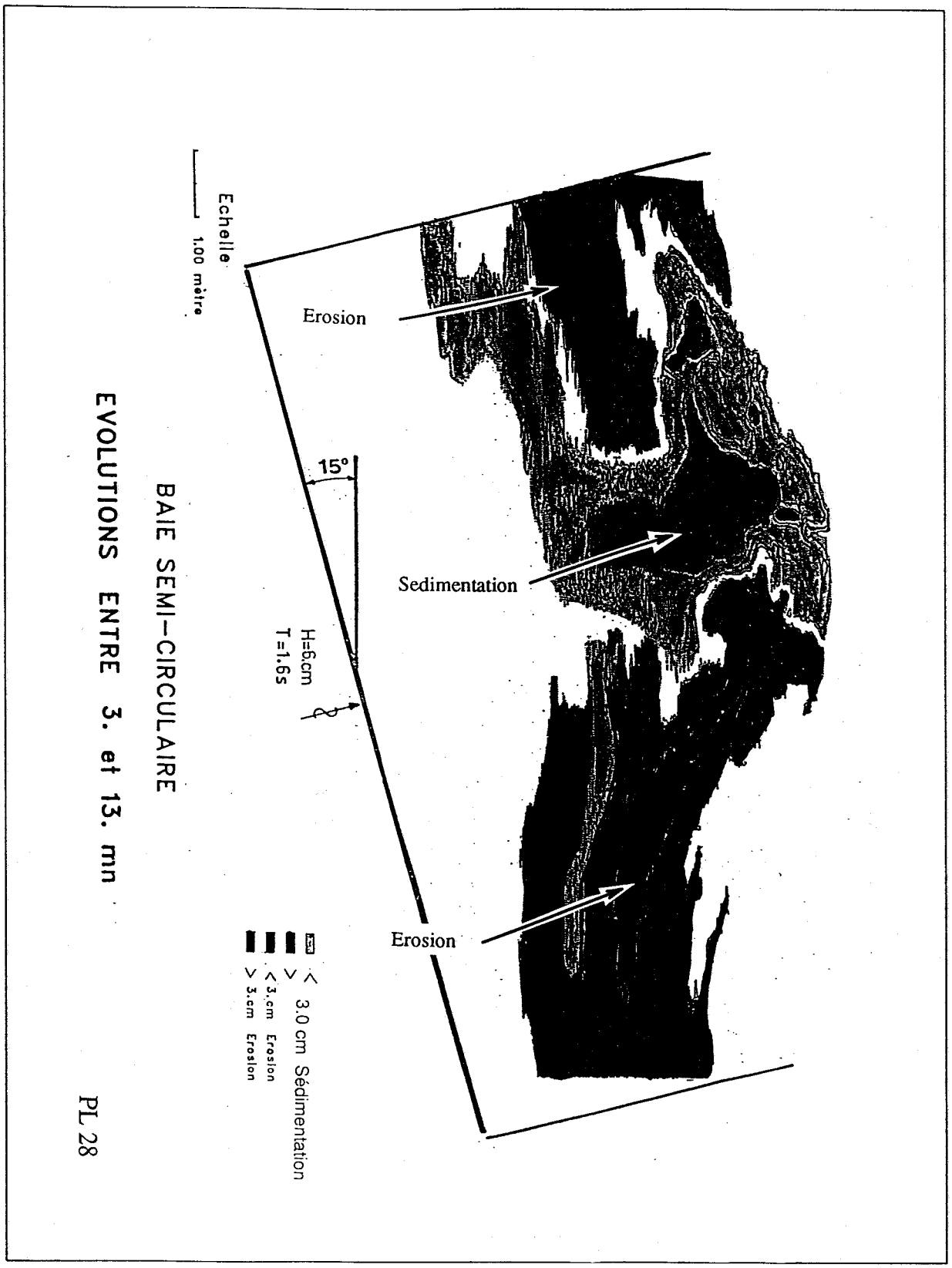

Figure 52 Semicircular bay test case
Physical model bed level changes

Appendices

Appendix 1

Description of FDWAVE model

Appendix 1 Description of FDWAVE model

This appendix describes a computational wave transformation model incorporating the combined effects of refraction and diffraction of waves using a time-independent finite-difference marching technique. This method has several potential advantages over alternative techniques. The inclusion of diffraction should give improved predictions of wave parameters compared with pure refraction methods in areas of irregular bathymetry where diffraction effects are strong. The method is also computationally quicker than most alternative refraction-diffraction methods, with the possibility of further increasing computational speed by the ability to use coarser grid sizes. Directional wave spectra, current refraction effects, and dissipation by bottom friction and wave breaking can be modelled. The model is designed for wave propagation in the open sea, rather than where structures are present. Wave directions are limited to a certain range either side of the forward grid direction, usually about 40° from this forward grid direction, but it depends upon the grid being used.

The model is based upon a theoretical approach originally put forward by Battjes (Reference 1) and extended by Yoo and O'Connor (References 2 and 3). The HR FDWAVE model uses the same theoretical basis as Yoo and O'Connor but adopts a different numerical modelling approach. Yoo and O'Connor used a time-dependent formulation which can require a considerable number of time steps to reach a steady state. The present model is time-independent and gives the steady state solution directly. The theory and equations used in the model are described in detail in Reference 4.

The sea area under study is represented by a grid composed of rectangular or square elements. The positive y direction is chosen to be in the main propagation direction of the waves (roughly perpendicular to the coastline). The method of solution uses a row-by-row marching technique with a predictor and corrector calculation at each row. The input values of wave height, period and direction are specified at each grid element on the offshore row. The finite-difference representation of the governing equations is then used to make a calculation of these parameters on the second row. This is the predictor step. Using these values, a more accurate estimate of the y-derivatives can be made, and the calculation of parameters on row two is repeated with these 'corrected' y-derivatives. This corrector step can, in principle, be repeated an indefinite number of times, but in most cases one calculation is found to be sufficient. The whole predictor-corrector process is then repeated for row three, and the process continues until the last row, furthest inshore, is reached. The method employed is explicit throughout.

The model has been tested on a circular shoal bathymetry which provides quite a severe test case (Reference 4). Classical ray theory predicts a cusped caustic for this problem and therefore, in nature, strong diffraction effects are present. It was found that the finite-difference scheme gave numerically unstable results, and as a consequence much of the work in developing the model has been devoted to devising modifications to ensure stability. The governing equations do not readily lend themselves to an analytical investigation of stability, and therefore a number of ad hoc approaches have been tried. The most successful of these has involved forming averages of

various quantities with neighbouring values along each row, according to the formula,

$$b_{n,i}=(\lambda b_{o,i-1}+2(2-\lambda)b_{0,i}+\lambda b_{o,i+1})/4$$

in which b denotes any predicted wave variable, and the subscripts o and n denote old (before averaging) and new (after averaging) values respectively. λ is an input parameter, between 0 and 2, which denotes the 'strength' of the averaging process. For example if $\lambda=1$ then the new value of b for the ith value in the row is half of the old ith value of b plus a quarter of each of the values either side of it. For $\lambda=0$ there is no averaging between values and $b_{n,i} = b_{o,i}$. The averaging process can be repeated a number of times.

The use of this averaging process introduces some numerical dispersion in the model which has the effect of decreasing maxima and increasing minima of wave height. The most accurate results are found to be obtained when just sufficient averaging is used to ensure stability.

Appendix
References

1. Battjes J A. Refraction of water waves. Journal of Waterway and Harbour Division, ASCE, Vol 94, WW4, pp 437-451, 1968.

2. Yoo D and O'Connor B A. Ray model for caustic gravity waves. Proc. 5th Conf. of Asian and Pacific Division of IAHR, Seoul, Vol 3, pp 1-13, 1986.

3. Yoo D and O'Connor B A. Diffraction of waves in caustics. Journal of Waterway, Port, Coastal and Ocean Division, ASCE, Vol 114, No 6, 1988.

4. Southgate H N and Goldberg D G. An efficient computational model for wave refraction and diffraction using finite differences. HR Report SR 213, June 1989.

Appendix 2

Description of Tideflow-2D model

Appendix 2 Description of Tideflow-2D model

Purpose

To calculate tidal levels, velocities and/or conservative discharges/unit width.

Method

The appropriate equations for studying water movements in tidal areas are the shallow water equations. These are obtained by vertically integrating the equations of motion governing mass and momentum and making the following simplifying assumptions:

(i) the flow is incompressible;
(ii) it is well mixed (no variations in density);
(iii) vertical accelerations are negligible (the hydrostatic pressure assumption);
(iv) the effective lateral stresses associated mainly with shearing in the horizontal, and to a small extent with the averaging of sub-grid scale turbulence, may be approximated by a constant eddy viscosity;
(v) bed stress can be modelled using a quadratic friction law.

The equations then take the following form:

Conservation of mass:

$$\frac{\partial z}{\partial t} + \frac{\partial}{\partial x}(ud) + \frac{\partial}{\partial y}(vd) = 0$$

Conservation of momentum:

$$\frac{\partial u}{\partial t} + u\frac{\partial u}{\partial x} + v\frac{\partial u}{\partial y} = -g\frac{\partial z}{\partial x} - f\frac{u}{d}\sqrt{u^2+v^2} + D\left[\frac{\partial^2 u}{\partial x^2} + \frac{\partial^2 u}{\partial y^2}\right] + \Omega v + \frac{\tau_x}{\rho d}$$

$$\frac{\partial v}{\partial t} + u\frac{\partial v}{\partial x} + v\frac{\partial v}{\partial y} = -g\frac{\partial z}{\partial y} - f\frac{v}{d}\sqrt{u^2+v^2} + D\left[\frac{\partial^2 v}{\partial x^2} + \frac{\partial^2 v}{\partial y^2}\right] - \Omega u + \frac{\tau_y}{\rho d}$$

where

z = elevation above datum (m)
u = depth averaged component of velocity in x direction (+ ve eastwards) (m/s)
v = depth averaged component of velocity in y direction (+ ve northwards) (m/s)
d = total depth, (z + h), where h is depth below datum (m)
f = friction coefficient
D = horizontal eddy viscosity coefficient (m^2/s)
Ω = Coriolis parameter(s^{-1}) which is derived from the latitude specified when setting up the model.
τ_x = component of wind stress and/or wave radiation stress in the x direction (N/m^2)
τ_y = component of wind stress and/or wave radiation stress in the y direction (N/m^2)
ρ = density of fluid (kg/m^3)

The friction coefficient is calculated by the models using the rough channel law:

$$f = \frac{1}{32}[\log_{10}(14.8d/k_s)]^{-2}$$

where

k_s = roughness length (m)

The roughness length is related to the size of the protuberances on the bed, either directly in the form of particle sizes (especially in the case of shingle and stones etc) or indirectly in the form of ripple lengths (in the case of fine particles, ripple lengths are about 1000 times median grain size). Typical values vary from around 0.2m for fairly stony rough estuaries, to 0.003m or smaller for muddy, smooth estuaries. The friction term affects mainly the amplitude of the tide and currents, with less effect on their spatial or temporal distribution.

For conditions with wave activity the calm conditions friction coefficient is calculated according to:

$$f_w = f(1 + \alpha\frac{W}{U})^n$$

where
α = 0.72
n = 1
W = peak wave orbital velocity (m/s)
U = current speed (m/s)

The formula for the eddy viscosity D is not well determined except in a few idealised cases. Fortunately the solutions to the equations are not in general critically dependent on D and an initial estimate of its value can be taken as:

D = (mean velocity). (mean depth)

Eddy viscosity mainly affects the spatial distribution of currents, eg lateral profiles and eddy sizes, thus by comparing model eddies with observations, the value of D can be approximately determined.

Numerical method

The equations are solved using explicit finite difference techniques. This entails covering the estuary with a mesh, or grid, and discretising elevations and velocities in space and time to fit on this grid. Having discretised the variables, derivatives are approximated by simple differences divided by the distance between (in a space or time sense). An explicit method, in order to be stable, must restrict its timestep to within the following:

$\Delta t \leq (\Delta x/\sqrt{(2gd)}$ + max velocity) (approximately)

where Δx is grid size (m)

Thus, deeper water, higher velocities or a finer grid result in a reduction of the maximum allowable timestep.

Spatial variation of roughness

The bed roughness gives a frictional resistance to the flow. Mud being the smoothest and rock boulders being the roughest. For most applications a median value of roughness for the whole of the model area will suffice, but occasionally it is necessary to vary the roughness spatially. Bed flags are used for this purpose, in Tideway. They are initialised to 1 when the model is first set up but may be changed to other numbers, up to a maximum value of 10. It is then possible to prescribe a roughness length associated with each bed flag.

Typical values are: 0 to 0.003 for mud and smooth sand

0.1 to 0.3 for rippled sand (approximately 1000 times the median grain size)

0.2 for gravel.